NASA CR-134631

TOPICAL REPORT

LIGHTWEIGHT THERMALLY EFFICIENT COMPOSITE FEEDLINES PRELIMINARY DESIGN AND EVALUATION

BY

D. E. SPOND, R. E. HOLZWORTH AND C. A. HALL

MARTIN MARIETTA CORPORATION

PREPARED FOR

NATIONAL AERONAUTICS AND SPACE ADMINISTRATION

NASA LEWIS RESEARCH CENTER

CONTRACT NAS3-17796

JOSEPH NOTARDONATO, PROJECT MANAGER

1. Report No.	2. Government Accession No.	3. Recipient's Catalog No.
NASA CR-134631		

4. Title and Subtitle	5. Report Date
Topical Report, Lightweight Thermally Efficient Composite Feedlines, Preliminary Design and Evaluation	June 1974
	6. Performing Organization Code 04236
7. Author(s) D. E. Spond, R. E. Holzworth and C. A. Hall	8. Performing Organization Report No.
9. Performing Organization Name and Address	10. Work Unit No.
Martin Marietta Corporation P. O. Box 179 Denver, Colorado 80201	11. Contract or Grant No. NAS 3-17796
	13. Type of Report and Period Covered Topical Report August 1973 to February 1974
12. Sponsoring Agency Name and Address	14. Sponsoring Agency Code
National Aeronautics and Space Administration Lewis Research Center Cleveland, Ohio 44135	

15. Supplementary Notes

16. Abstract

Six liquid hydrogen feedline design concepts are developed for the cryogenic Space Tug. The feedlines include composite and all-metal vacuum jacketed and non-vacuum jacketed concepts, and incorporate the latest technology developments in the areas of thermally efficient vacuum jacket end closures and standoffs, radiation shields in the vacuum annulus, thermal coatings, and lightweight dissimilar metal flanged joints. The feedline design concepts are evaluated on the basis of thermal performance, weight, cost, reliability, and reusability. It is shown that composite tubing provides improved thermal performance and reduced weight for each design concept considered. Approximately 12 kg (26 lb.) can be saved by the use of composite tubing for the LH_2 feedline and the other propulsion lines in the Space Tug.

17. Key Words	18. Distribution Statement
Composite Feedline Cryogenic Overwrap Thermal efficiency Lightweight	Unclassified - Unlimited

19. Security Classif. (of this report)	20. Security Classif. (of this page)	21. No. of Pages	22. Price
Unclassified	Unclassified		

FOREWORD

The work described herein was conducted by Martin Marietta Corporation, Denver Division, under NASA Contract NAS3-17796, under the management of the NASA Project Manager, Mr. Joseph Notardonato, Propulsion Systems Branch, NASA Lewis Research Center, Cleveland, Ohio.

In addition to the stated authors, the following persons provided major assistance: Messrs Dan J. Laintz, John M. Phillips, Lyle L. Mason and Dr. Tom Howerton.

PAGES MISSING FROM AVAILABLE VERSION

TABLE OF CONTENTS

Table

TABLE OF CONTENTS (Continued)

TABLE OF CONTENTS (Continued)

SYMBOLS

A	Area, cm^2 ($in.^2$)
A_s	Projected area normal to solar radiation, cm^2 ($in.^2$)
A_c	Conductive area, cm^2 ($in.^2$)
A_M	MLI area, cm^2 ($in.^2$)
a	Membrane width, cm (in.)
b	Membrane length, cm (in.)
b	Base, cm (in.)
β	Liquid bulk modulus, N/cm^2 ($lb/in.^2$)
C	Circumference, cm (in.)
C_p	Specific heat, cal/g/^oK (Btu/lb/^oF)
D	Diameter, cm (in.)
D_T	Total deflection, cm (in.)
d	Resonant frequency, Hz
dB	Decibel
ϵ	Emittance
$\overline{\epsilon}$	Effective emittance
E_c	Composite modulus of elasticity (metal liner plus overwrap), N/cm^2 (psi)
E	Modulus of elasticity, N/cm^2 (psi)
E_θ	Circumferential modulus of elasticity, N/cm^2 (psi)
E_ϕ	Meridional modulus of elasticity, N/cm^2 (psi)
e	Strain, cm/cm (in./in.)
e_L	Strain in liner, cm/cm (in./in.)
e_o	Strain in overwrap, cm/cm (in./in.)

e_x	Strain in x direction (along tube centerline), cm/cm (in./in.)
e_h	Strain in hoop direction, cm/cm (in./in.)
F	Force, N (lb)
F_S	Factor of safety
f_{mn}	Frequency for mode shape, Hz
G	Acceleration (number of g's)
g	Acceleration of gravity, M/sec^2 (ft/sec^2)
g_o	Acceleration spectral density, g^2/Hz
Hz	Frequency in Hertz
$(\overline{HA})$	Effective conductance of end fitting, $W/^oK$ ($Btu/hr-^oF$)
$(HA)_F$	End fitting conductance, $W/^oK$ ($Btu/hr-^oF$)
$(HA)_C$	Joint contact conductance, $W/^oK$ ($Btu/hr-^oF$)
h	Gaseous heat transfer coefficient, W/m^2-^oK ($Btu/hr-ft^2-^oF$)
h	Height, cm (in.)
h_M	Film coefficient of MLI, W/m^2-^oK ($Btu/hr-ft^2-^oF$)
h_p	Film coefficient of purge bag exterior, W/m^2-^oK ($Btu/hr-ft^2-^oF$)
I	Moment of inertia, cm^4 ($in.^4$)
i	Current, amperes
K	Thermal conductivity, $W/m-^oK$ ($Btu/hr-ft-^oF$)
k	Unit conversion constant
L	Length, cm (in.)
L_x	Point of contact between line and end fitting
ΔL	Change in length, cm (in.)
δ	Hottel gray body factor

SYMBOLS (Continued)

M	Moment, cm-N (in.-lb)
m	Bending moment, cm-N (in.-lb)
mn	Mode shape
N	Number of radiation shields
n	Number of cycles
p	Pressure, N/cm^2 (psi)
P	Load, kg (lb)
Pc	Critical collapse pressure, N/cm^2 (psi)
P_N	Load per unit length, N/cm (lb/in.)
P_L	Load in liner, N/cm (lb/in.)
P_o	Load in overwrap, N/cm (lb/in.)
P_u	Uniform load intensity, N/cm (lb/in.)
ΔP	Pressure drop, N/cm^2 (psi or microns)
Q	Flowrate, kg/sec (lbm/sec)
Q_F	Magnification factor
q_R	Radiation heat transfer, W/m (Btu/hr-ft)
q_c	Conduction heat transfer, W/m (Btu/hr-ft)
R	Ring radius, cm (in.)
R	Ideal gas constant, $8.3143 J\,{}^{o}K^{-1}mol^{-1}\left(1544\ Ft\text{-}Lb\,{}^{o}F^{-1}Lb\text{-}mol^{-1}\right)$
R	Resistance, ohms
r_1	Radius of curvature, cm (in.)
r	Radius, cm (in.)
s	Time, seconds
S_{bc}	Critical buckling stress, N/cm^2 ($lb/in.^2$)
S	Stress, N/cm^2 ($lb/in.^2$)

S_c	Solar constant, W/m^2 ($Btu/hr\text{-}ft^2$)
S_h	Stress in hoop direction, N/cm^2 ($lb/in.^2$)
S_L	Stress in liner, N/cm^2 ($lb/in.^2$)
S_o	Stress in overwrap, N/cm^2 ($lb/in.^2$)
S_x	Stress in x direction, N/cm^2 ($lb/in.^2$)
S_y	Yield stress, N/cm^2 ($lb/in.^2$)
S_z	Stress in z direction, N/cm^2 ($lb/in.^2$)
S_ϕ	Meridional stress, N/cm^2 ($lb/in.^2$)
T	Temperature, ^oK (^oF or ^oR)
ΔT	Change in temperature, ^oK (^oR)
T	Torque, cm-N (in.-lb)
t	Thickness, cm (in.)
ΔT_L	Change in liner temperature, ^oK (^oR)
ΔT_o	Change in overwrap temperature, ^oK (^oR)
U	Overall transmittance, $W/m^2\text{-}^oK$ ($Btu/hr\text{-}ft^2\text{-}^oR$)
U_M	MLI transmittance, $W/m^2\text{-}^oK$ ($Btu/hr\text{-}ft^2\text{-}^oR$)
V	Volume, liters ($in.^3$)
v	Velocity, m/sec (ft/sec)
W	Weight, kg (lb)
w	Weight/unit area, kg/cm^2 ($lb/in.^2$)
w	Specific weight, Kg/cm^3 (lb/ft^3.)
x	Conductive length, cm (in.)
X	Deflection ratio
Y	Distance from neutral axis to extreme fiber, cm (in.)
Z	Stefan-Boltzmann constant, 1.798×10^{-8} $W/m^2\text{-}K^4$ (0.1713×10^{-8} $Btu/ft^2\text{-}hr\text{-}^oR^4$)

Z_L	Uniform tension per unit length, N/cm (lb/in.)
σ	Sigma (statistical)
$\Delta\theta$	Angular deflection, rad. (degrees)
Δ	Change in angle, rad. (degrees)
δ	Damping ratio
ϕ	Fluctuating pressure spectral density, $\left[\frac{(N/cm^2)}{Hz}\right]^2$ $\left[\frac{(psi)}{Hz}\right]^2$
μ	Microns of Hg
α	Coefficient of thermal expansion, cm/cm/^oK (in./in./^oF)
α_L	Liner coefficient of thermal expansion in axial direction, cm/cm/^oK (in./in./^oF)
α_o	Overwrap coefficient of thermal expansion in axial direction, cm/cm/^oK (in./in./^oF)
α_s	Solar absorptivity
ν	Poisson's ratio
ρ	Density, kg/cm^3 (lb/in.^{3})

SUBSCRIPTS

AT	Axial tension
B	Bending
BL	Bending in liner
c	Composite
c	Curved section
DTC	Differential thermal contraction
F	End fitting
He	Helium
IP	Internal pressure
i	Outside surface of inner line or inner liner
L	Liner
M	Multi layer insulation
OL	Longitudinal overwrap
OH	Hoop overwrap
o	Overwrap, or the inside surface of the vacuum jacket
p	Purge bag
rms	Route mean squared
st	Shear stress due to torsion
s	Straight section
T	Total
TC	Tensile stress in inner line liner
x	Longitudinal direction

DEFINITION OF TERMS

A listing of commonly used terms and their definitions follows. Familiarity with these terms should help the reader to understand the technical aspects of the document.

Inner Line	Line carrying the commodity.
Vacuum Jacket	Concentric line installed over the inner line providing an evacuated annulus for insulation.
Composite Vacuum Jacket	A vacuum jacket concept that incorporates a thin metallic liner and composite material to provide strength and handling damage resistance.
Overwrap	Fiberglass composite applied on exterior surface of the thin metal tubing liner.
Liner	Thin wall metal tube under the overwrap.
Standoff	Support between the vacuum jacket and the inner line.
End Closure	Metal membrane that seals the vacuum annulus between the inner line and the vacuum jacket.
End Fitting	Metal ring welded to the ends of the liner providing a surface for welding the end closure and a butt weld end for attaching one tube to another.
Solid State Bonding	Explosive bonding technique used to join two dissimilar metals such as aluminum to Inconel or stainless steel.

PAGE MISSING FROM AVAILABLE VERSION

SUMMARY

This Topical Report presents the analytical studies and conceptual design developed during Task I of an 18 month program being performed under Contract NAS3-17796. The objective of this program is to develop lightweight thermally efficient composite feedlines for the Cryogenic Space Tug propulsion system.

Six liquid hydrogen (LH_2) feedline design concepts were developed consisting of composite and all-metal vacuum jacketed and non-vacuum jacketed concepts. The non-vacuum jacketed feedlines incorporate purged and non-purged multi-layer insulation (MLI) systems with the system prevalve located at the engine turbopump and at the LH_2 tank outlet respectively. The six design concepts incorporate the latest technology developments in the areas of thermally efficient vacuum jacket end closures and standoffs, radiation shields in the vacuum annulus, thermal coatings, and lightweight dissimilar metal flanged joints. The LH_2 feedline routting and design conditions are representative of the current Space Tug configuration. All design concepts include straight line sections, curved sections, elbows, tees, flanged joints and gimbal installations. The composite feedline designs have sufficient flexibility to incorporate future changes in design requirements.

The all-metal and composite feedline designs are evaluated on the basis of thermal performance, weight, cost, reliability and reusability. It is shown that the composite designs offer improved thermal performance and reduced weight for each concept considered, with little increased cost. Composite feedlines also exhibit superior damage resistance which makes them desirable from reliability, reusability and maintainability aspects. In addition to the LH_2 feedline, other propulsion systems are evaluated for potential weight savings. It is shown that the Space Tug propulsion system weight can be reduced by a total of 11.7 kg (25.9 lb) by the use of composite tubing.

One of the composite and one of the all-metal feedline design concepts are recommended for further evaluation. The evaluation program will include fabricating one all-metal and three composite LH_2 feedline assemblies and subjecting them to identical test programs. This evaluation will provide a direct comparison of the fabrication, cost and performance characteristics of the all-metal and composite designs.

INTRODUCTION

In the continuing development of optimum performance cryogenic propulsion systems, there is considerable interest in the optimization of several system parameters. These parameters include thermal flux, total weight, cost, reliability and maintainability. The Space Tug will require optimization of each of these parameters. Techniques have now been developed to produce feedlines using low heat-leak composite materials which also offer significant weight reduction, when compared to conventional all-metal feedlines. Because of the weight savings and improved thermal efficiency that is possible with composite tubing technology, the use of this concept may be effective as feedlines for the Space Tug and for other thermally optimized, reusable vehicles. The capability, performance and reliability of composite tubing, however, must be demonstrated.

The objective of this program is to develop lightweight, thermally efficient composite feedlines for the Space Tug cryogenic propellant feed system. The program will be performed in eight tasks, as follows:

Task I	-	Definition of Technology Requirements
Task II	-	Subscale Testing and Analysis
Task III	-	Feedline Detailed Design
Task IV	-	Fabrication
Task V	-	Testing
Task VI	-	Analysis
Task VII	-	Reporting
Task VIII	-	Reliability and Quality Assurance

The purpose of this report is to document the results of Task I. The primary activities performed during Task I included:

1) A literature search to obtain the information necessary to develop a representative feedline design configuration and design parameters;

2) An assessment of technology developments that improve the relative merits of composite feedlines;

3) Producing conceptual designs for six liquid hydrogen feedline configurations;

4) Performing structural analyses to define the required feedline wall thickness;

5) Evaluating each of the conceptual designs on the basis of thermal performance, system weight, cost, reliability and reusability;

6) Selecting the optimum concept for detail design, fabrication and test; and

7) Assessing the relative magnitude of potential benefits to be derived from the use of composite feedlines on the Space Tug compared to the standard metal feedlines.

LITERATURE SURVEY

A literature search was conducted to obtain the information necessary to determine the Space Tug liquid hydrogen feedline design conditions and physical configuration. This search included a review of the Space Tug Point Design Studies, conducted by McDonnell-Douglas Astronautics Co., and North American Rockwell (Ref. 1 and 2), the Baseline Tug Definition Document - Rev. A (Ref. 3), Space Tug Systems Study by General Dynamics/Convair (Ref. 4), Space Tug Systems Study (Storable) by the Martin Marietta Corporation (Ref. 5), preliminary Space Tug design drawings obtained from the NASA George C. Marshall Space Flight Center, and telephone conversations with numerous personnel who participated in these studies.

During the literature search, it became clear that Space Tug design conditions and physical configuration are not yet firmly established and will continue to change for some time. Therefore, data obtained from the literature surveyed was used to develop a set of design parameters and a liquid hydrogen feedline configuration which provides design flexibility for future application.

FEEDLINE DESIGN CONDITIONS

The conditions which affect the liquid hydrogen feedline design are system operating requirements and environments within the Space Shuttle cargo bay and during the Space Tug mission. The conditions defined in the contract statement of work are considered representative and are used in the development of the feedline design concepts. These conditions are defined in Tables I, II, III & IV. The random vibration environment, Figure 1, was developed, based upon available Space Shuttle data. A representative mission timeline, consisting of a synchronous equatorial orbit-retrieval mission, was selected from Ref. 4, see Table 5.

The primary design objective is to demonstrate all types of composite tubing technology which may be required for future feedline design conditions and requirements.

ASSESSMENT OF TECHNOLOGY DEVELOPMENTS

Known state-of-the-art technology developments were evaluated to assure that optimum components were used in the development of the liquid hydrogen feedline design concepts. This activity included an evaluation of:

1. High modulus composites for overwrapping the metallic liner on both the inner line and vacuum jacket;

2. Effect of multi-layer insulation (MLI) in the annulus between the vacuum jacket and the inner line;

3. Lightweight and thermally efficient vacuum jacketed line end closures and standoffs;

4. Dissimilar metal joints as a technique of reducing the weight of connections between sections of line; and

5. Application of thermal coatings to the composite to reduce radiation heat transfer for those sections of feedline exposed to solar radiation.

High Modulus Composites. - The following composites were selected as candidate overwrap materials: S-glass, Kevlar 49 DP-01, graphite and boron. These composites were evaluated by comparing mechanical properties, thermal conductivity, resistance to fatigue failure, weight and cost. Evaluation of the application of the composite materials will be performed during Task II, when subscale test specimens are overwrapped using each of the candidate composites except boron.

Composite properties: The physical properties and cost of the candidate composite materials are defined in Table VI.

The thermal conductivity of S-glass, boron and graphite over a temperature range of 28°K to 305°K (50°F to 550°R) as reported by Gille, Ref. 8, is defined in Figure 2. The thermal conductivity of Kevlar 49 at ambient temperature is reported in Ref. 7, as follows:

Conductivity (transverse to fibers) = 0.149 W/m-°K (0.086 Btu/hr-ft-°F)

Conductivity (parallel to fibers) = 1.747 W/m-°K (1.01 Btu/hr-ft-°F)

The key differences in composite properties are minimum wrap thickness, density, cost and thermal coefficient of expansion. It is noted that the thiner minimum wrap thickness and the lower density of graphite results in a high percentage of composite weight reduction. The negative coefficient of expansion characteristic of Kevlar 49 DP-01 is very undesirable for use with LH_2, but would probably be acceptable for use on feedlines having less temperature extremes. S-glass is superior to the other composites from a cost and fabrication experience standpoint.

Resistance to fatigue failure: A comparison of the fatigue behavior of the unidirectional composites, stainless steel and aluminum (as reported in Ref. 7), is shown in Figure 3. The difference between the fatigue behavior of a composite and that of a metal structure, Ref. 9, is depicted in Figure 4. The primary mode of damage in a metal structure is cracking. Cracks propagate in a well defined manner with respect to the applied stress, and the critical crack size and rate of crack propagation can be related to specimen data through analytical fracture mechanics. In this discussion, the critical damage size is defined as that amount of damage at which the composite will no longer be structurally adequate. In general, the crack initiation time [defined as the time to detectable cracking (inspection threshold)] occupies a large part of the fatigue life of a metal part. It should be noted that all structures have some initial damage in the form of micro-cracks, surface imperfections, inclusions and other stress risers and that much of the so-called crack initiation time involves propagation of this damage to detectable size. With composite structures there is no single damage mode which dominates. Matrix cracking, delamination, debonding, voids, fiber fracture and composite cracking can all occur separately or in combination, and the predominance of one or more is highly dependent on the laminae orientations and the loading conditions. In addition, the unique joints and attachments used for composite structures often introduce modes of failure different from those typified by the laminate itself.

Referring to Figure 4, the composite damage propagates in a less regular manner and damage modes can change. Present experience with composites indicates that the rate of damage propagation in composites does not exhibit the two distinct regions of initiation and propagation. Although, as mentioned above, the crack initiation range in metals is actually propagation, there is a significant quantitative difference in rate. This quantitative difference appears to be less apparent with composites. This observation is quite subjective and apparently dependent upon the observer's definition of initiation. Some investigators have observed matrix crazing and other indications early in their tests, but have reported short time rapid propagation, because they define the latter, based upon their experience with metals, as crack propagation. Indeed, composite cracking may occupy only a small part of the fatigue life at the very end, but we can certainly make use of all the earlier indications which are prevalent.

It is expected that composite materials will be more damage tolerant than metals. This expectation is based upon limited experience and will depend upon the laminae orientations (unidirectional composites are subject to splitting) and the loading conditions, but in general, it can be argued that each fiber is a separate load path and that a composite is, therefore, highly redundant.

Thermal stresses: The computation of the stresses induced into the composite, as a result of delta temperature, assumes that the liner and overwrap deflect an equal amount with temperature changes, i.e., the overwrap is attached to the liner end fittings or its movement is restricted by the end fittings. The derivation of an equation to determine axial stresses in the liner and overwrap is presented below:

The deflection (ΔL) of the composite tube due to temperature change = $\alpha(\Delta L)L$ and the deflection due to internal forces = $\frac{FL}{AE}$

where,

α = Coefficient of thermal expansion

ΔT = Change in temperature, (negative if temperature is lowered and positive if temperature rises)

L = Tube length

F = Force

A = Cross sectional area

E = Modulus of elasticity.

Subscripts:

L indicates liner
OL indicates longitudinal overwrap
OH indicates hoop overwrap.

The deflection of the tube in the longitudinal direction can be expressed as:

$$\Delta L = \alpha_L (\Delta T)L_L + \frac{F_L L_L}{A_L E_L} = \alpha_{OL} (\Delta T)L_{OL} + \frac{F_{OL} L_{OL}}{A_{OL} L_{OL}} = \alpha_{OH} (\Delta T)L_{OH} + \frac{F_{OH} L_{OH}}{A_{OH} E_{OH}}$$

But, $L_L = L_{OL} = L_{OH}$

and $F_L = (\Delta L_{/L} - \alpha_L \Delta T)(A_L E_L)$

$F_{OL} = (\Delta L_{/L} - \alpha_{OL} \Delta T)(A_{OL} E_{OL})$

$F_{OH} = (\Delta L_{/L} - \alpha_{OH} \Delta T)(A_{OH} E_{OH})$

Since the forces in the liner and overwrap must be equal at equilibrium conditions:

$\sum F = 0$ or $F_L + F_{OL} + F_{OH} = 0$ then,

$$A_L E_L (\Delta L/L - \alpha_L \Delta T) + A_{OL} E_{OL} (\Delta L/L - \alpha_{OL} \Delta T) + A_{OH} E_{OH} (\Delta L/L \alpha_{OH} \Delta T) = 0$$

$$\Delta L/L (A_L E_L + A_{OL} E_{OL} + A_{OH} E_{OH}) - \Delta T(\alpha_L A_L E_L + \alpha_{OL} A_{OL} E_{OL} + \alpha_{OH} A_{OH} E_{OH}) = 0$$

$$\text{or } \frac{\Delta L}{L} = \frac{\Delta T\left(\alpha_L A_L E_L + \alpha_{OL} A_{OL} E_{OL} + \alpha_{OH} A_{OH} E_{OH}\right)}{A_L E_L + A_{OL} E_{OL} + A_{OH} E_{OH}}$$

Now, since the axial stress (S) is equal to the force divided by the cross sectional area, the axial stresses in the liner, the longitudinal overwrap and the hoop overwrap can be determined from:

$$S_L = \frac{F_L}{A_L} = (\Delta L/L - \alpha_L \Delta T) E_L$$

$$S_{OL} = \frac{F_{OL}}{A_{OL}} = (\Delta L/L - \alpha_{OL} \Delta T) E_{OL}$$

$$S_{OH} = \frac{F_{OH}}{A_{OH}} = (\Delta L/L - \alpha_{OH} \Delta T) E_{OH}$$

The following properties were constant for each overwrap material:

Liner - 0.013 cm (0.005 in.) wall Inconel 718

Overwrap pattern - consists of two hoop layers and a 1/2 longitudinal layer of cloth strips.

E_L - 22,100,000 N/cm^2 (32,000,000 psi)

α_L - 2.68 x 10^{-6} cm/cm/^{o}K (4.82 x 10^{-6} in/in/^{o}F)

ΔT - 272^{o}K (490^{o}F)

The stresses predicted by this analysis for a 10.2 cm (4 in.) diameter composite line overwrapped with the candidate composite materials are as follows:

Composite Material	AXIAL STRESS WITH RESPECT TO TUBE CENTERLINE	
	Composite Hoop Overwrap N/cm^2 (psi)	Composite Longitudinal Overwrap, N/cm^2 (psi) (1)
S-Glass	1,193 (1,730)	-6315 (-9160)
Kevlar 49 DP-01	7,726 (10,555)	-27,030 (-39,210)
Graphite	3,164 (4,590)	-17,225 (-24,985)
Boron	3,433 (4,980)	-20,402 (-29,594)

(1) Negative sign indicates compression.

The compressive stress in the Kevlar 49 DP-01 approaches the allowable for this material, Ref. Table VI. The stresses for boron, graphite and S-Glass are well within the allowable limits.

Summary-evaluation of composites: The evaluation parameters for each of the candidate composites are summarized in Table VII. The cost and weight comparison is based upon the composite material required to overwrap one liquid hydrogen feedline assembly. S-Glass or graphite are the two most promising materials. The final selection, however, should be based on system sensitivity to weight, assuming difficulties are not encountered in the application of the overwrap or test. This will be determined during the overwrap of the subscale test specimens in Task II.

Effect of Radiation Shields in Vacuum Jacketed Line Annulus. - The primary requirement for radiation shields in the vacuum jacketed lines is to reduce the radiation component of heat transfer. Radiation shields exhibit a low emittance, thereby reducing the effective emittance and consequently the overall heat flux. The key considerations for radiation shields in a vacuum annulus are effective emittance, system heat flux, weight and cost. These parameters versus the number of layers of radiation shields are depicted in Figure 5.

The addition of radiation shields also reduces gas conduction at higher gas pressures because the voids between components of insulation are reduced; thus the mean free path of gas molecules is no longer an influence. This is especially true in ground operations where vacuum maintenance is critical to maintaining low LH_2 boiloff rates.

Effective emittances: Emissivity measurements made of vacuum annuli without radiation shields and data from the literature of candidate materials (see Table VIII) indicate that the emissivity of cleaned Inconel surfaces is about 0.20 at ambient temperatures. Under these conditions, the effective emissivity for radiation exchange across the vacuum jacket is approximately 0.0758. This is equivalent to a net radiation transfer rate of 46.4 W/m^2 (14.7 $Btu/hr\text{-}ft^2$) or about 51% of the total heat leak on the LH_2 vacuum jacketed metal line without radiation shields. A corresponding composite line has an effective emissivity of 0.225 and net radiation transfer rate of 138 W/m^2 (43.6 $Btu/hr\text{-}ft^2$) or about 75% of the total heat flux for a jacket temperature of 322°K (120°F). The effective emissivity of a composite line can be reduced by applying a thermal coating on the composite overwrap surface or by the addition of radiation shields. Eight radiation shields will yield an effective emissivity of 0.00147 and eliminate 98.1% of the heat flux due to radiation. The "Superfloc" radiation shields proposed approach an idealized assembly, i.e., where the radiation shield is defined as an isothermal surface of low emittance having no direct contact with adjoining surfaces and/or boundaries. "Superfloc" is a high performance superinsulation (aluminized mylar separated by flocked tufts of Dacron fibers) manufactured by General Dynamics/Convair, San Diego, California.

The solid conduction component of heat transfer from the Superfloc radiation shields contributes approximately 0.4 W (1.5 Btu/hr) or less that 0.6% of the total heat flux for the vacuum jacketed feedline.

Weight and cost of radiation shields: The density of the eight radiation shields consisting of 6 layers of Superfloc and an inner and outer protection shield is 0.22 kg/m^2 (0.0445 lb/ft^2) or 0.21 kg (0.47 lb) for the entire feedline. The cost of eight layers of Superfloc is $1,145 for one feedline assembly. The Superfloc insulation is used in the analyses presented herein and is depicted in the feedline conceptual designs. A less expensive MLI, however, will be used on the test specimens, because of the higher cost for Superfloc. Both composite and non-composite test specimens will be insulated identically for comparison of thermal performance. The difference in the thermal characteristics of Superfloc and the test insulation will be considered in comparing test and theoretical results.

Vacuum Jacketed Line Standoffs and End Closures. -The conventional vacuum jacket proposed is a double walled construction with the annulus between the concentric walls evacuated. The thermal effectiveness of this design is dependent upon the level of vacuum and the method of outer to inner wall support and attachment. The liquid hydrogen line vacuum jacket is supported from the inner line by nine standoffs. End closures sealing the vacuum jacket to the inner line are provided at six locations and are adjacent to the flanges. Figures 7 and 8 describe the concepts evaluated for standoffs and end closures respectively with corresponding heat flux and weight values.

Concept (a), Figure 7, was selected as the optimum vacuum jacket standoff for the following reasons:

Low heat flux;
Good load carrying characteristics;
Resistance to damage and good maintainability.

The proposed standoff design consists of a stainless steel ring with a hat-shaped cross section welded to the vacuum jacket. Thermal losses through the standoffs are minimized by the tortuous leak path through the metal spring which is isolated from the cold surface of the inner line by Teflon blocks. The Teflon blocks also prevent surface wear by preventing metal-to-metal contact of the standoffs to the inner line. The non-metallics will require vacuum baking at elevated temperatures to reduce outgassing. A clearance of 0.15 cm (0.06 in.) is provided between the base of the hat section and the inner line. This allows the hat-section to uniformly distribute loads from the vacuum jacket to the inner line.

The other designs, although lighter weight, do not provide uniform load dissipation, overload protection or competitive thermal characteristics.

Concept (c), Figure 8, was selected as the optimum vacuum jacket end closure, because it offers the highest thermal efficiency and acceptable structural and fabrication characteristics.

The end closures consist of a number of contracting and expanding cones of increasing diameter welded together. The design concept may be incorporated both at the flexible joints and at the vacuum jacket terminations adjacent to the line flanges.

Lighter weight end closure concepts, shown in Figure 8, were not selected, because of poor thermal characteristics, higher fabrication costs and poor structural reliability. A heat flux of 33 W (113 Btu/hr) per concept (a), Figure 8, would approximately double the total liquid hydrogen boiloff that will exist with concept (c).

Evaluation of Dissimilar Metal Joints. - Four techniques of joining dissimilar metal (304L stainless steel to 2219-T851 aluminum) tubes were evaluated. The techniques consisted of inertia welding, coextrusion bonding, swaged and explosive welding. Fifteen joints 6.4 cm (2.5 in.) O.D., by 0.3 cm (0.125 in.) thick wall, by 7.6 cm (3.0 in.) long were fabricated using each of the joining techniques. The joints were subjected to a test program and evaluated for application in the liquid hydrogen feedline design. The fabrication and testing of these joints was performed under Contract NAS9-13570, Dissimilar Metals Joint Evaluation, Report No. MCR 74-88, The Martin Marietta Corporation, April, 1974. The results and conclusions of this contract are discussed in the following paragraphs.

Results of dissimilar metal joint evaluation under Contract NAS9-13570: The purpose of this contract was to develop the production technique for 6.35 cm (2.50 in.) diameter bimetallic transition joints from 2219-T851 aluminum to 304L stainless steel by four methods, and to compare their relative performance through a series of tests. Also, an evaluation was made of the costs and constraints of applying the production methods to larger joints up to 43 cm (17 in.) diameter.

A total of twenty-one joints were fabricated by inertia welding (friction welding) using a Caterpillar Tractor Co. welder. The joints were manufactured by Interface Welding Company of Carson, California. Attempts were made to weld the 2219 directly to the 304L by exploring all adjustable machine parameters, by using different configurations and by using both T851 and T351 tempers. This resulted in a poor quality bond, so it was elected to provide an intermediate layer of 6061-T6 aluminum, which is more readily weldable to each of the other materials. The production process which evolved welded the 6061-T6 to 2219-T851, then welded the refaced 6061 to 304L. The completed joint was artificially aged to recover 6061-T6 aluminum properties in the thin intermediate layer.

A total of eighteen joints were fabricated by explosive welding. They were manufactured by Martin Marietta Corporation, Denver Division. The configuration chosen featured a scarf angle at the interface, in order to provide more bond area to dissipate stresses. The joints used an intermediate layer of sterling silver bonded to the T851 condition aluminum, with the 304L stainless steel then bonded to the silver. No ageing or stress relieving operations were performed during assembly of these joints.

Fifteen joints were fabricated by coextrusion bonding. To fabricate a joint, the 2219 aluminum was placed in intimate contact with the 304L stainless steel within an extrusion billet. After heating, the billet was extruded to promote the diffusion between the aluminum and stainless steel. After preliminary machining, the joint was solutionized and quenched, subjected to 1 to 3% cold deformation and artificially aged to bring the aluminum to T851 condition.

Fifteen joints were prepared by swaged construction. They were manufactured by Metal Bellows Corporation of Chatsworth, California. The joint was formed by mechanically swaging a cylindrical section of 304L stainless steel within a serrated 2219 aluminum collar. The sharp edges of the serrations were held in intimate contact with the opposing piece due to the high residual stresses following swaging (tensile in the aluminum and compressive in the stainless).

Tests were performed to compare the structural integrity and leakage resistance of the four joint types. Tests consisted of proof, leakage, NDT, thermal cycle, pressure cycle, galvanic corrosion, burst and metallographic inspection.

The overall results of the test program were excellent. A parametric evaluation of the four joint configurations is provided in Table IX. Each joint type (in at least one phase of testing) exhibited an advantage over the other joint types, when all test results were compared. Thus, one fabrication technique could prove to be more suitable than the others for a given application. A brief summary of the test results follows. All joint types exhibited good mechanical strength. All joint types were essentially leak-free except for the swaged construction and some of the explosive welded joints. All joint types exhibited a yield pressure of from 2100 N/cm^2 (3000 psig) to 2800 N/cm^2 (4000 psig) and a burst pressure of approximately 5000 N/cm^2 (8000 psig). All joint types withstood exposure to thermal cycling without apparent degradation and exhibited reasonable life when subjected to pressure cycling. The inertia welded joints showed the best resistance to pressure cycling (at a stress level equivalent to that produced by proof pressure), surviving to about 170,000 cycles, and failed in the parent aluminum material. The galvanic corrosion test, while harsh (items unprotected while immersed in a $NaCl/H_2O$ bath), indicated that the swaged construction and explosive welded joints exhibited a reasonable resistance to galvanic corrosion. Of all joint types, the inertia welded joints were more severely attacked.

Unfortunately, manufacturing problems forced delivery of most of the coextruded joints too late for complete evaluation under this test program.

Conclusions, dissimilar metal joint evaluation: The following determinations were made with respect to the 6.4 cm (2.5 in.) O.D. joints produced by inertia welding.

1. A weld between 2219-T851 and 304L could not be made without an intermediate material.

2. A layer of 6061-T6 is a suitable intermediate material between 2219-T851 and 304L.

3. The process was found to be consistent and reliable, as critical paremeters are controlled by machinery rather than by personnel.

4. The joints exhibited excellent fatigue strength when compared to the parent 2219 aluminum.

5. The joints exhibited poor galvanic corrosion resistance compared to the explosive welded and swaged construction joints, when submerged in a $NaCl/H_2O$ electrolyte.

6. The joints exhibited excellent thermal cycle resistance when cycled between 78K (-320°F) and 375K (+215°F).

7. The joints exhibited excellent leakage resistance.

8. The joints failed axially at the 304L/6061 bond interface when hydroburst, with little apparent ductility.

9. The 2219/6061 and 6061/304L bonds were found to have metallurgical diffusion.

The following determinations were made with respect to the 6.4 cm (2.5 in.) O.D. joints produced by explosive welding.

1. The process is more subject to inconsistency when compared with inertia welding or swaged construction, as several critical parameters are controlled by workmanship of personnel.

2. A tubular weld between 2219-T851 and 304L can be successfully made on a scarf angle, using a sterling silver intermediate layer.

3. The joints exhibited about 20% of the fatigue strength of the parent 2219 aluminum.

4. The joints exhibited galvanic corrosion resistance between inertia welded and swaged construction joints when submerged in a $NaCl/H_2O$ electrolyte.

5. The joints exhibited good thermal cycle resistance when cycled between 78K (-320°F) and 375K (+215°F).

6. The joints exhibited good leakage resistance when once verified leak free after manufacture.

7. The joints failed in an axial shear mode partly in the 304L/Ag bond, and partly in the aluminum parent metal when hydroburst.

8. The 304L/Ag and Ag/2219 bonds were found to have metallurgical diffusion.

The following determinations were made with respect to the 6.4 cm (2.5 in.) O.D. joints produced by swaged construction.

1. A tubular joint may be made between 2219-T851 and 304L, but additional development is necessary.

2. The joints exhibited about 40% of the fatigue strength of the parent 2219 aluminum.

3. The joints exhibited better galvanic corrosion resistance than inertia welded or explosive welded joints when submerged in a $NaCl/H_2O$ electrolyte. This resistance is due to anodization of the aluminum portion prior to assembly which is not feasible on the other joint types.

4. The joints exhibited excellent thermal cycle resistance when cycled between 78K (-320°F) and 375K (+215°F).

5. Most of the joints were not leak free. It is felt that the leakage could be remedied through development.

6. The joints failed in an axial shear mode in the stainless portion or the the joint pulling slightly apart, but always in a leak-before-burst mode.

The following determinations were made with respect to the 6.4 cm (2.5 in.) O.D. joints produced by coextrusion.

1. A joint between 2219-T851 and 304L, although possible, presents serious problems during fabrication, particularly during the heat treatment portion of the process.

2. The joint tested exhibited excellent thermal cycle resistance when cycled between 78K (-320°F) and 375K (+215°F).

3. The joints tested exhibited excellent leakage resistance.

The following determinations were made with respect to producing larger size 20.3 cm (8.0 in.), 30.5 cm (12.0 in.) and 43.2 cm (17.0 in.) O.D. joints.

1. The least expensive joint to manufacture in larger sizes (once tooling has been purchased) is the swaged construction.

2. Inertia welded, explosive welded and swaged construction joints appear practical to manufacture in larger sizes. The coextruded joint is not a good candidate for larger sizes in 2219 aluminum alloy if it must be heat treated.

3. The construction method which is potentially lightest weight is inertia welding, due to its butt joint configuration.

The successful development of dissimilar metal joint fabrication techniques provides the capability of using lightweight overwrapped Inconel tubing and lightweight aluminum flanges. A typical dissimilar metal flange joint configuration is depicted in Figure 9. As shown, the thin stainless steel tubular section of the flange is welded to the thin Inconel tubing liner. The thick section of the flange is aluminum. This flange reflects the low profile design developed by NASA MSFC. The flange dimensions were determined by computer analysis developed by the Lockheed Missiles and Space Company under Contract NAS8-28614, Ref. 10. The resulting flange dimensions are charted in Figure 9 for the Space Tug liquid hydrogen feedline. A comparison of the all-stainless and dissimilar metal joint flange weights shows 0.14 kg (0.3 lb) can be saved per flange using dissimilar metal joints.

The cost for fabrication of the dissimilar metal joints are compared below. These costs are based on a quantity of 12 each and do not include machining of the flange face which would be the same for each type of joint. It should be noted that the costs for machining the aluminum flange on a dissimilar metal joint would be less than for the all stainless steel flange, because of the easier machinability of aluminum. This would partially offset the cost of the dissimilar metal joint, when compared to the all stainless steel flange.

TYPE OF DISSIMILAR METAL JOINT	COST/JOINT
Coextrusion Bond	$485.00
Explosive Welding	$310.00
Swaged Construction	$200.00
Inertia Welding	$170.00

Evaluation of Thermal Coatings on Composite Lines. - The temperature of a surface exposed to solar radiation in a space environment will reach an equilibrium temperature consistent with an energy balance between the rate of solar energy absorption and the rate of infrared emission. The solar energy absorbed is a function of the solar absorptivity (α_s) and the projected area normal to the incident radiation, and the emitted energy is a function of the surface emissivity and the total radiation area. The equilibrium temperature is given by:

$$T = \left[\frac{S_c A_s \alpha_s}{Z A \epsilon}\right]^{1/4}$$

where S_c = Solar constant, 1355 W/m^2 (430 Btu/hr-ft^2) in near-Earth environment;

A_s = Projected area normal to solar radiation, m^2 ($ft.^2$)

α_s = Solar absorptivity

Z = Stefan Boltzmann Constant, 1.798×10^{-8} $W/m^2\text{-}^oK^4$

(0.1713×10^{-8} $Btu/hr\text{-}ft^2\text{-}^oR^4$)

A = Radiation area, m^2 ($ft.^2$)

ϵ = Surface emissivity

Typical temperatures for an insulated flat plate, a semi-cylinder, an uninsulated flat plate and a bare cylinder are given in Table X for an $\alpha_s/\epsilon = 1$ and $\alpha_s/\epsilon = 0.24/0.88$. The feedline solar radiation surface approximates a semi-cylinder, i.e., the line is assumed to be routed adjacent to a tank or structure so that the back side is not exposed. The predicted equilibrium temperatures for metal and composite lines with and without thermal coatings are compared in Table XI. As indicated the composite lines without thermal coatings will reach an equilibrium temperature of 350°K (170°F). This will not cause structural degradation but will reduce thermal performance. Thus, exposed sections of the feedline which have the potential of reaching high localized temperatures should be covered with a coating having a low α_s/ϵ. Recommended coatings are given in Table XII.

The feedline design concepts that include multi-layer insulation (Superfloc made from double aluminized Mylar film with Dacron flock tufts) should be configured so that the outer layer of insulation has the aluminized coating facing inward. The outer non-aluminized Mylar surface will have an $\alpha_s/\epsilon \approx 0.25$ and will, therefore, reach an equilibrium temperature of approximately the same as the thermally coated surfaces.

The thermal coating adherence characteristics are a function of material, surface finish and environments. If thermally coated composite lines without multi-layer insulation are to be used in a solar radiation environment, coating application techniques should be developed and tested.

Summary - Assessment of Technology Developments. - The following conclusions are drawn from the evaluation of technology developments applicable to composite feedlines:

1. Graphite/epoxy provides the lightest weight structurally acceptable overwrap material of the composites evaluated.

2. The radiation component of heat transfer in the vacuum jacketed feedline is minimized by the installation of eight radiation shields in the vacuum jacket annulus.

3. Thermally efficient vacuum jacketed line end closures and standoffs significantly reduce liquid hydrogen boil-off, as compared to non-optimum designs. The boil-off losses are more significant from a system aspect than the end closure or standoff component weight.

4. The fabrication and testing of dissimilar metal joints that has been completed shows promising results. When fully developed, dissimilar metal joining techniques will provide the capability of using lightweight aluminum flanges with lightweight composite tubing.

5. All-metal or composite lines which are exposed to solar radiation and not covered with insulation should be thermally coated to reduce line surface equilibrium temperature.

LIQUID HYDROGEN FEEDLINE DESIGN CONCEPTS

Six concept designs for the Space Tug liquid hydrogen feedline were developed. These concepts are defined, as follows:

CONCEPT NUMBER	CONFIGURATION	LINE CONDITION	INSULATION
1	Vacuum Jacketed Metal	Wet	None
2	Vacuum Jacketed Composite	Wet	None
3	Non-Vacuum Jacketed Metal	Wet	Purged MLI
4	Non-Vacuum Jacketed Metal	Dry	MLI
5	Non-Vacuum Jacketed Composite	Dry	MLI
6	Non-Vacuum Jacketed Composite	Wet	Purged MLI

Concept No. 3 is the baseline concept for evaluation and comparison with the other concepts. The line condition "wet" is defined as a configuration that has a prevalve located near the engine turbo pump and the feedline is full of liquid from the time of ground propellant loading until the flight mission is complete and propellant is dumped prior to reentry. The line condition "dry" is defined as a configuration that has a prevalve located at the feedline/LH_2 tank interface. Two operational plans were evaluated for the dry line condition:

1. Mode II: The prevalve is closed during propellant loading and remains closed until the first engine burn during the mission; the valve then remains open, leaving the feedline full of propellant from that time until the mission has been completed.

2. Mode III: The prevalve is closed during propellant loading and remains closed at all times during the mission except during engine burn. The line is dumped after each burn.

These designs are depicted by the concept design drawings included in Appendix A. All design concepts include curved and straight line sections and are representative of anticipated Space Tug feedline routing and interface characteristics. The feedline assemblies consist of three flanged line sections to facilitate installation and handling. All configurations include three gimbal joints to accomodate structural and thermal deflections.

The vacuum jacketed configurations have eight layers of multi-layer insulation (MLI) in the vacuum annulus, a thermal coating on the exterior surface of the vacuum jacket and lightweight/thermally efficient end closures and standoffs.

The composite lines are overwrapped with a layer of machine hoop wrapped 20 end roving, a half layer of longitudinally oriented glass cloth, and a final layer of hoop wrap. The use of graphite epoxy would reduce the feedline assembly weight by approximately 0.8 kg (1.7 lb) but was not selected because overwrap application has not yet been demonstrated.

All composite feedline concepts include inertia welded dissimilar metal (aluminum to stainless steel) flanged joints. This dissimilar metal flange configuration reduces the LH_2 feedline system weight by 0.8 kg (1.8 lb) and could be used with the all metal configurations, as well as with the composite lines. They were not used in the all-metal configurations, because dissimilar metal joints are not shown on any of the current Space Tug feedline preliminary designs.

Feedline Routing Considerations. - The key considerations and rationale used in the development of the feedline configurations depicted by the drawings in Appendix A are:

1. Current cryogenic Space Tug feedline design concepts;
2. Influence of vehicle configurations drivers; and
3. Line motions resulting from structural and thermal deflections.

Current Space Tug feedline design concepts: A review of available Space Tug literature and contacts with contractor personnel continuing to work cryogenic Tug studies indicated that the design conditions are still preliminary and will continue to change. Anticipated feedline routing requirements will include straight line sections, curved line sections, short radius elbows, tees, fittings, flexible joints and external supports. The feedline routing developed for the six design concepts will demonstrate composite line technology for each of these requirements.

Configuration drivers: The anticipated influence of the various Space Tug Vehicle configuration drivers was determined and factored into the feedline configurations. Examples of configuration drivers are: feedline design conditions (defined earlier), type of LH_2 tank insulation system, interface and packaging constraints and operational requirements. Table XIII depicts the anticipated configuration drivers, effected feedline characteristics and plan for evaluation.

Line motions: The feedline design must accommodate the effects of temperature extremes 367°K to 21°K (200°F to -423°F), system operation pressure, propellant weight and interface translational and rotational motions resulting from vehicle acceleration and vibration. An analysis was performed to predict the thermal effects and establish the interface motions. The resulting line deflections and angulation requirements are defined in Figure 10.

Each of the feedline assemblies include three gimbal joints to accommodate the interface motions and temperature extremes. These joints are a standard design by Stainless Steel Products, Inc. The design was used on the Saturn SIVB stage in liquid hydrogen vent lines. The joint is designed for low pressure and light weight, 0.9 kg (2.01 lb). The joint is capable of 0.087 rad. ($\pm$ 5°) motion and 55 N/cm^2 (80 psig) proof pressure at ambient temperature.

Multi-Layer Insulation. - Various multi-layer insulation (MLI) systems were investigated for the LH_2 feedlines. The objectives were to find a system which is lightweight, readily purgeable during ground operations, easily installed on the feedline, thermally acceptable for insulation performance over all phases of the mission and reusable with minimum degradation and maintenance for the life of the vehicle. A description of the proposed system, rationale for component selection, system performance and weight sensitivities are presented in the following paragraphs.

The MLI consists of 0.00064 cm (0.00025 in.) doubly aluminized mylar radiation shields separated 0.08 cm (0.030 in.) by Dacron flock tufts. The MLI is helically wrapped from a 5.1 cm (2 in.) wide spool with a 2.54 cm (1 in.) overlap, on the non-vacuum jacketed feedlines to a thickness of 2.54 cm (1 in.) (approximately 30 layers per inch). A protective purge bag, G. T. Schjeldahl Co., Northfield, Minnesota, P/N X-850 or equivalent laminate, 0.0178 cm (0.007 in.) thick and 0.078 kg/m^2 (0.016 lb/ft^2), is wrapped around the MLI for protection from handling damage and external environment including water vapor, salt spray, dust, etc. The purge bag axial and circumferential seams are bonded with a Crest Product Co., P/N 7410 A & B, adhesive. Only the inside of the purge bag is aluminized to reduce the exterior operation temperature. The externally mounted purge bag can be effectively preconditioned to remove constituents such as absorbed water vapor which will outgas in space, purged to remove condensible gases prior to propellant loading and repressurized during entry to prevent ambient gas from contaminating the system. The inclusion of a sealed purge bag eliminated the requirement for expensive gold-coating of the MLI radiation shields to prevent damage of the shields from moisture.

A helium purge system is installed at one end of the feedline for the design concepts using a purged MLI insulation system. Phenolic standoffs are bonded to the feedline providing an enclosure at the MLI ends for application of the helium purge. The helium will flow from one end of the feedline to the other where it will be vented to the atmosphere. A hot helium purge will be initiated prior to propellant loading to drive off any residual moisture. The configuration of the MLI (both purged and non-purged designs) are depicted on the concept design drawings in Appendix A.

The Dacron flock (Superfloc) between radiation shields was selected over other spacer materials, e.g., foam, glass fabric, crinkled film, silk, nylon screen, etc., because of the following:

1. Low weight per unit area 0.316 kg/m^2 (0.0648 lb/ft^2) for 30 layers Superfloc;

2. Excellent dimensional stability; and

3. Excellent capability to carry compressive loads (94% compression recovery).

Superfloc has been subjected to considerable subscale thermal and structural testing and has been wrapped successfully on a 7.6 cm (3.0 in.) cryogenic feedline complete with purge system and purge bag. The Superfloc system possesses excellent interstitial gas venting characteristics and offers maximum thermal performance for a given number of layers. It exhibits a balance between the desire to reduce weight and the capability of the spacer material to carry loads without suffering a substantial increase in heat transfer. The weight of the MLI has been calculated as follows:

	kg/m^2 (lb/ft^2)
30 layers of Superfloc	0.32 (0.0648)
Laminated aluminized purge bag	0.08 (0.0160)
Total	0.40 (0.0808)

Concept 1, Vacuum Jacketed Metal Configuration Description. - Concept 1 consists of an all-metal conventional vacuum jacketed line assembly.

The inner line is 0.058 cm (0.023 in.) thick stainless steel sheet, formed to the configuration shown in Appendix A. Low profile stainless steel flanges are welded to the inner line for interfacing with the prevalve, located at the engine interface and with the liquid hydrogen tank. Two additional flange joints are provided which divide the feedline assembly into three line sections. A tee connection is provided for LH_2 fill and drain through the feedline, if required.

Each of the line sections are vacuum jacketed for thermal insulation. The vacuum jacket consists of a 12.7 cm (5.0 in.) O.D. by 0.06 cm (0.025 in.) thick stainless steel tube supported to the inner line by standoffs and sealed at the ends by end closures. The standoffs and end closures are of the optimum configurations shown in Figures 7 concept (a) and 8 concept (c) respectively. Eight layers of Superfloc insulation are installed in the vacuum annulus to reduce radiation heat flux. Internal 0.06 cm (0.25 in.) radius convolutes on 22.8 cm (9.0 in.) centers are formed in the vacuum jacket for resistance to external pressure loading.

Each of the line sections contain a flight weight vacuum sensing connection, vacuum acquisition valve and a burst disc for over pressure relief.

The feedline assembly contains three vacuum jacketed gimbals welded into the inner line and into the vacuum jacket. The vacuum annulus is continuous through the gimbals.

Concept 2, Vacuum Jacketed Composite Configuration. - Concept 2 is of the same physical geometry as Concept 1. The gimbals, prevalve location, vacuum components, MLI insulation, standoffs and end closure designs are identical to Concept 1.

The vacuum jacket consists of a 0.021 cm (0.009 in.) thick Inconel 718 liner overwrapped with 2 hoop layers of S-Glass roving applied in a $\pm$ 0.09 rad ($\pm$ 5 degrees) helical pattern. Convolutes of 0.64 cm (0.25 in.) radius are formed in the vacuum jacket on 3.8 cm (1.5 in.) centers for resistance to external pressure loading.

The inner line consists of a 0.02 cm (0.008 in.) thick Inconel 718 tube liner overwrapped with two hoop layers of S-Glass roving and longitudinal strips of glass-fiber cloth sandwiched between the hoop layers. The flange locations are identical to Concept 1. The flanges are inertia welded stainless steel to aluminum joints of the configuration discussed earlier.

Concept 3, Non-Vacuum Jacketed Metal, Wet, Purged MLI, Configuration. - Concept 3, a conventional all-metal feedline insulated with helium purged MLI, was established by NASA as the baseline for competitive comparison with the other design concepts. The prevalve is located at the engine turbo pump interface. The gimbal system (except non-vacuum jacketed), flange designs and routing are identical to Concept 1. The feedline is 10 cm (4.0 in.) O.D. by 0.05 cm (0.020 in.) thick stainless steel tubing.

The insulation system consists of 30 layers of double aluminized Superfloc, as defined earlier.

Concept 4, Non-Vacuum Jacketed Metal, Dry, MLI, Configuration. - Concept 4 is identical to Concept 3 except the prevalve is located at the liquid hydrogen tank interface and the insulation system is not purged.

Concept 5, Non-Vacuum Jacketed Composite, Dry, MLI, Configuration. - Concept 5 is identical to Concept 4 except the pressure line is a composite overwrapped design and dissimilar metal (aluminum to stainless steel) flanges are used. The pressure line is 0.013 cm (0.005 in.) thick Inconel 718 overwrapped with two layers of S-Glass roving and longitudinal strips of glass-fiber cloth identical to the overwrap on the Concept 2 inner line.

Concept 6 Non-Vacuum Jacketed Composite, Wet, Purged, MLI Configuration. - Concept 6 is identical to Concept 3 except, as in Concept 5, the pressure line is a composite overwrapped design and dissimilar metal flanges are used.

STRUCTURAL EVALUATION

Because of the feedline low operating pressure and external loads, the non-vacuum jacketed feedline concepts are essentially designed for handling and manufacturing limitations. The vacuum jacketed lines are designed to withstand an external pressure loading of 15 N/cm^2 (22 psi) on both the pressure carrying inner line and the vacuum jacket. Handling loads are also a major consideration in the vacuum jacketed line design.

The NASA Marshall Space Flight Center has recommended the minimum duct wall thickness for handling, see Figure 11. As shown, the minimum gage for 10.2 and 12.7 cm (4.0 and 5.0 in.) diameter steel tubing is 0.05 and 0.06 cm (0.02 and 0.025 in.) respectively. These are the line gages selected for the all-metal design concepts, except for the inner line of the all-metal vacuum jacketed line, Concept 1. This line gage was dictated by an internal over pressure consideration per the following analysis. The composite line gages, considering the combined metal liner and overwrap thickness, slightly exceed these minimum gage requirements. Stress levels are checked for the pressure carrying lines using maximum anticipated line pressure. The maximum line pressures may be as high as 58 N/cm^2 (85 psig) assuming an operating pressure of 21 N/cm^2 (30 psig) added to a surge pressure of 38 N/cm^2 (55 psig). The surge pressure is calculated based on a fast closing engine shutoff valve. From Ref. 12, surge pressure is given by:

$$\text{Surge Pressure} = \frac{k\, w\, v}{g\sqrt{w\left(\frac{1}{\beta} + \frac{D}{E\,t}\right)}} = 38\ N/cm^2\ (55\ psi)$$

where: w = 71 kg/m^3 (4.43 lb/ft^3), specific weight of LH_2

v = 4.6 m/sec (15 ft/sec)

g = 9.7 m/sec^2 (32.2 ft/sec^2)

β = 9996 N/cm^2 (14,500 psi)

D = 10 cm (4 in.)

t = 0.05 cm (0.02 in.)

k = Unit conversion constant

E = Modulus of elasticity, 20 x 10^6 N/cm^2 (29 x 10^6 psi)

The stress in the all-metal pressure carrying lines, where t = 0.05 cm (0.02 in.), P = 58 N/cm^2 (85 psig) and r = 5 cm (2 in.) is provided by the relation:

$$S = \frac{Pr}{t} = 5860\ N/cm^2\ (8500\ psi).$$

The stress in the composite overwrapped lines where t = 0.013 cm (0.005 in.) will be 23,400 N/cm^2 (34,000 psi) assuming no structural support from the composite overwrap. Comparing these stress levels to stress allowables for stainless steel (all-metal lines) and Inconel 718 (composite lines), it is obvious that handling conditions and not pressure dictate the line wall thickness.

The inner line liner for the composite vacuum jacketed line, Concept 2, is designed from a possible failure mode consideration, where a liner leak would allow a pressure buildup in the vacuum annulus. For this condition, the vacuum jacket burst disc rupture pressure, 10.3 N/cm^2 (15 psi), establishes an external pressure loading on the inner line liner. Assuming no structural support from the composite overwrap, the inner line liner material thickness may be determined by the relation from Roark, Ref. 13:

$$Pc = 0.807 \frac{Et^2}{Lr} \sqrt[4]{\left(\frac{1}{1-\nu}\right)^3 \frac{t^2}{r^2}}$$

where: Pc = Critical collapse pressure, 10.3 N/cm^2 (15 psi)

L = Length of tube, 127 cm (50 in.)

ν = Poisson's ratio, 0.3

r = Radius, 5.1 cm (2.0 in.)

t = Liner thickness, cm (in.)

E = Modulus of elasticity, 20 x 10^6 N/cm^2 (29 x 10^6 psi)

Solving the above equation yeilds a required liner thickness of 0.058 cm (0.023 in.). It has been demonstrated, however, through work done by Johns and Kaufman, Ref. 14, and by Martin Marietta the composite overwrapping does substantially improve the buckling strength of thin metallic liners. Although test data is limited, preliminary indications are that the liner thickness may be determined by multiplying the theoretical thickness by 0.6, yielding a thickness requirement of:

$$t = 0.6\ (0.058) = 0.035 \text{ cm } (0.013 \text{ in.})$$

The composite vacuum jacket liner thickness is determined by using the same relationship for critical collapse pressure (P_c) as above where: r = 6.4 cm (2.5 in.), L = 3.8 cm (1.5 in.) the distance between convolutes, and P_c = 15.2 N/cm^2 (22 psi). Solving for thickness yields: t = 0.018 cm (0.007 in.). The composite overwrap factor was not used to reduce vacuum jacket thickness, because of the desire to provide structural margin for handling.

Bending Stresses. - An analysis was performed to evaluate the stresses induced in the composite line due to bending loads. For this analysis, the line was considered as being made up of a series of short, straight sections, as shown in the following sketch.

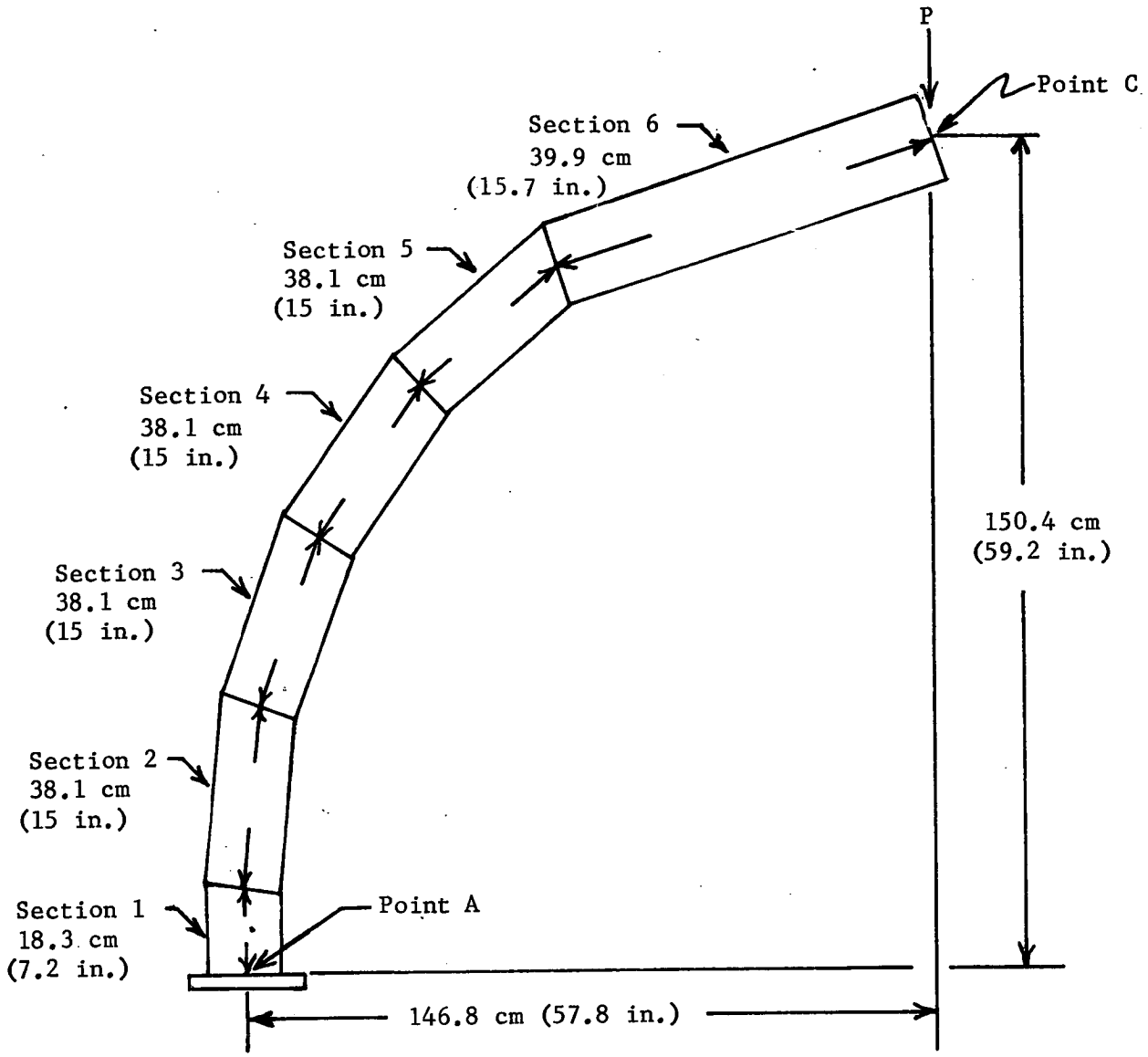

For this analysis, point A was assumed to be fixed and a load P was applied at point C. The angular deflection of each section was determined from the relation:

$$\Delta\theta = \int \frac{M}{EI}\, dx$$

where M (refer to sketch below) = P (R + x COSβ) through the limits of x = 0 to x = L

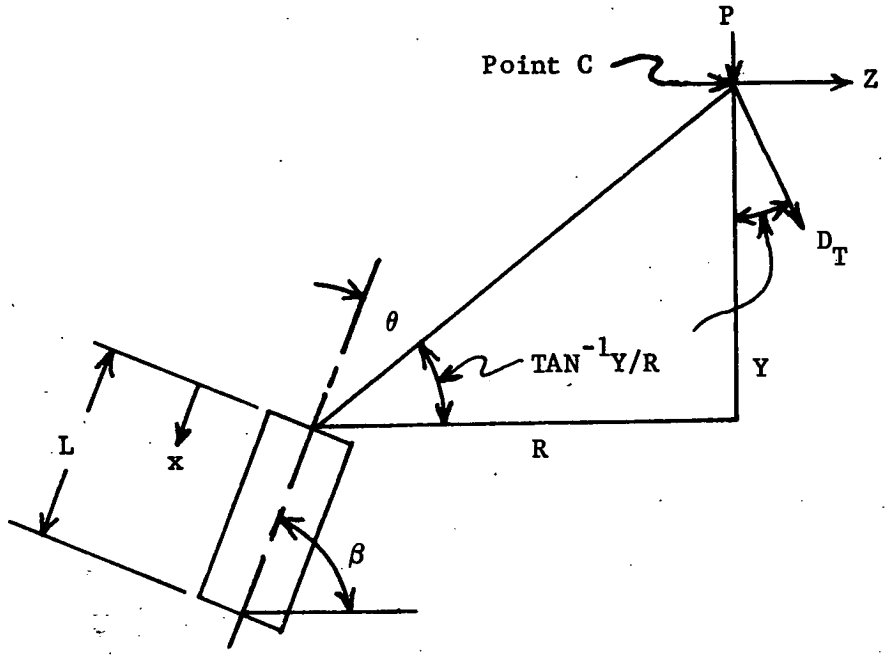

The total deflection (D_T) of point C for each section was then determined from:

$$D_T = \Delta\theta \sqrt{R^2 + Y^2} \text{ at an angle } TAN^{-1} Y/R \text{ from the vertical.}$$

This total deflection was then resolved into the Y and Z components by using:

$$D_Z = D_T \text{ SIN } (TAN^{-1} Y/R) \text{ and } D_Y = D_T \text{ COS } (TAN^{-1} Y/R).$$

From motion analysis the deflection of point C in the Y direction was determined to be 2.3 cm (0.9 in.). Since the numerical values of E, I, R, Y and x are known or can be determined from system geometry, the D_Y deflections can be expressed in terms of the load added.

The load required to produce a deflection of 2.3 cm (0.9 in.) in the Y direction was determined to be 10.5 kg (22.8 lb) from:

$$\sum D_Y = 0.04 \text{ (P)} = 2.3 \text{ cm (0.9 in.)}$$

The stresses in the liner at section 1 were then determined. The stress due to the moment at section 1 is:

$$S_1 = \frac{MC}{I} = \frac{PLC}{I} = 14{,}500 \text{ N/cm}^2 \text{ (21,000 psi)}$$

The stress due to the load is:

$$S = F/A = 250 \text{ N/cm}^2 \text{ (362.5 psi)}$$

The critical compressive buckling stress S_{bc} in the liner can be determined from:

S_{bc} = 0.3 E (t/r) where:

S_{bc} = Critical compressive buckling stress in axial direction;

t = Liner thickness;

r = Liner radius (nominal); and

E = Liner modulus of elasticity.

For a dry, unpressurized line at ambient temperature, the critical buckling stress would be 15,200 N/cm^2 (22,000 psi) which is just slightly greater than sum of the stresses due to the moment and the load.

The results of this analysis show that the stresses in the 10.2 cm (4.0 in.) diameter 0.013 cm (0.005 in.) wall Inconel liner would most likely cause buckling of the liner in section 1.

Therefore, the wall thickness of the liner must be increased to provide a safe margin between the actual stress and the allowable stress, or bellows/gimbals must be added to eliminate the bending stresses. Both of these options increase the total weight of the line. However, the addition of gimbals to the line provides other advantages, such as:

1. Allowing for misalignment during installation;
2. Reducing axial stresses due to cooldown and pressurization;
3. Reducing vibration loads; and
4. Reducing handling loads.

THERMAL ANALYSIS

The thermal insulation systems consist of two basic types -- vacuum jacketed and multilayer insulation (MLI). "Wet" or "dry" lines are designations given to a feedline depending on the location of the LH_2 tank isolation valve (prevalve). A "wet" line is one in which the prevalve is located at the turbopump interface (see Figure 12). A "dry" line has the prevalve located at the tank outlet, thereby keeping the line dry until engine firing.

Heat can flow through an insulation system by the simultaneous action of several different mechanisms:

1. Solid conduction through the materials making up the insulation and conduction between individual components of the insulation across areas of contact;

2. Gas conduction in void spaces contained within the insulation system; and

3. Radiation across these void spaces and through the components of the insulation.

Because these heat-transfer mechanisms operate simultaneously and interact with each other, it is, therefore, useful to refer to an apparent thermal conductivity, which is definable analytically or measured experimentally during steady-state heat transfer and evaluated from the basic Fourier equation:

$$q = \frac{KA}{t} (T_1 - T_2)$$

where:

q = Heat flux through the material

K = Apparent thermal conductivity

A = Area

T_1, T_2 = Boundary temperatures

t = Thickness of the insulation

The primary effort in the development of more efficient thermal insulation systems is directed toward reducing the different heat transfer mechanisms. To aid in these efforts, the effects of variables - solid conduction, gas conduction and radiation, on thermal conductivity had to be determined.

Liquid Hydrogen Feedline Boiloff. - Table XIV lists the liquid hydrogen boiloff of three operational modes: Mode I - Ground operations and Modes II and III - Space residency. The boiloff values given represent the additional propellant required due to thermal and operational losses. Table V presents the timeline used in determination of the total boiloff values for a typical Space Tug mission requiring six engine burnes.

Ground operations, Mode I: Mode I defines the liquid hydrogen boiloff during two hours of prelaunch operations. During this time, a ground support LH_2 replenish system is active, maintaining the Tug propellant tank in a launch-ready, loaded condition. A helium purge within the Space Shuttle Cargo Bay will temper the prelaunch 322°K (120°F) wall temperature so that the Tug feedlines should not exceed 300°K (80°F) on the external surfaces, during ground operations.

It is apparent from Table XIV that the purged MLI lines yield the highest losses, because of the convection component of heat transfer in the insulation for Mode I. Non-purged MLI-Dry lines exhibit the lowest boiloff losses with the composite line showing about a 50% advantage over the all-metal line. All MLI insulated lines were assumed to have a natural insulation density of 12 layers/cm (30 layers/in.). Concepts 4 and 5 have the least boiloff losses, because the lines were dry and the only heat flux was that due to the axial conduction along the warm line to the cold LH_2 tank.

The LH_2 losses during Mode I are not very significant, due to the ground support replenish system. This system replaces any LH_2 boiloff up until launch. Therefore, the losses prior to launch are not considered as unusable propellant.

Space residency, Mode II: The feedline configuration for both the wet and dry feedline systems are shown schematically in Figure 12. Space residency is defined as the total time in space including storage in the Space Shuttle cargo bay. Mode II and Mode III define two operational modes for the dry feedline configurations during space residency. Figure 13 depicts the conditions and timelines for the two operational configurations for the dry feedlines (Concepts 4 and 5). The total LH_2 boiloff was determined for each mode. For Mode II the LH_2 feedline is void of propellant for the first 14.7 hours. The Space Tug is in the Space Shuttle cargo bay during this time. For the balance of the mission, 31.86 hours, the feedline is full of propellant.

Table XIV, Boiloff Values for Mode II, shows the non-vacuum jacketed, dry, MLI insulated composite line, Concept 5, with the lowest LH_2 loss. It is closely followed by the similar but all-metal feedline, Concept 4. The MLI, Wet lines, Concepts 3 and 6, will of course, exhibit a higher LH_2 boiloff over the dry lines, because of the added time (14.74 hours) of having LH_2 in the line. Line chilldowns are not required of the wet lines and this can be as much as a 3.8 kg (8.3 lbs) advantage. The vacuum jacketed lines suffer from the solid conduction element of heat transfer contributed by the standoffs and end closures. It is to be noted that

the radiation shields reduced the overall LH_2 boiloff by 46% in the case of the metal lines. The boiloff of the composite line was reduced 72% with the addition of eight radiation shields. This reduction was possible because of high emissivity differential between radiation shields and the bare overwrap.

Space residency, Mode III: Mode III synchronizes the prevalve actuation (opening and closing) with that of the engine valve. After each engine firing, the line would be vented to space, resulting in the feedline being void of any propellant between engine firings. The time required for the empty feedline to return to ambient temperature was calculated to be 2 to 7 hours. Therefore a complete LH_2 line chilldown and fill is required prior to the next engine firing. The venting of the feedline after each engine firing accounts for more LH_2 loss than that of the heat flux, due to engine soak-back (see Mode II). Again, the composite line exhibits the lowest LH_2 boiloff. Engine soak back was insignificant and, therefore, not included.

Heat transfer by engine to feedline: The engine thermal effects are shown in Figures 14 and 15. Liquid hydrogen boiloff due to engine heat transfer is shown in Table XIV. The heat input to the dry feedline is a function of the L/D and the engine temperature. The feedline is 10.2 cm (4.0 in.) diameter stainless steel with a wall thickness of 0.051 cm (0.020 in.). Since the length of the dry section is greater than 73.7 cm (29.0 in.) and the turbopump to feedline interface temperature is 278°K (40°F), the heat flux is about 3.81 watts (13 Btu/hr). Both radiation and conduction modes of heat transfer were considered.

Vacuum Jacketed Insulation Systems. - The vacuum jacketed concept consists thermally of an inner line, an outer concentric vacuum jacket, flexible joints, standoffs, 8 radiation shields and end closures. For Concept 1 the inner line and the vacuum jacket are of an all-metal design and Concept 2 uses a composite tubing design for both the inner and outer line. The main advantage of vacuum jacketed insulation is the low heat flux during ground operations in a wet configuration. The disadvantages are increased weight and increased operations required for vacuum maintenance of the vacuum annulus.

Vacuum jacketed line thermal analysis: A heat flux analysis of the vacuum jacketed line concepts was performed and the results are shown in Tables XV and XVI. Thermal performance is given for environments of one-G at 300°K (80°F) and space residency at the following conditions:

256°K (0°F)	-	Thermal coated lines during Tug operation
322°K (120°F)	-	Lines during Tug storage in Space Shuttle
367°K (200°F)	-	Lines during Tug storage in Space Shuttle

Data is provided for lines with and without radiation shields.

Heat transfer between the environment and the feedline occurs by radiation through the vacuum annulus, by conduction through noncondensible gases in the annulus and by conduction through standoffs, flexible joints, and end closures. Radiation transfer through the vacuum jacket is determined primarily by the emissivity and temperature difference of the enclosure surfaces. In this analysis, the annular spacing is small relative to the line radius, because of the shields, and the effective emissivity for radiation transfer is essentially independent of the annular spacing.

The mechanism for steady-state radiation transfer through a vacuum jacket containing several radiation shields can be considered in terms of two conductances in series; one through the radiation shields next to the inner wall (1) and the other between the outer radiation shield (2) and the vacuum jacket (3), as shown in Figure 6.

The effective emmittance for these series conductances is:

$$\bar{\epsilon} = \epsilon_{12}\,\epsilon_{23}/(\epsilon_{12} + \epsilon_{23}) \text{ - with radiation shields, or}$$

$$\bar{\epsilon} = \frac{1}{1/\epsilon_1 + A_1/A_3\,(1/\epsilon_3 + 1)} \text{ - without radiation shields,}$$

where $\bar{\epsilon}$ is the overall effective emittance.

ϵ_{12} is the effective emittance through the shield blanket and ϵ_{23} is the gap emittance.

For a gap thickness which is small relative to the line radius, the gap emittance can be expressed in terms of the emissivities of surfaces 2 and 3 by the relation:

$$\epsilon_{23} = (\epsilon_2)(\epsilon_3)/(\epsilon_2 + \epsilon_3 - \epsilon_2\,\epsilon_3)$$

Emissivities of the vacuum jacket components were taken as:

ϵ_1 = {0.10 (metal), 0.80 (composite)} - Inner Line
ϵ_2 = 0.025 (radiation shields)
ϵ_3 = 0.20 (vacuum jacket)

then,

ϵ_{23} = 0.0227

For multiple radiation shields all having the same emissivity (ϵ_2), the blanket emittance is approximately:

$$\epsilon_{12} = \epsilon_2/N(2 - \epsilon_2)$$

for ϵ_2 = 0.025

$$\epsilon_{12} = 0.0126/N$$

Therefore, eight radiation shields will result in a vacuum jacket effective emissivity, $\bar{\epsilon}$ of 0.00147 for both metal and composite lines. It should be noted that the effective emissivity is largely dependent on the radiation shield emissivity for vacuum jackets incorporating radiation shielding.

The effective emissivity of the metal and composite lines without radiation shields is 0.0758 and 0.225 respectively. The emissivity of the composite line can be reduced through the usage of thermal coatings.

The radiation component of heat transfer was derived from the classical Stefan Boltzmann equation. Radiation heat flux involving the determination of net heat transferred between surfaces in a vacuum, separated by a non-absorbing medium, is given by the following expression:

$$q_R = Z\ \bar{\epsilon}\ A_2(T_3^4 - T_1^4)$$

The presence of noncondensible gases, such as H_e or H_2, in the vacuum jacket under operating conditions can contribute to the total heat transfer rate by gaseous conduction. The gas conductivity can be reduced by decreasing the jacket pressure to the point where the mean free path is greater than the system dimension. For a 1.27 cm (0.50 in.) gap thickness (vacuum annulus without radiation shields), the noncondensible gas pressure must be less than 0.015 torr in order to reduce the gas conductivity below that existing at a pressure of 1 atmosphere. In the rarefied gas region below 0.015 torr, the gaseous heat transfer coefficient (h) is roughly proportional to the gas pressure for the specified temperature boundaries. For hydrogen, h = 596.2 x pressure in torr, Watt/$m^2 \cdot {}^oK$ (h = 105 x pressure torr, Btu/hr-ft^2-^oF) and the free molecular gas conduction rate is approximately h = 165,632 x pressure in torr, Watt/m^2 (52,500 x pressure in torr, Btu/hr-ft^2) for a 278^{o}K (500^{o}R) temperature difference across the vacuum jacket. To maintain the gaseous conduction rate at a value less than an acceptable allowable for a LH_2 line, 94.7 W/m^2 (30 Btu/hr-ft^2), the noncondensible gas pressure (resulting from H_2 or helium leakage into the vacuum annulus) must be less than 6×10^{-4} torr. The noncondensible gas pressure must be less than 1×10^{-4} torr to reduce the gas conduction rate to a value below 16.7% of the total allowable. In this analysis the vacuum annulus pressure was assumed to be less than 10^{-5} torr. Therefore, heat transfer due to gas conduction was considered negligible.

The expression for the conductive component of heat transfer through the vacuum jacket standoffs and end closures is given by the following expression:

$$q_c = UA(T_3 - T_1), \text{ where:}$$

$$UA = \frac{1}{x/KA}$$

Finally, the total heat flux of a vacuum jacketed line is the summation of the heat transfer due to radiation and conduction. Total heat flux = $q_R + q_c$.

Multilayer Insulation Systems. - The multilayer insulation consists of 30 layers of 0.000635 cm (0.00025 in.) double-aluminized mylar radiation shields (Superfloc) separated by low-conductive flocked tufts of Dacron fibers. The tufts, arranged triangularly, provide positive spacing of the radiation shields, thus providing a direct path for interstitial gases, during purging, evacuation (ascent) and repressurization (descent), and to reduce the heat transferred from shield to shield by solid conduction. Solid conduction accounts for approximately 10% of the apparent conductivity of the insulation material. The gas in the space between the shields is expelled during ascent to decrease the conduction by gas molecules. The MLI was verified during compression and recovery tests, to recover up to 94%. This indicates that the method of spacing withstands mechanical compression during manufacturing or high g-loads during Shuttle boost, without deterioration of thermal performance.

Other features of the MLI are high strength, density control, good gas absorption/outgassing characteristics and integral spacer material with radiation shields achieving the lowest weight density versus conductivity rating.

MLI Thermal Analysis. - The thermal performance of the MLI was determined for both purged (wet), Concepts 3 and 6, and unpurged (dry), Concepts 4 and 5, MLI systems. Equilibrium heat flux values are presented in Table XVI. In multilayer insulations, the principles used to obtain more effective evacuated insulations were used recognizing the importance of radiation heat transfer once the mechanisms of gas conduction and solid conduction have been reduced. In this insulation, radiation shields of low emittance (0.025) are separated by spaces of low conductivity (less than 10% of the overall apparent conductivity) and are exposed to the high vacuum of deep space. In an idealized assembly of radiation shields, radiation is directly proportional to the emittance of the surfaces and inversely proportional to the number of radiation shields between the two temperature boundaries. In practical MLI systems, radiation heat transfer between two radiation shields involves complex interactions between the reflective properties of the radiation shield and the adsorption and scattering properties of the spaces. Because of the complexity of the heat transfer phenomena, data obtained from laboratory tests are essential in predicting the thermal performance. Figure 16 shows the relationship of MLI apparent thermal conductivity versus density [(layers/cm(in.)], as exhibited in tests over the range of 300°K to 78°K (540°R to 140°R).

The performance of the MLI in the actual installation will be affected by the following variables:

1. Applied compressive loads;
2. Gas pressure within the MLI;
3. Flow passages permitting outgassing; and
4. Temperatures of the warm and cold boundaries.

Compressive loads, either those caused by atmospheric pressure or those developed during application of MLI, reduce overall insulating effectiveness. External forces such as tension applied during wrapping of the MLI around the feedlines, thermal expansion or contraction of the insulation mylar purge covering, and localized loads in the vicinity of the feedline support, can compress the insulation. These compressive loads may be in the range from 0.0069 to 0.69 N/cm^2 (0.01 to 1 psi). When compression up to 1.38 N/cm^2 (2 psi) is applied, the apparent thermal conductivity is about 200 times greater than the no-load condition [natural density of 12 layers/cm (30 layers/in.)].

Figure 17 relates the apparent thermal conductivity to the gas pressure in the MLI. At pressures below 10^{-5} torr, the heat transferred by a gas is directly proportional to the gas pressure and density. However, the heat conducted by a gas at that pressure is only a small portion of the total heat transferred through the insulation. Therefore, the apparent thermal conductivity of the multilayer insulation decreases only slightly at pressures below 10^{-5} torr and heat transfer is by solid conduction within and through the components of the MLI and by radiation across the voids and through these components.

To assure that the MLI will operate at the desired low pressure, the interstitial gas caused by outgassing has to be evacuated through the edges of the insulation. Because of the positive separation, 0.089 cm (0.035 in.) between the radiation shields, rapid evacuation is possible. Tests have indicated that the proposed MLI will reduce a pressure of 2 torr within the layers to 10^{-4} torr within 5 minutes in a vacuum chamber environment of 10^{-5} torr. This method of venting is preferred over penetrations in the MLI which can cause an increase in heat flux as much as 278% for 0.32 cm (1/8 in.) holes, Ref. 15.

Effects of boundary temperatures on apparent conductivity are shown in Figure 18 of a typical MLI (Ref. 15). The one that represents a cold-boundary temperature of 21°K (-423°F) indicates a lower thermal conductivity than the one representing a cold-boundary temperature of 77°K (-320°F).

The equations and assumptions used in calculating the heat flux values for MLI systems are presented in the following paragraphs. Heat flux values were computed for both metal and composite feedlines, however, there is no appreciable difference for filled LH_2 lines in a space environment between the two concepts. A delta does exist during Space Shuttle storage, when the Tug feedlines are dry. The heat transfer from a "warm" feedline to the tank is approximately 50% more for the metal line than it is for the composite line. The heat flux, prior to launch, is considerable for the "wet" purged MLI line, because of the helium purge required to maintain the insulation free of moisture and contaminants. The space heat flux values for wet MLI lines were increased by approximately 800% to account for previously mentioned variables of the MLI apparent thermal conductivity.

One G environment, purged, wet MLI analysis: Natural convection was assumed in the MLI annuli and external surface of the purge bag. Film coefficients, h_M and h_p used were 17.6 to 5.7 W/m^2-^oK (3.1 and 1.0 Btu/hr-ft^2-^oR) respectively. End losses were considered negligible, because the line length is greater than 10 times the line diameter. The external purge bag temperature, Tp, was assumed to be 300^oK (80^oF). The expression for the heat transfer rate from the LH_2 in the feedline through the MLI and helium to the surrounding ambient medium is given by:

$$q = UA_M(T_P - T_i)$$

where:

$$U = \frac{1}{\frac{1}{h_M} + \frac{t}{K_{He}} + \frac{1}{h_P}}$$ for metal and composite lines.

A_M = MIL area, m^2

h_M = Film coefficient within MLI, $Watt/m^2-^oK$

h_p = Film coefficient of purge bag exterior, $Watt/m^2-^oK$

K_{He} = Helium conductivity, $Watt/m-^oK$

q = Heat flux, Watts

t = Thickness of MLI, m

T_P = Purge bag exterior surface temperature, ^oK

T_i = Inner line temperature, ^oK

U = Overall transmittance, $Watt/m^2-^oK$

The thermal conductivity of helium, K_{He} was assumed to be 0.095 $Watt/m-^oK$ (0.055 Btu/hr-ft-^oF).

One G environment, dry MLI analysis: Heat flux equations used were typical of those used in analyzing the heat flux from insulated feedline end sections (see space environment dry MLI analysis). Exterior surface temperatures were assumed to be 300^oK (80^oF). The only heat flux considered was that of the warm feedline interfacing with the LH_2 tank prevalve.

Space environment, purged, wet MLI analysis: High emissivities of the Tug and Space Shuttle structural surfaces will dictate a feedline surface temperature, T_p equivalent, to the internal Shuttle cargo bay temperature 367^oK (200^oF) during storage. During the Space Tug mission the surface temperature was assumed to be 256^oK (0^oF) because of thermal coatings on the feedlines. Apparent thermal conductivity of the MLI includes both heat transfer components of radiation and solid conduction. Gas conduction was considered negligible with a MLI annulus pressure less than 10^{-5} torr. Heat flux is given by the typical Fourier expression:

$$q = U_M A_M (T_P - T_i)$$

where

$$U_M = \frac{K_M}{t_M}$$

K_M = MLI apparent thermal conductivity, W/m-^oK

t_M = MLI thickness in direction of heat flux, m.

Space environment, dry MLI analysis: This analysis deals with the axial thermal conduction through flanged or welded line connections attached to both composite and all-metal lines. The lines are insulated with MLI under both vacuum and helium purge conditions. The heat flux values calculated represent the heat transfer from the warm, dry line to the LH_2 propellant tanks. See Figure 19 for the configuration of the axial heat transfer configuration for a warm line to a cold line.

Axial conduction of the glass-fiber overwrap is considered negligible relative to that of the metal liner. The MLI annulus pressure, during space residency, is considered to be less than 10^{-5} torr. The prevalve provides the LH_2 isolation required between the warm and cold lines.

The steady state axial heat conduction in a symmetrical fin immersed in a constant temperature environment is described by the differential equation:

$$(d^2t/dx^2) = (U_M/k_i t_i)(T_x - T_p) = 0$$

for which the general solution is

$$(T_x - T_p) = \bar{A} \sinh (mx) + \bar{B} \cosh (mx)$$

where:

$$m = \sqrt{U_M/K_i t_i} \quad \text{for space residency}$$

$$m = \sqrt{U_{He}/K_i t_i} \quad \text{for ground purge}$$

where:

$$U_{He} = \frac{K_{He}}{t_{He}} \text{ and } U_M = \frac{K_M}{t_M}$$

T_x = Line temperature at joint, X = L

$\bar{A}$ = Constant of integration

$\bar{B}$ = Constant of integration

When subject to boundary conditions of:

1) $K_L Ct_L \, (dt/dx)_L = (\overline{HA})(T_L - T_i)$ at $x = L_x$

and

2) $(dt/dx) = 0$ at $x = 0$

the heat conduction rate in the line at $x = L_x$ is

$$q_L = \frac{(\overline{HA})(T_P - T_i)}{1 + \left[(\overline{HA})/mK_L Ct_L \coth (mL_x) \right]}$$

For the alternate boundary condition of 2):

$$T_x = T_p \text{ at } x = 0$$

the heat conduction rate at $x = L_x$ is

$$q_L = \frac{(\overline{HA})(T_P - T_i)}{1 + \left[(\overline{HA})/mK_L Ct_L \tanh (mL_x) \right]}$$

Under conditions that $(mL_x) > 2$, both coth (mL_x) and tanh (mL_x) are approximately equal to 1, and the heat conduction rate for both sets of boundary conditions approaches:

$$q_L = (UA)(t_P - t_i)$$

where

$$(UA) = \frac{(\overline{HA})(mK_L Ct_L)}{(\overline{HA}) + (mK_L Ct_L)}$$

The end fitting resistance is made up of two conductances in series; the conductance through the metallic structure and the contact conductance between bolted flanges. The conductance through the metallic structure of the end fitting is given by:

$$(\overline{HA})_F = \frac{K_F}{t_F} A_F$$

where subscript (F) refers to end fitting.

The joint contact conductance $(\overline{HA})_C$ is estimated to be the product of a contact coefficient of 568 W/m^2-^{o}K (100 Btu/hr-ft^2-^{o}F) and the contact area of 0.01 m^2 (0.109 ft^2) or 5.8 W/m-^{o}K (10.9 Btu/hr-^{o}F).

The end fitting effective conductance for the two bolted flanges is then:

$$(\overline{HA}) = \frac{(\overline{HA})_F \, (\overline{HA})_C}{(\overline{HA})_F + (\overline{HA})_C}$$

In these cases, the contact resistance of a bolted joint is negligible relative to the resistance in a stainless steel flange, but it could be roughly equal to the thermal resistance through an aluminum flange. The heat flux values calculated are shown in Tables XV and XVI. Values for the axial length (X = L) of line downstream of the cold fitting interface were 2.6 m (8.5 ft) and 4.7 m (15.5 ft) for the composite and all-metal line respectively.

WEIGHT AND COST ANALYSIS

Weight Analysis. - The weight of each feedline design concept, depicted by the drawings in Appendix A, was calculated and is presented in Table XVII.

As noted in Table XVII, the wet concepts may require a recirculation and purge system, depending upon the selected propulsion system concept. One cryogenic propulsion system, being studied, circulates cold hydrogen boiloff gases through the engine rather than use a closed loop recirculation system. This concept would not require a recirculation system. If required, the recirculation and purge systems would add approximately 5.2 kg (11.3 lb) to the total weight of the wet feedlines (Concepts 1, 2, 3 and 6).

The following conclusions are drawn from the weight analysis:

1. The vacuum jacketed concepts are significantly heavier than the non-vacuum jacketed concepts. The composite vacuum jacketed feedline is 28 percent lighter weight than the all-metal vacuum jacketed line.

2. The composite non-vacuum jacketed concepts are approximately 26% lighter weight than the all-metal non-vacuum jacketed concepts. This percentage is based on total line weight. The composite line is 42% lighter weight if only the bare line weight is considered, i.e., gimbals, flanges and insulation are excluded from the weight calculations.

3. Concept 5, Non-Vacuum Jacketed Composite (Dry-MLI), is the lightest weight concept, weighing 10.3 kg (22.6 lb). Concept 6, Non-Vacuum Jacketed Composite (Wet-Purged MLI) is only 0.5 kg (1.3 lb) heavier, but may require the addition of a recirculation and purge system of approximately 5.2 kg (11.2 lb) .

Cost Analysis. - The producibility costs including labor and material were determined for the six feedline concepts, see Table XVIII. The costs shown are unit costs based on a quantity of twelve feedline assemblies. The costs do not include design, qualification and acceptance testing. The design costs would be somewhat higher for the composite feedlines due to the additional processes required. This added cost, however, would be very minor. The qualification and acceptance requirements for the composite and all-metal configurations should be the same, these costs, however (qualification and acceptance), will be higher for the vacuum jacketed feedlines than the non-vacuum jacketed concepts.

The feedline assembly costs gain significance when the costs and weight are compared for the various design concepts. For example, compare the lightest weight feedline, Concept 5, with the baseline configuration, Concept 3:

	Feedline Weight kg (lb)	Feedline Cost ($)
Concept 5:	10.3 (22.6)	24,400
Concept 3:	14.6 (32.2)	20,500
Delta:	-4.3 (9.6)	+ 3,900

Concept 5 saves 4.3 kg (9.6 lb) of weight for an additional cost of $3,900. The cost for a pound of weight saved by the composite LH_2 feedline is $907/kg ($406/lb). This is a very attractive value for the Space Tug where the cost per kg (lb) may be several thousand dollars.

Weight Reduction Potential for Other Systems. - The use of composite lines provides potential for additional weight savings when all the propulsion systems are considered. An indication of the total weight that may be saved by the use of composite lines is provided by a preliminary evaluation of the other systems.

Propulsion Systems	Estimated All-Metal Weight, kg (lb.)
GH_2 Vent, 7.6 cm (3.0 in.) dia. by 330 cm (130 in.) long.	4.0 (8.9)
GH_2 Zero-G Vent Line, 1.3 cm (0.5 in.) dia. by 330 cm (130 in.) long.	0.7 (1.5)
LH_2 Abort Pressurization, 2.5 cm (1 in.) dia. by 330 cm (130 in.) long.	1.3 (2.9)
LH_2 Fill/Drain/Abort Dump, 15.2 cm (6.0 in.) dia. by 203 cm (80 in.) long.	4.9 (10.9)
GO_2 Vent, 7.6 cm (3.0 in.) dia. by 163 cm (64 in.) long	2.0 (4.4)
LO_2 Fill/Drain/Abort Dump, 12.7 cm (5.0 in.) dia. by 163 cm (64 in.) long.	3.3 (7.3)
LO_2 Abort Pressurization, 2.5 cm (1.0 in.) dia. by 127 cm (50 in.) long	0.5 (1.1)
LO_2 Feedline, 6.4 cm (2.5 in.) dia. by 89 cm (35 in.) long.	0.9 (1.9)
TOTAL:	17.6 (38.9)

The estimated weight for the propulsion systems listed above are based on the use of 0.06 cm (0.025 in.) thick wall stainless steel tubing. Assuming that composite tubing would reduce the weight of all-metal tubing by 42% (as is the case with the LH_2 feedline) an additional 7.4 kg (16.3 lb) potential weight savings exists. Thus, it is concluded that composite tubing should reduce Space Tug propulsion system weight by 11.7 kg (25.9 lb), if LH_2 feedline weight savings are added to the weight savings for the other systems.

System Weight Considerations. - To consider the total system weight resulting from each of the various feedline concepts the propellant losses must also be considered. These losses were defined earlier in the thermal analysis section and are combined with the feedline weight in the system evaluation summary discussed later.

RELIABILITY AND REUSABILITY EVALUATION

A comparison of each of the design concepts from a reliability aspect was made by performing a failure modes and effects analysis (FMEA), see Table XIX. The analysis included determining the failure modes, the potential method of failure detection, the impact of failure on the propulsion system and on the Space Tug mission, the most probable corrective action required and the recommended procedure for failure prevention, for each feedline assembly component.

The negative features applicable to each of the design concepts, as indicated by the FMEA, are summarized in Table XX.

An evaluation of the FMEA and the negative features indicates that Concept 5, Non-Vacuum Jacketed Composite (Dry-MLI), is the superior configuration from a reliability standpoint because: 1) There are fewer components to fail; and 2) the consequence of potential failures result in less impact on the propulsion system and the Space Tug mission.

A relative reliability ranking of the concept configurations in order of desirability is: Configuration 5, 4, 6, 3, 1 and 2. The order of Configurations 1 and 2 would be reversed, if only the vacuum jacket is overwrapped, using a conventional all-metal inner line.

The key considerations for feedline reusability are damage susceptibility, vacuum maintainability, and repairability. The feedline concepts are compared on the basis of these considerations in Table XXI. The composite vacuum jacketed and non-vacuum jacketed concepts are considered less susceptible to damage than the all-metal lines. The non-vacuum jacketed concepts should require less maintenance than the vacuum jacketed feedlines because of the problems associated with vacuum maintainability. The installed repairability of the MLI insulated feedlines should be equal, except the dry configurations have fewer components than the wet configurations. It is, therefore, concluded that Concept 5, Non-Vacuum Jacketed Composite (Dry-MLI), should be the most desirable based on reusability and maintainability aspects.

SYSTEM EVALUATION SUMMARY

A comparison of the six design concepts from a Space Tug System aspect is provided in Table XXII. The total system weight was determined by adding the feedline hardware weight and the weight of LH_2 boiloff losses. The boiloff losses reflect the results of the thermal analysis and the optimum systems operational modes considered. The different operational modes had a significant effect on the dry feedline concepts. The operational mode resulting in the least boiloff is Mode II, for which the prevalve remains open after the initial engine firing.

Considering the combined feedline weight and the weight of propellant lost due to boiloff, feedline Concept 6, consisting of a non-vacuum jacketed, composite feedline with purged multi-layer-insulation and the prevalve located at the engine (wet), offers the least weight system. It is noted, however, that the wet feedline concepts may require a recirculation and purge system which would add 5.1 kg (11.2 lb). If this were the case, then Concept 5, Non-Vacuum Jacketed Composite (MLI-Dry) would provide the least weight system. Concept 5 also shows the highest desirability from reliability, reusability and maintainability aspects. Concept 4 shows the lowest producibility costs. The difference in costs, however, between the non-vacuum jacketed concepts is considered insignificant.

It may be assumed that system considerations, other than feedline boiloff losses, will ultimately determine the issue of a "wet versus dry" feedline configuration, and also the MLI design. Then the key issue is what are the advantages of composite versus all-metal feedlines. When this comparison is made of like designs, the composite feedline saves hardware weight and propellant weight in every case. This comparison is made as follows:

	FEEDLINE DESIGN CONCEPT	FEEDLINE WEIGHT kg (lb)	BOILOFF WEIGHT kg (lb)	TOTAL kg (lb)
1.	Vacuum Jacketed Metal (Wet):	29.4 (64.9)	35.6 (78.6)	65.0 (143.5)
2.	Vacuum Jacketed Composite (Wet):	21.3 (46.9)	35.0 (77.3)	56.3 (124.2)
	Weight Saved by Composite Design:	8.1 (18.0)	0.6 (1.3)	8.7 (19.3)
3.	Non-Vacuum Jacketed Metal (Purged MLI - Wet):	14.6 (32.2)	3.6 (8.0)	18.2 (40.2)
6.	Non-Vacuum Jacketed Composite (Purged MLI - Wet):	10.8 (23.9)	3.0 (6.7)	13.8 (30.6)
	Weight Saved by Composite Design:	3.8 (8.3)	0.6 (1.3)	4.4 (9.6)
4.	Non-Vacuum Jacketed Metal (MLI - Dry):	14.1 (31.0)	6.2 (13.8)	20.3 (44.8)
5.	Non-Vacuum Jacketed Composite (MLI - Dry):	10.3 (22.6)	4.1 (9.1)	14.4 (31.7)
	Weight Saved by Composite Design:	3.8 (8.4)	2.1 (4.7)	5.9 (13.1)

In summary, the composite design for the LH_2 feedline will save from 4.4 kg (9.6 lb) to 8.7 kg (19.3 lb) depending upon the design selected.

CONCLUSIONS, POTENTIAL BENEFITS AND RECOMMENDATIONS

Several conclusions and potential benefits to the Space Tug vehicle are evident from the analyses included herein. A feedline design concept is recommended for further evaluation.

Conclusions. - The conclusions which can be made from the Task I studies and analyses are summarized as follows:

1. The Space Tug design conditions and physical configurations are not yet firmly established. The design parameters and the configuration selected for the development of composite feedlines should provide the flexibility necessary to meet all future requirements.

2. S-Glass or graphite are the two most promising overwrap materials. The final selection should be based on system sensitivity to weight, assumming dificulties are not encountered in the application of the overwrap. The final selection of the overwrap material should be delayed until after the overwrap of the subscale test specimens is complete.

3. The addition of radiation shields in the vacuum annulus of the vacuum jacketed lines significantly reduces the effective emissivity. Eight radiation shields will eliminate 98.1% of the heat flux due to radiation. The solid conduction component of heat transfer through the radiation shields is less than 0.6% of the total heat flux for the vacuum jacketed feedline.

4. Propellant boil-off losses for the vacuum jacketed feedlines are significantly reduced by thermally optimized standoffs and end closures.

5. The development of dissimilar metal joints shows promising results. When fully developed, dissimilar metal joining techniques will provide the capability of using lightweight aluminum flanges with lightweight composite tubing.

6. All metal or composite feedlines which are exposed to solar radiation and not covered with insulation should be thermally coated to reduce line surface equilibrium temperature.

7. Feedline wall thickness will be dictated based upon handling and/or manufacturing limitations. System design pressures and anticipated external loads will not add to these wall thicknesses.

8. The vacuum jacketed feedline configurations are more thermally efficient for ground operations and are less thermally efficient during the space mission than the feedlines insulated with MLI. Because the LH_2 tank is topped until launch the boil-off losses which occur prior to launch are not significant to the mission.

9. The feedline operational mode may be influenced by system considerations other than propellant boil-off. However, propellant boil-off losses are reduced by the use of composite tubing for all design configurations compared with an all-metal feedline.

10. The vacuum jacketed feedline weight is approximately double the weight of the non-vacuum jacketed concepts.

11. The composite design with dissimilar metal flanges for the LH_2 feedline will save from 4.4 kg (9.6 lb.) to 8.7 kg (19.3 lb.) depending upon the design concept selected. An additional 7.4 kg (16.3 lb.) can be saved by the use of composite lines for the other Space Tug propulsion systems.

12. The design Concept 5 - Non-Vacuum Jacketed Composite (Dry-MLI), provides the most desirable configuration from reliability, reusability and maintainability aspects because: 1) composite tubing provides superior damage resistance; 2) there are fewer components to fail; and 3) the consequence of potential failures result in less impact on the propulsion system and on the Space Tug mission than the other design concepts.

Potential Benefits. - The use of composite tubing in the Space Tug propulsion system will improve thermal efficiency and reduce overall system weight at a very small increase in cost. It is estimated that the Space Tug propulsion system weight can be reduced by 11.7 kg (25.9 lb.) which is a 36% weight reduction. The additional cost of composite tubing over all-metal tubing is minor for space vehicles where minimum weight is extremely important. The cost per kg (lb.) for the Space Tug has been estimated in the thousands of dollars. Analysis shows that the cost per kg (lb.) of weight saved by the use of composite tubing in the Space Tug propulsion system is $907/kg ($406/lb.). In addition, the thermal analysis shows that composite tubing will reduce the quantity of non-usable LH_2, due to boil-off losses, by 0.6 kg (1.3 lb.) to 2.1 kg (4.7 lb.) depending upon the system configuration.

Composite tubing should also provide a more reliable and maintenance free feedline system than the all-metal design because of the superior damage resistant characteristics of composites.

Recommendations. - It is recommended that feedline design, Concept 5, be selected for further evaluation by fabricating and testing four LH_2 feedline assemblies, consisting of three composite and one all-metal configurations. This will provide a direct comparison of fabrication, cost, and performance characteristics of the composite and all-metal feedlines.

TABLE I.- CRYOGENIC FEEDLINE DESIGN CONDITIONS

CONDITION	LH_2 LINE
Operating Pressure	20.7 N/cm^2 (30 psia)
Proof Pressure	41.4 N/cm^2 (60 psia)
Burst Pressure	62.1 N/cm^2 (90 psia)
Diameter	10.2 cm (4.0 in.)
Flow Rate	2.72 kg/sec (6.0 lb/sec)

TABLE II.- SHUTTLE PAYLOAD LOAD FACTORS

CONDITION	AXIS		
	X(g)	Y(g)	Z(g)
Launch	1.4 ± 1.6	± 1.0	± 1.0
High-Q Booster Thrust	1.9 ± 0.3	± 1.0	0.8 ± 0.2
End Boost (Booster Thrust)[a]	3 ± 0.3	± 0.6	± 0.6
End Burn (Orbiter Thrust)	3 ± 0.3	± 0.5	± 0.5
Orbiter Entry	- 0.5	± 1.0	$- 3.0 \pm 1.0$
Orbiter Flyback	- 0.5	± 1.0	± 1.0 $- 2.5$ ± 1.0
Landing	- 1.3	± 0.5	$- 2.7 \pm 0.5$

[a] Excludes booster-orbiter separation loads

TABLE III.- SHUTTLE CARGO BAY INTERNAL WALL TEMPERATURE ENVIRONMENTS

CONDITION	TEMPERATURE K (°F)	
	Minimum	Maximum
Prelaunch	200 (-100)	322 (120)
Launch	200 (-100)	367 (200)
On Orbit (Door Closed)	200 (-100)	367 (200)
Entry and Post Landing	200 (-100)	367 (200)

TABLE IV.- ORBITER PAYLOAD COMPARTMENT INTERNAL ACOUSTIC DESIGN CRITERIA SOUND PRESSURE LEVEL (dB) - 10^{-5} N/m^2

1/3 Octave Center Band Frequency (H_z)	Liftoff	Boundary Layer
5	124	124.5
6.3	127	125.0
8	128	126.0
10	129	126.5
12.5	131	127.0
16	132	128.0
20	134	128.5
25	135	129.0
31.5	137	130.0
40	138	130.5
50	139	131.0
63	140	132.0
80	141	132.5
100	143	133.0
125	144	134.0
160	145	134.5
200	145	135.5
250	145	136.0
315	144	136.5
400	143	137.0
500	142	137.5
630	141	138.0
800	140	138.5
1K	139	138.0
1.25K	138	137.0
1.6K	137	136.5
2K	135	135.5
2.5K	134	134.5
3.15K	133	134.0
4K	132	133.0
5K	131	132.0
6.3K	130	131.0
8K	129	130.0
10K	128	129.0
	OASPL155 dB	OASPL149 dB

TABLE V.- SYNCHRONOUS EQUATORIAL ORBIT-RETRIEVAL MISSION

EVENT	SEQ. NO.	TIME (HR)		TUG MAIN ENGINE				ACS ΔV (FPS)
				FULL THRUST ΔV (FPS)			BURN TIME (2)(MIN)	
		Δ	TOTAL	IDEAL	GRAV. LOSS (1)	TOTAL		
Shuttle Liftoff			0					
Shuttle Burnout	1		0.14					
Coast to 100 n.mi.	1-2a	0.73						
Shuttle 100x160 n.mi. Insertion	2a		0.87					
Coast to 160 n.mi.	2a-2	0.76						
Circularize at 160 n.mi.	2		1.63					
Tug Deploy & Coast	2-3	13.11						10
Phasing Orbit Insertion	3		14.74	1,824	16	1,840	4.1	
Coast to TOI	3-4	1.92						
Transfer Orbit Insert.	4		16.66	6,222	33	6,255	9.9	
Coast to 19,323 n.mi.	4-5	5.27						50(3)
Mission Orbit Insert.	5		21.93	5,849	0	5,849	6.1	
Retrieve P/L & Coast	5-6	11.15						115(4)
Transfer Orbit Insert.	6		33.08	5,844	0	5,844	5.1	
Coast to POI	6-7	5.27						50(3)
Phasing Orbit Insert.	7		38.35	3,720	10	3,730	2.3	
Coast	7-8	3.02						
Circularize for Rend.	8		41.37	4,309	7	4,316	2.0	
Shuttle Rend. & Coast	8-9	4.53						
Shuttle Deorbit	9		45.90					
Touchdown	10		46.60					

(1) Based on 15,000 lb thrust engine.
(2) Approx. burn time - 15,000 lb main engine.
(3) Midcourse correction.
(4) Rendezvous & dock with P/L.

Reference: Space Tug Systems Study NAS8-29676. DATA DUMP General Dynamics/ Convair Aerospace Division, 18 September 1973

TABLE VI.- CANDIDATE COMPOSITE PROPERTIES

Fiber With 58-68R Resin System	S-Glass, Ref. 6	Graphite, Ref. 6	Boron, Ref. 6	Kevlar 49 DP-01 Ref. 7
Thickness/Layer cm (in.)	0.020 (0.008)	0.010 (0.004)	0.013 (0.005)	0.020 (0.008)
Minimum Wrap Thickness cm (in.) and Layup Configuration	0.051 (0.020) H-½L-H	0.025 (0.010) H-½L-H	0.033 (0.013) H-½L-H	0.051 (0.020) H-½L-H
Density kg/cm^3 (lb/in.^{3})	0.002 (0.085)	0.0015 (0.055)	0.0019 (0.072)	0.0014 (0.052)
Cost of Prepreg, $/kg ($/lb.)	29 (13)	552 (250)	552 (250)	77 (35)
% Resin Content	25	45	50	25
Modulus of Elasticity, E_{OL} N/cm^2 (psi)	3.8 x 10^6 (5.5 x 10^6)	25.5 x 10^6 (37.0 x 10^6)	21.0 x 10^6 (30.0 x 10^6)	7.6 x 10^6 (11.x 10^6)
Modulus of Elasticity, E_{OH} N/cm^2 (psi)	1.1 x 10^6 (1.6 x 10^6)	2.1 x 10^6 (3.0 x 10^6)	2.1 x 10^6) (3.0 x 10^6)	0.6 x 10^6 (0.8 x 10^6)
Thermal Coefficient of Expansion, α_{OL} cm/cm/K (in/in/^{o}F	0.8 x 10^{-6} (1.4 x 10^{-6})	1.4 x 10^{-6} (2.5 x 10^{-6})	1.4 x 10^{-6} (2.5 x 10^{-6})	-1.2 x 10^{-6} (-2.2 x 10^{-6})
Thermal Coefficient of Expansion, α_{OH} cm/cm/K (in/in/^{o}F)	3.9 x 10^{-6} (7.0 x 10^{-6})	3.9 x 10^{-6} (7.0 x 10^{-6})	4.4 x 10^{-6} (7.9 x 10^{-6})	17.8 x 10^{-6} (32. x 10^{-6})
Allowable Compression Stress, N/cm^2 (psi)	-65,500 (-95,000)	-68,900 (-100,000)	-124,100 (-180,000)	-27,600 (-40,000)
Allowable Tension Stress, N/cm^2 (psi)	212,300 (308,000)	68,900 (100,000)	124,000 (180,000)	137,900 (200,000)

Subscripts: OL - Longitudinal Overwrap
OH - Hoop Overwrap

Note: Values for modulus of elasticity and thermal coefficient of expansion are for axial direction with respect to the tube centerline, ie., transverse to the fibers for the hoop overwrap and parallel to the fibers for the longitudinal overwrap

TABLE VII.- SUMMARY-EVALUATION OF HIGH MODULUS COMPOSITES

Overwrap Material	Thermal Stresses	Thermal Conductivity at 21 K (-423°F) W/m - K (Btu/ft-hr-°F)	Fatigue Strength	LH_2 Feed-line Composite Wt., kg (lbs)	LH_2 Feed-line Overwrap Mat'l Cost ($)	Fabrication
S-Glass	Acceptable Margin	0.17 (0.1)	Best	2.2 (4.8)	62	Most Development Experience
Kevlar 49 DT-01	Kevlar DT-01 Provides low Margin	0.35 (0.2)	Acceptable	1.3 (2.9)	102	TBD
Graphite	High Margin	0.52 (0.3)	Acceptable	1.4 (3.1)	775	TBD
Boron	High Margin	1.38 (0.8)	Acceptable	1.8 (4.0)	1000	TBD

TABLE VIII.- VACUUM JACKETED LINE SURFACE EMISSIVITIES

Material	Temp.K (^{o}F)	Surface Finish, μ- cm. (μ- in.)	ϵ	Reference
SS 17-7 PH	83 (-310)	5 (2)	0.022	1
	83 (-310)	38 (15)	0.044	1
SS 321	83 (-310)	Bright	0.044	1
	83 (-310)	5 (2)	0.036	1
	83 (-310)	15 (6)	0.111	1
	83 (-310)	15 (6)	0.155	1
		Oxidized in air at reduced heat for 30 minutes		
SS 316	83 (-310)	5 (2)	0.027	1
	83 (-310)	38 (15)	0.045	1
SS 301	300 (80)	Cleaned	0.160	Measured *
Inconel B	89 (-299)		0.180	2
	139 (-209)		0.205	2
	364 (195)		0.230	2
Inconel X	98 (-284)		0.200	2
	151 (-90)		0.240	2
	372 (210)		0.230	2
Inconel 718	300 (80)		0.230	Measured *

Reference 1. WADC TR-56-222, Pt II, Pg 1-184, 1957
Betz, H. T., Olson, O. H., Shurin, B. D., Morris, J. C.

Reference 2. WADC TR-54-22, Pg 1-94, 1954
Walker G. B.

* Measured by Martin Marietta Corp.

TABLE IX.- SUMMARY, DISSIMILAR METAL JOINT TEST RESULTS

		INERTIA WELDING	COEXTRUSION	EXPLOSIVE WELDING	SWAGED
1. Cost		Low cost after development, all sizes.	Higher cost after development, small size only.	Moderate cost after development, all sizes.	Low cost after development, all sizes.
2. Availability		Most available, many potential suppliers.	Few suppliers	Few suppliers	Single supplier
3. Test Item Consistency		Most consistent test evaluation results. Good process control.	Unknown - only 2 specimens evaluated.	Consistency involves craftsmanship and explosive characteristics, and both are variable.	Fair consistency in this evaluation; should be very consistent with more development.
4. Thermal Tolerance		Minimal effect, 373K to 78K (+212°F to -320 °F) cycles.	Minimal effect, 373K to 78K (+212°F to -320°F) cycles (one joint only.) Survives solutionizing and quench during manufacture.	Minimal effect, 373K to 78K (+212°F to -320°F) cycles.	Minimal effect, 373K to 78K (+212°F to -320°F) cycles.
5. Joint Length		May be short due to butt joint.	Scarf joint requires more length than butt joint.	Scarf joint requires more length than butt joint.	Multiple serrations require more length than other types.
6. Weight		May be same thickness as basic tube.	May be same thickness as basic tube.	May be same thickness as basic tube.	Must be heaviest due to necessary thicker section in serrated area.
7. Loads	A. Pressure Cycle	Near 100% of parent metal tolerance.	Not tested.	20% of parent metal tolerance.	40% of parent metal tolerance.
	B. Bending C. Torsion D. Vibration	These were not tested but will need evaluation prior to firm commitment to use			

TABLE IX.- SUMMARY, DISSIMILAR METAL JOINT TEST RESULTS (CONTINUED)

	INERTIA WELDING	COEXTRUSION	EXPLOSIVE WELDING	SWAGED
8. Leakage A. Vacuum	No helium leak at 1×10^{-5} torr internal (15 of 15 specimens)	No helium leak at 1×10^{-5} torr internal (2 of 2) specimens)	No helium leak at 1×10^{-5} torr internal (10 of 15 specimens)	No helium leak at 1×10^{-5} torr internal (10 of 15 specimens)
B. Pressure	Less than 3×10^{-10} scc/sec GHe at operating pressure (15 of 15 specimens)	Less than 3×10^{-10} scc/sec GHe at operating pressure (2 of 2 specimens)	Less than 3×10^{-10} scc/sec GHe at operating pressure (7 of 13 specimens)	All units leaked 1×10^{-5} scc/sec GHe minimum (off scale on MSLD)
9. Repairability	Not repairable.	Not repairable.	Not repairable.	Not repairable.
10. Replaceability	Replaceable by cutting out old joint and welding in new if adjacent heat treat requirements are not violated.	Replaceable by cutting out old joint and welding in new if adjacent heat treat requirements are not violated.	Replaceable by cutting out old joint and welding in new if adjacent heat treat requirements are not violated.	Replaceable by cutting out old joint and welding in new if adjacent heat treat requirements are not violated. Possibly swaged in field.
11. Corrosion Resistance (Without protection)	Poor in $NaCl/H_2O$	Not tested	Fair resistance to $NaCl/H_2O$ solution	Process allows use of anodized aluminum interface. Good resistance. Difficult to inspect.
12. Failure Mode	11 of 11 6.4cm (2.5 in.) specimens separated into two pieces when hydroburst.	2 of 2 6.4cm (2.5 in.) specimens separated into two pieces when hydroburst.	7 of 8 6.4cm (2.5 in.) specimens failed axially in and near the bond; 1 of 8 failed in hoop mode: when hydroburst.	8 of 9 6.4cm (2.5 in.) specimens failed by axial slip and leakage; 1 of 9 failed in axial stainless shear: when hydroburst.

TABLE X.- TYPICAL SURFACES EXPOSED TO SOLAR RADIATION

CONFIGURATION	TEMPERATURE K (°F) $\alpha_s/\epsilon = 1$	TEMPERATURE K (°F) $\alpha_s/\epsilon = 0.24/0.88$
Insulated Flat Plate 	394 (250)	283 (50)
Semi-cylinder 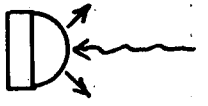	350 (170)	255 (0)
Uninsulated Flat Plate 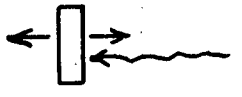	329 (133)	239 (-30)
Bare Cylinder 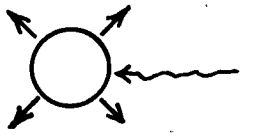	294 (70)	214 (-75)

TABLE XI.- PREDICTED FEEDLINE EQUILIBRIUM TEMPERATURES WHEN EXPOSED TO SOLAR RADIATION

FEEDLINE CONFIGURATION	$\frac{\alpha_s}{\epsilon}$	TEMPERATURE K (^{o}F)
Vacuum Jacketed Metal	2 to 3	418 to 463 (293 to 373)
Vacuum Jacketed Metal (with thermal coating)	0.27	255 (0)
Vacuum Jacketed Composite	1	350 (170)
Vacuum Jacketed Composite (with thermal coating)	0.27	255 (0)

TABLE XII.- RECOMMENDED THERMAL COATINGS

COATING	α_s/ϵ
Thermatrol (TiO_2 in 92-007 silicone)	0.18/0.85
Martin Marietta STP 72712 (ZnO in silicone)	0.25/0.85
GE S-13G	0.24/0.88
The GE S-13G is recommended because it is stable to long exposure to solar radiation and can be applied to organic surfaces.	

TABLE XIII.- SPACE TUG CONFIGURATION DRIVERS AND EFFECTS

VEHICLE CONFIGURATION DRIVERS	FEEDLINE CHARACTERISTICS												EVALUATION PLAN	
	Line Size	Mat'l Gage	Mat'l Selection	Flexible Joints	Supports	Wet	Dry	Tees & Elbows	Curved Lines	Purged MLI	MLI	Vacuum Jacketed	ANALYSIS	TEST
1. Feedline Design Conditions (LH_2)	X	X	X	X	X	X	X	X	X	X	X	X	X	X
2. LH_2 Tank Insulation :														
a. Purged MLI						X				X		X	X	
b. Non Purged MLI							X				X		X	X
c. Vacuum Jacket						X				X		X	X	
d. SOFI							X				X			
e. Uninsulated							X				X			
3. Propellant Dump	X	X	X	X	X	X	X	X	X	X	X	X		
4. Fill and Drain	X	X	X	X	X	X	X	X	X	X	X	X		
5. Packaging	X			X	X	X	X	X	X	X	X	X	X	
6. Storable Tug Considerations:														
a. Pressure & Flowrate	X	X	X											
b. Loads (Acoustic, Dynamic)		X	X	X	X									
c. Packaging				X	X			X	X				X	X
d. Propellant Compatibility			X											X

TABLE XIV. - WET SYSTEMS - PREVALVE AT LH_2 ENGINE INTERFACE - LH_2 BOILOFF, Kg (LBS)

WET SYSTEMS - PREVALVE AT LH_2 ENGINE INTERFACE - LH_2 BOILOFF, Kg (lbs.)

DESIGN CONCEPT	CONFIGURATION	GROUND OPERATIONS	FLIGHT OPERATIONS			
		MODE I (2 HRS.)	ENGINE HEAT TRANSFER	SHUTTLE STORAGE	TUG FLIGHT	TOTAL
1. Vacuum Jacketed - Metal Wet	Without Radiation Shields	2.8(6.1)	1.4(3.1)	34.3(75.6)	30.5(67.3)	66.2(146.0)
	With 8 Radiation Shields	1.5(3.4)	1.4(3.1)	14.2(31.2)	20.1(44.3)	35.7(78.6)
2. Vacuum Jacketed - Composite Wet	Without Radiation Shields	5.2(11.4)	0.8(1.8)	74.8(164.9)	51.4(113.3)	127.0(280.0)
	With 8 Radiation Shields	1.5(3.4)	0.8(1.8)	14.2(31.2)	20.1(44.3)	35.1(77.3)
3. Non-Vacuum Jacketed - Metal, MLI, Purged Wet	--	15.8(34.9)	1.4(3.1)	0.8(1.7)	1.4(3.2)	3.6(8.0)
6. Non-Vacuum Jacketed - Composite, MLI, Purged, Wet	--	15.8(34.9)	0.8(1.8)	0.8(1.7)	1.4(3.2)	3.0(6.7)

DRY SYSTEMS - PREVALVE AT LH_2 TANK - LIQUID HYDROGEN BOILOFF, Kg (lbs)

DESIGN CONCEPT	GROUND OPERATIONS	FLIGHT OPERATIONS				
	MODE I (2 HRS.)	MODE II - PREVALVE REMAINS OPEN AFTER INITIAL FIRING				
		ONE LINE CHILLDOWN	SHUTTLE STORAGE	TUG FLIGHT	ENGINE HEAT TRANSFER	TOTAL
4. Non-Vacuum Jacketed - Metal, MLI, Dry	0.2(0.4)	3.8(8.3)	.05(0.1)	1.5(3.3)	1.0(2.1)	6.2 (13.8)
5. Non-Vacuum Jacketed - Composite, MLI, Dry	0.1(0.2)	2.1(4.6)	.05(0.1)	1.5(3.2)	0.5(1.2)	4.1(9.1)

DRY SYSTEMS - PREVALVE AT LH_2 TANK - LIQUID HYDROGEN BOILOFF, Kg (lbs)

DESIGN CONCEPT	FLIGHT OPERATIONS				
	MODE III - PREVALVE CLOSED AFTER EACH FIRING AND LINE DUMPED				
	6 LINE CHILLDOWNS	SHUTTLE STORAGE	TUG FLIGHT	6 LINE DUMPS	TOTAL
4. Non-Vacuum Jacketed - Metal, MLI, Dry	22.5(49.5)	--	0.1(0.2)	19.3(42.6)	41.9(92.3)
5. Non-Vacuum Jacketed - Composite, MLI, Dry	12.6(27.8)	--	.05(0.1)	19.3(42.6)	31.9(70.5)

TABLE XV.- THERMAL PERFORMANCE OF FEEDLINE CONCEPTS (TOTAL FEEDLINE ASSEMBLY)

FEEDLINE DESIGN CONCEPT	CONFIGURATION	FEEDLINE HEAT FLUX - WATTS (Btu/hr)			
		ONE-G ENVIRONMENT 300 K (80°F)	SPACE ENVIRONMENT		
			256 K (0°F)	322 K (120°F)	367 K (200°F)
1. Vacuum Jacketed Metal Wet	Without Radiation Shields	173 (590)	120 (410)	205 (700)	292 (995)
	With 8 Radiation Shields	95 (325)	79 (270)	103 (350)	120 (410)
2. Vacuum Jacketed Composite Wet	Without Radiation Shields	325 (1110)	202 (690)	410 (1400)	636 (2170)
	With 8 Radiation Shields	95 (325)	79 (270)	103 (350)	120 (410)
3. Non-Vacuum Jacketed Metal Purged MLI Wet		994 (3390)	5.9 (20.0)	6.1 (20.8)	6.4 (21.8)
4. Non-Vacuum Jacketed Metal MLI Dry	CRES End Fitting	12.0 (41.1)	0.19 (0.64)	0.22 (0.76)	0.25 (0.87)
	Al End Fitting	12.8 (43.6)	0.19 (0.64)	0.22 (0.76)	0.25 (0.87)
5. Non-Vacuum Jacketed Composite MLI Dry	CRES End Fitting	6.8 (23.3)	0.11 (0.37)	0.13 (0.43)	0.15 (0.50)
	Al End Fitting	7.0 (24.0)	0.11 (0.37)	0.13 (0.43)	0.15 (0.50)
6. Non-Vacuum Jacketed Composite Purged MLI Wet		994 (3390)	5.9 (20.0)	6.1 (20.8)	6.4 (21.8)

TABLE XVI.- THERMAL PERFORMANCE OF FEEDLINE CONCEPTS (PER UNIT AREA)

FEEDLINE DESIGN CONCEPT	CONFIGURATION	FEEDLINE HEAT FLUX - WATTS/M^2 (Btu/hr-Ft^2)			
		ONE-G ENVIRONMENT 300 K (80°F)	SPACE ENVIRONMENT		
			256 K (0°F)	322 K (120°F)	367 K (200°F)
1. Vacuum Jacketed Metal Wet	Without Radiation Shields	77.0 (24.4)	53.3 (16.9)	91.2 (28.9)	129.7 (41.1)
	With 8 Radiation Shields	42.3 (13.4)	35.3 (11.2)	45.7 (14.5)	53.3 (16.9)
2. Vacuum Jacketed Composite Wet	Without Radiation Shields	144.8 (45.9)	89.9 (28.5)	182.7 (57.9)	283.0 (89.7)
	With 8 Radiation Shields	42.3 (13.4)	35.3 (11.2)	45.7 (14.5)	53.3 (16.9)
3. Non-Vacuum Jacketed Metal Purged MLI Wet		441.7 (140)	2.62 (0.83)	2.71 (0.86)	2.84 (0.90)
4. Non-Vacuum Jacketed Metal MLI Dry	CRES End Fitting	5.4 (1.7)	0.082 (0.026)	0.098 (0.031)	0.114 (0.036)
	Al End Fitting	5.7 (1.8)	0.082 (0.026)	0.098 (0.031)	0.114 (0.036)
5. Non-Vacuum Jacketed Composite MLI Dry	CRES End Fitting	3.0 (0.96)	0.047 (0.015)	0.057 (.018)	0.065 (0.021)
	Al End Fitting	3.2 (1.0)	0.047 (0.015)	0.057 (0.018)	0.065 (0.021)
6. Non-Vacuum Jacketed Composite Purged MLI Wet		441.7 (140)	2.62 (0.83)	2.71 (0.86)	2.84 (0.90)

TABLE XVII.- WEIGHT STATMENT, LH_2 FEEDLINE

CONCEPT 1		CONCEPT 2		CONCEPT 3		CONCEPT 4		CONCEPT 5		CONCEPT 6	
ITEM	WEIGHT kg (lb.)	ITEM	WEIGHT kg (lb.)	ITEM	WEIGHT kg (lb.)	ITEM	WEIGHT kg (lb.)	ITEM	WEIGHT kg (lb.)	ITEM	WEIGHT kg (lb.)
Inner Line	8.3(18.5)	Inner Line	4.8(10.7)	Metal Line	7.3(16.1)	Metal Line	7.3(16.1)	Metal Liner	1.9(4.1)	Metal Liner	1.9(4.1)
Vacuum Jacket	11.4(25.1)	Wrap, Inner Line	2.2(4.8)	2 Layers Mylar 0.013cm (0.005 in.)	0.7(1.4)	1 Layer Mylar 0.013cm (0.005 in.)	0.3(0.7)	Wrap, Metal Liner	2.3(4.9)	Wrap, Metal Liner	2.3(4.9)
Gimbals	4.7(10.5)	Vacuum Jacket Liner	4.2(9.3)	30 Layers Mylar 0.00064cm (0.00025 in.)	0.6(0.3)	30 Layers Mylar 0.00064cm (0.00025 in.)	0.6(1.3)	1 Layer Mylar 0.013cm (0.005 in.)	0.3(0.7)	2 Layers Mylar 0.013cm (0.005 in.)	0.7(1.4)
		Flanges	2.2(4.8)								
Standoffs	0.5(1.1)	Wrap, Vacuum Jacket	2.2(4.8)	Purge Bag	0.1(0.3)	Velcro	0.1(0.3)	30 Layers Mylar 0.00064cm (0.00025 in.)	0.6(1.3)	30 Layers Mylar 0.00064cm (0.00025 in.)	0.6(1.3)
End Closures	0.7(1.5)	Gimbals	4.8(10.5)	Nylon Attachments	0.05(0.1)	Nylon Attachments	0.05(0.1)	Velcro	0.1(0.3)	Purge Bag	0.1(0.3)
Vacuum Valves	0.6(1.4)	Standoffs	0.5(1.1)	Velcro	0.1(0.3)	Gimbals	2.7(6.0)	Nylon Attachments	0.05(0.1)	Nylon Attachments	0.05(0.1)
Burst Discs	0.7(1.5)	End Closures	0.7(1.5)	Gimbals	2.7(6.0)	Flanges	2.9(6.5)	Gimbals	2.7(6.0)	Velcro	0.1(0.3)
Vacuum Gages	0.3(0.7)	Vacuum Valves	0.6(1.4)	Insulation End Closure	0.1(0.3)	Purge Bag For Protection Only	0.1(0.3)	Purge Bag	0.1(0.3)	Gimbals	2.7(6.0)
Flanges	2.9(6.5)	Burst Discs	0.7(1.5)	Purge Tubing	0.05(0.1)			Flanges	2.2(4.8)	End Closures	0.1(0.3)
8 Layers	0.2(0.4)	Vacuum Gages	0.3(0.7)	Flange	2.9(6.5)					Purge Tubing	0.1(0.1)
Nylon Ties	0.05(0.1)	8 Layers MLI	0.2(0.4)							Flanges	2.2(4.8)
		Nylon Ties	0.05(0.1)								
Total	30.5(67.3)	Total	23.4(51.6)	Total	14.6(32.2)	Total	14.1(31.0)	Total	10.3(22.6)	Total	10.8(23.9)

Concept 1 - Vacuum Jacketed Metal (Wet)
Concept 2 - Vacuum Jacketed Composite (Wet)
Concept 3 - Non Vacuum Jacketed Metal (Wet-Purged MLI)
Concept 4 - Non Vacuum Jacketed Metal (Dry-MLI)
Concept 5 - Non Vacuum Jacketed Composite (Dry-MLI)
Concept 6 - Non Vacuum Jacketed Composite (Wet-Purged MLI)

Note: Concepts 1, 2, 3 and 6 (Wet concepts) may require a recirculation and a purge system. It is estimated that this would add approximately 5.2 kg (11.2 lbs) to each of these concepts.

RECIRCULATION SYSTEM

6.1 m (20 ft.) of 1.3 cm (0.5 in.) Tubing:	1.0 kg (2.2 lb.)
3 Tubing Supports	0.7 kg (1.5 lb.)
Pump	1.4 kg (3.0 lb.)
Total:	3.1 kg (6.7 lb.)

Purge System

Valve:	0.5 kg (1.0 lb.)
Regulator	0.9 kg (2.0 lb.)
3 m (10 ft.) of 0.6 cm (0.25 in.) Tubing	0.2 kg (0.5 lb.)
Tubing Supports	0.5 kg (1.0 lb.)
Total:	2.1 kg (4.5 lb.)

TABLE XVIII.- WEIGHT AND COST COMPARISON OF LH_2 FEEDLINE CONCEPTS

FEEDLINE CONCEPTS	WEIGHT kg (lbs)	COST ($)
1. Vacuum Jacketed Metal (Wet)	29.4 (64.9)	37,900
2. Vacuum Jacketed Composite (Wet)	21.3 (46.9)	45,400
3. Non-Vacuum Jacketed Metal (Wet - Purged MLI)	14.6 (32.2)	20,500
4. Non-Vacuum Jacketed Metal (Dry - MLI)	14.1 (31.0)	19,900
5. Non-Vacuum Jacketed Composite (Dry - MLI)	10.3 (22.6)	24,400
6. Non-Vacuum Jacketed Composite (Wet - Purged MLI)	10.8 (23.9)	25,000

TABLE XIX.- FAILURE MODES AND EFFECTS ANALYSIS

CONFIGURATION	FAILURE MODE	FAILURE DETECTION	IMPACT ON SYSTEM	IMPACT ON MISSION		CORRECTIVE ACTION	FAILURE PREVENTION
				PREFLIGHT	INFLIGHT		
1. Vacuum Jacketed Metal (Wet)							
a) Inner Line	Leak	Vacuum Gage Readout, Blow Burst Disc	Loss of Propellant. Hazardous Gases in Compartment	Flight Abort	Potential Loss of Mission	Replace Line	Design with Margin, Qualification and Acceptance Test
b) Vacuum Jacket	Vacuum Loss - Inner Line Leak - Vacuum Jacket Leak - Outgassing Condensibles in Vacuum Annulus. External Damage.	Vacuum Gage Readout, Blow Burst Disc, Inspection	Degradation in Thermal Performance	Potential Abort	Minor	Replace Line if Due to Leak. CO_2 Purge and Evacuate if Due to Condensibles. Vacuum Bakeout if Due to Outgassing	Same as Above to Prevent Leak in Inner Line and Vacuum Jacket. Contamination Control and Vacuum Bakeout to Prevent Outgassing and Condensibles. To Prevent Damage Provide Thicker Gage Jacket or Provide Overwrap Protection
c) Vacuum Valve	Leak	Vacuum Gage Readout	Loss of Vacuum, Condensibles in Annulus, Degradation in Thermal Performance.	Potential Abort	Minor	Repair Leak (Line Replacement may be Required) CO_2 Purge and Re-evacuate to Remove Condensibles.	Acceptance Test, Weld Valve Into Vacuum Jacket
d) Vacuum Gage	Leak	Same as (1c)	Same as (1c)	Potential Abort	Minor	Same as (1c)	Same as (1c)
e) Burst Disc	Leak, Failure to Rupture	Same as (1c)	Same as (1c) if Leak. Inner Line Implosion if Failure to Rupture Causing Flow Restriction. Potential Rupture of Vacuum Jacket.	Potential Abort	Potential Loss of Mission	Replace Burst Disc	Qualification and Acceptance Test. Design Inner Liner to Carry Pressure in Excess of That Required to Rupture Burst Disc. Design Vacuum Jacket to Carry Internal Pressure in Excess of That Required to Rupture Burst Disc
f) Flange	Leak	System Leak Test, Leak Detection Ports	Loss of Propellant. Hazardous Condition in Compartment. Could be catastrophic.	Potential Abort	Minor if Leak Not Severe	Replace Seal, Remove and Repair Flange if Required	Same as (1a)

TABLE XIX.- FAILURE MODES AND EFFECTS ANALYSIS (CONTINUED)

CONFIGURATION	FAILURE MODE	FAILURE DETECTION	IMPACT ON SYSTEM	IMPACT ON MISSION		CORRECTIVE ACTION	FAILURE PREVENTION
				PREFLIGHT	INFLIGHT		
2. Vacuum Jacketed Composite (Wet)							
a) Inner Line	Leak	Same as (1a)	Same as (1a)	Flight Abort	Potential Loss of Mission	Replace Line	Same as (1a)
b) Vacuum Jacket	Same as (1b)	Same as (1b)	Same as (1b)	Potential Abort	Minor	Same as (1b)	Same as (1b), Except for Damage. Composite Overwrap Provides Damage Protection on This Configuration.
c) Vacuum Valve	Same as (1c)	Same as (1c)	Same as (1c)	Same (1c)	Same (1c)	Same as (1c)	Same as (1c)
d) Vacuum Gage	Same as (1d)	Same as (1d)	Same as (1d)	Same (1d)	Same (1d)	Same as (1d)	Same as (1d)
e) Burst Disc	Same as (1e)	Same as (1e)	Same as (1e)	Same (1e)	Same (1e)	Same as (1e)	Same as (1e)
f) Flange	Same as (1f)	Same as (1f)	Same as (1f)	Same (1f)	Same (1f)	Same as (1f)	Same as (1f)
3. Nonvacuum Jacketed Metal (Wet-Purged MLI)							
a) Metal Line	Leak. External Damage.	Pressure Loss in Tank. System Leak Test. Inspection.	Loss of Propellant. Hazardous Gas Collected in MLI and Purged with Helium Gas to Safe Area.	Potential Abort	Hazardous Gas May Collect in The MLI	Repair in Place May be Possible. Line Replacement is Most Likely.	Design With Margin. Qualification and Acceptance Test. Careful Procedures to Prevent Damage.
b) MLI	External Damage, Tear or Rip. Iceing in the MLI. Damage MLI by Purge Over Pressure or Restrictive Gas-Expulsion During Launch.	Inspection. Most Probable Cause is Loss of Purge or Contamination in the MLI.	Minor Degradation in Thermal Performance. Significant Degradation in Thermal Performance Resulting in Loss of Propellant. Formation of LO_2 Around LH_2 Feedline.	Minor. Potential Hazard from Liquid Air.	Minor. N/A	Repair in Place is Most Feasible.	Careful Handling. Strong Protective Purge Bag. Contamination Control Procedures and GHe_2 Purge. Should Purge System Upon Re-entry into Atmosphere to Keep Dry. Control Purge Pressure & Gas Expulsion.
c) MLI Purge System	Loss of Purge. Purge Overpressure.	Same as (3b)	Same as (3b)	Same (3b)	N/A	Same as (3b)	Hardware Design and Procedure Control
d) Flange	Same as (1f)	Same as (1f)	Same as (1f)	Same (1f)	Same (1f)	Same as (1f)	Same as (1f)

TABLE XIX.- FAILURE MODES AND EFFECTS ANALYSIS (CONTINUED)

CONFIGURATION	FAILURE MODE	FAILURE DETECTION	IMPACT ON SYSTEM	IMPACT ON MISSION		CORRECTIVE ACTION	FAILURE PREVENTION
				PREFLIGHT	INFLIGHT		
4. Nonvacuum Jacketed Metal (Dry - MLI)							
a) Metal Line	Leak, External Damage,	System Leak Test. Inspection.	Loss of Propellant	None	Reduce Flight Time. Potential Abort.	Same as (3a)	Same as (3a)
b) MLI	External Damage, Tear or Rip. Restrictive Gas Expulsion During Launch.	Inspection.	Minor. Significant Degradation in Thermal Performance.	Potential Liquid Air	Minor Reduction in Thermal Efficiency	Same as (3b)	Same as (3b)
c) Flange	Same as (1f)	Same as (1f)	Same as (1f)	Same (1f)	Same (1f)	Same as (1f)	Same as (1f)
5. Nonvacuum Jacketed Composite (Dry - MLI)							
a) Metal Line	Same as (4a)	Same as (4a)	Same as (4a)	Same (4a)	Same (4a)	Same as (4a)	Same as (4a), Except Less Susceptible to Damage.
b) MLI	Same as (4b)	Same as (4b)	Same as (4b)	Same (4b)	Same (4b)	Same as (4b)	Same as (4b)
c) Flange	Same as (1f)	Same as (1f)	Same as (1f)	Same (1f)	Same (1f)	Same as (1f)	Same as (1f)
6. Nonvacuum Jacketed Composite (Wet - Purged MLI)							
a) Metal Line	Same as (3a)	Same as (3a)	Same as (3a)	Same (3a)	Same (3a)	Same as (3a)	Same as (3a)
b) MLI	Same as (3b)	Same as (3b)	Same as (3b)	Same (3b)	Same (3b)	Same as (3b)	Same as (3b)
c) MLI Purge System	Same as (3c)	Same as (3c)	Same as (3c)	Same (3c)	Same (3c)	Same as (3c)	Same as (3c)
d) Flange	Same as (1f)	Same as (1f)	Same as (1f)	Same (1f)	Same (1f)	Same as (1f)	Same as (1f)

TABLE XX.- COMPARISON OF NEGATIVE FEATURES

CONCEPT CONFIGURATION	NEGATIVE FEATURES
1. Vacuum Jacketed Metal (Wet)	More susceptible to external damage than 2. More components to fail than 3, 4, 5, or 6.
2. Vacuum Jacketed Composite (Wet)	More apt to have outgassing problems than 1. Less resistant than 1 to inner line implosion if overpressure condition developes in the vacuum annulus. More components to fail than 3, 4, 5, or 6.
3. Non-Vacuum Jacketed Metal (Wet-Purged MLI)	More susceptible to external damage than 2, 5, or 6. More susceptible to liquid air hazards on ground than 4 and 5. More components to fail than 4 or 5.
4. Non-Vacuum Jacketed Metal (Dry - MLI)	Less apt to detect leakage problems on ground than 3. More susceptible to external damage than 5 or 6.
5. Non-Vacuum Jacketed Composite (Dry - MLI)	Less apt to detect leakage problems on ground than 1, 2, 3, or 6.
6. Non-Vacuum Jacketed Composite (Wet - Purged MLI)	More Components to fail than 4 or 5. More susceptible to liquid air hazards on ground than 4 and 5.

TABLE XXI.- REUSABILITY AND MAINTAINABILITY EVALUATION

FEEDLINE DESIGN CONCEPT	KEY CONSIDERATIONS	RANKING
1. Vacuum Jacketed Metal (Wet)	a. More susceptible to asthetic damage (dings, dents,etc.) than vacuum jacket composite or MLI. b. Vacuum maintainability requirements greater than for concepts using MLI.	6
2. Vacuum Jacketed Composite (Wet)	a. Overwrapped vacuum Jacket is more durable and less susceptible to damage than the all-metal vacuum jacket or the MLI (especially true for resisting puncture from sharp objects). b. Vacuum maintainability requirements greater than for concepts using MLI.	5
3. Non-Vacuum Jacketed Metal (Wet - Purged MLI)	a. Installed repairability of MLI system is more feasible than vacuum jacketed configurations. b. Requires dedicated dry gas purge during re-entry.	4
4. Non-Vacuum Jacketed Metal (Dry - MLI)	a. Installed repairability of MLI system may be more feasible than for vacuum jacketed configurations. b. No maintainability required for purge system.	2
5. Non-Vacuum Jacketed Composite (Dry - MLI)	a. Installed repairability of MLI system is more feasible than vacuum jacketed configurations. b. No maintainability required for purge system. c. Metal line less susceptible to damage, due to overwrap, than the all-metal line.	1
6. Non-Vacuum Jacketed Composite (Wet - Purged MLI)	a. Installed repairability of MLI system is more feasible than vacuum jacketed configurations. b. Requires dedicated dry gas purge during re-entry.	3

TABLE XXII. - SYSTEM COMPARISON OF FEEDLINE DESIGN CONCEPTS

Design Concept	Configuration	System Weight kg (lbs)			Cost ($x1000)	**Reliability	**Reusability and Maintainability
		Feedline Weight	*Boil-off Weight	Total System Weight			
1. Vacuum Jacketed Metal (Wet)	With Radiation Shields	29.4 (64.9)	35.6 (78.6)	65.0 (143.5)	37.9	5	6
2. Vacuum Jacketed Composite (Wet)	With Radiation Shields	21.3 (46.9)	35.1 (77.3)	56.3 (124.2)	45.4	6	5
3. Non-Vacuum Jacketed Metal (Purged MLI - Dry)		14.6 (32.2)	3.6 (8.0)	18.2 (40.2)	20.5	4	4
4. Non-Vacuum Jacketed Metal (MLI - Dry)	Prevalve Open After Initial Firing	14.1 (31.0)	6.2 (13.8)	20.3 (44.8)	19.9	2	2
5. Non-Vacuum Jacketed Composite (MLI - Dry)	Prevalve Open After Initial Firing	10.3 (22.6)	4.1 (9.1)	14.4 (31.7)	24.4	1	1
6. Non-Vacuum Jacketed Composite (Purged MLI-Wet)		10.8 (23.9)	3.0 (6.7)	13.8 (30.6)	25.0	3	3

* Sum of boil-off during storage in cargo bay and during flight.

** Ranking is in order of preference (1 is best)

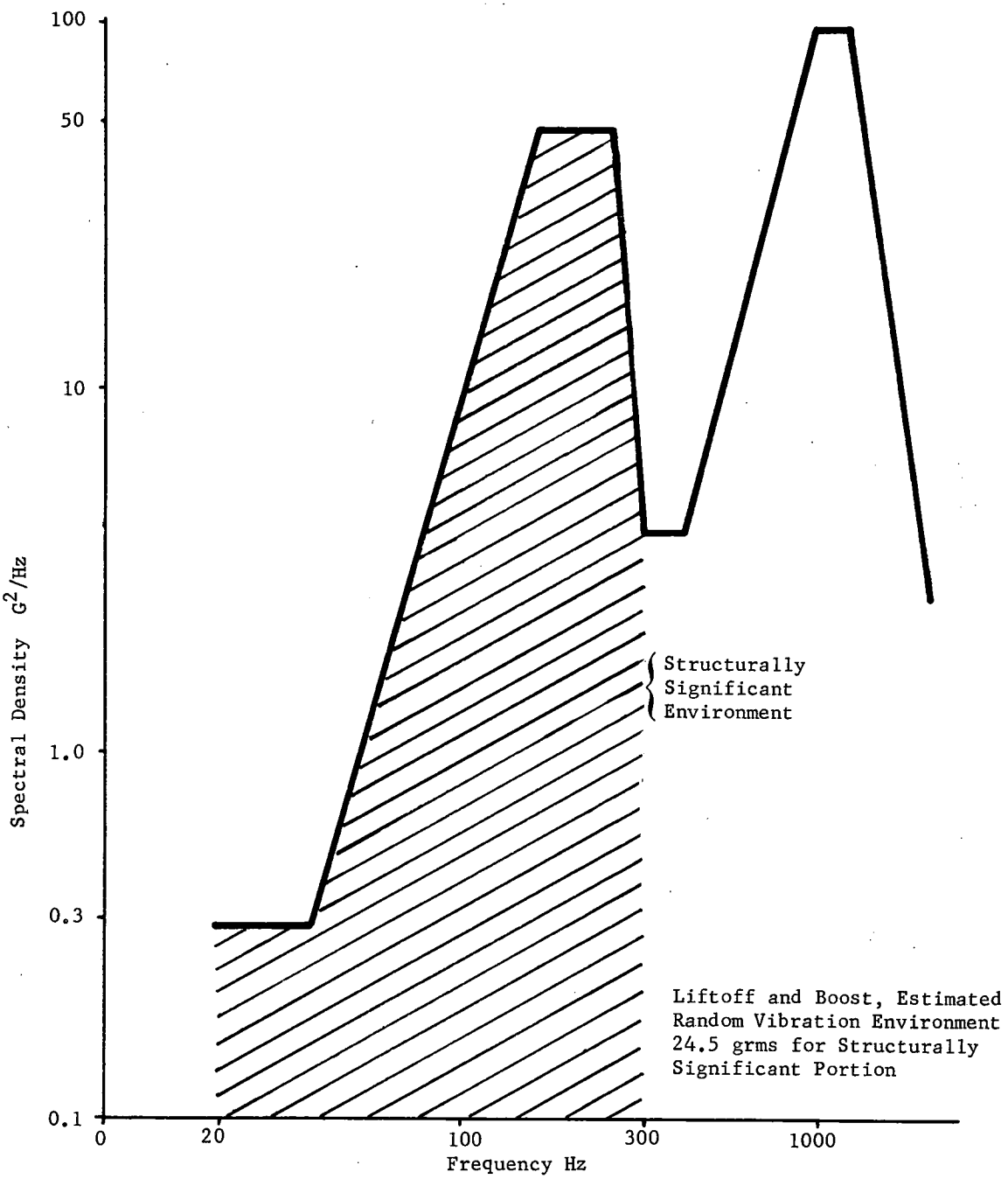

FIGURE 1.- LIFTOFF AND BOOST, ESTIMATED RANDOM VIBRATION ENVIRONMENT

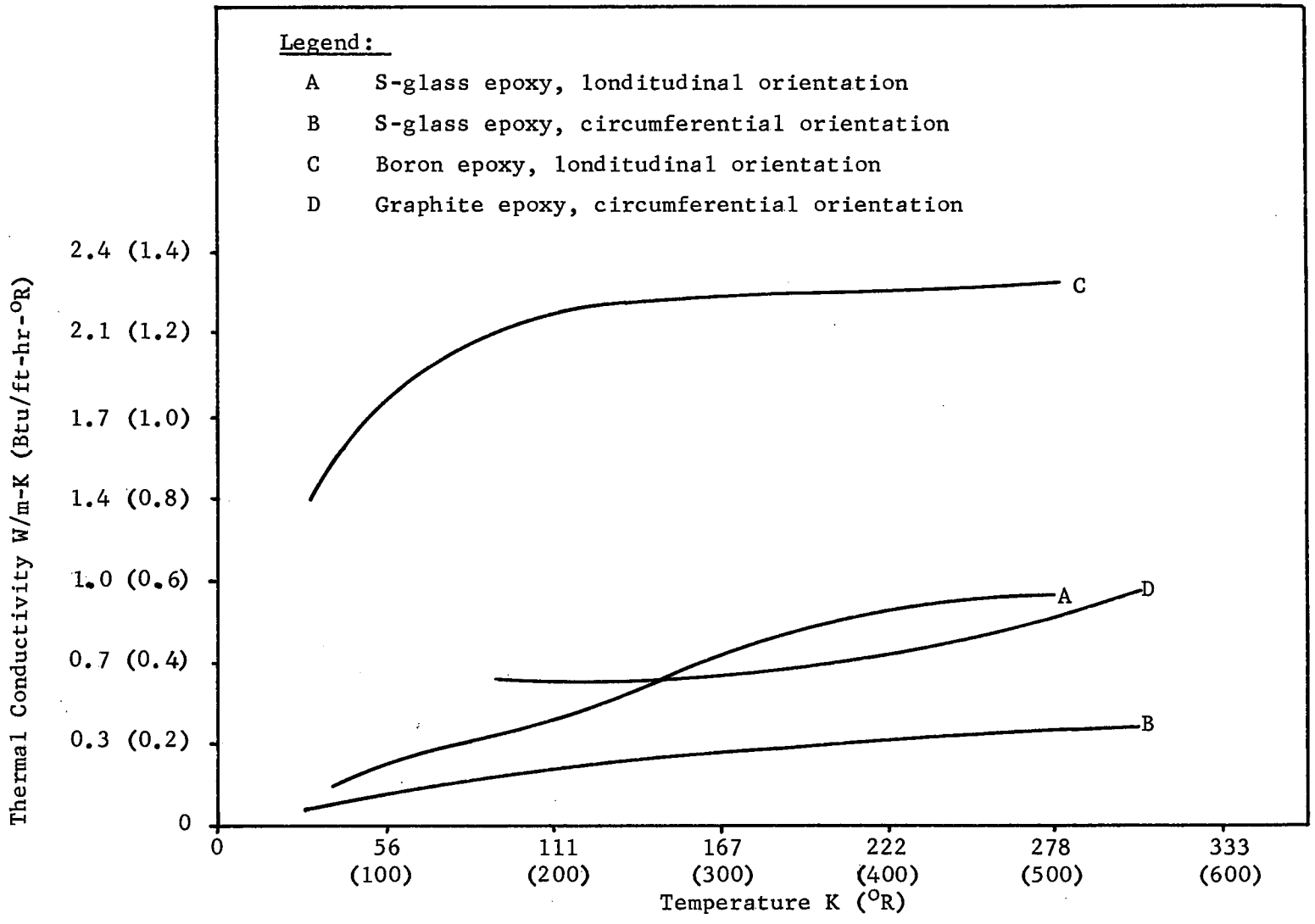

FIGURE 2.- Comparison of Thermal Conductivity Versus Temperature for Candidate Overwrap Materials

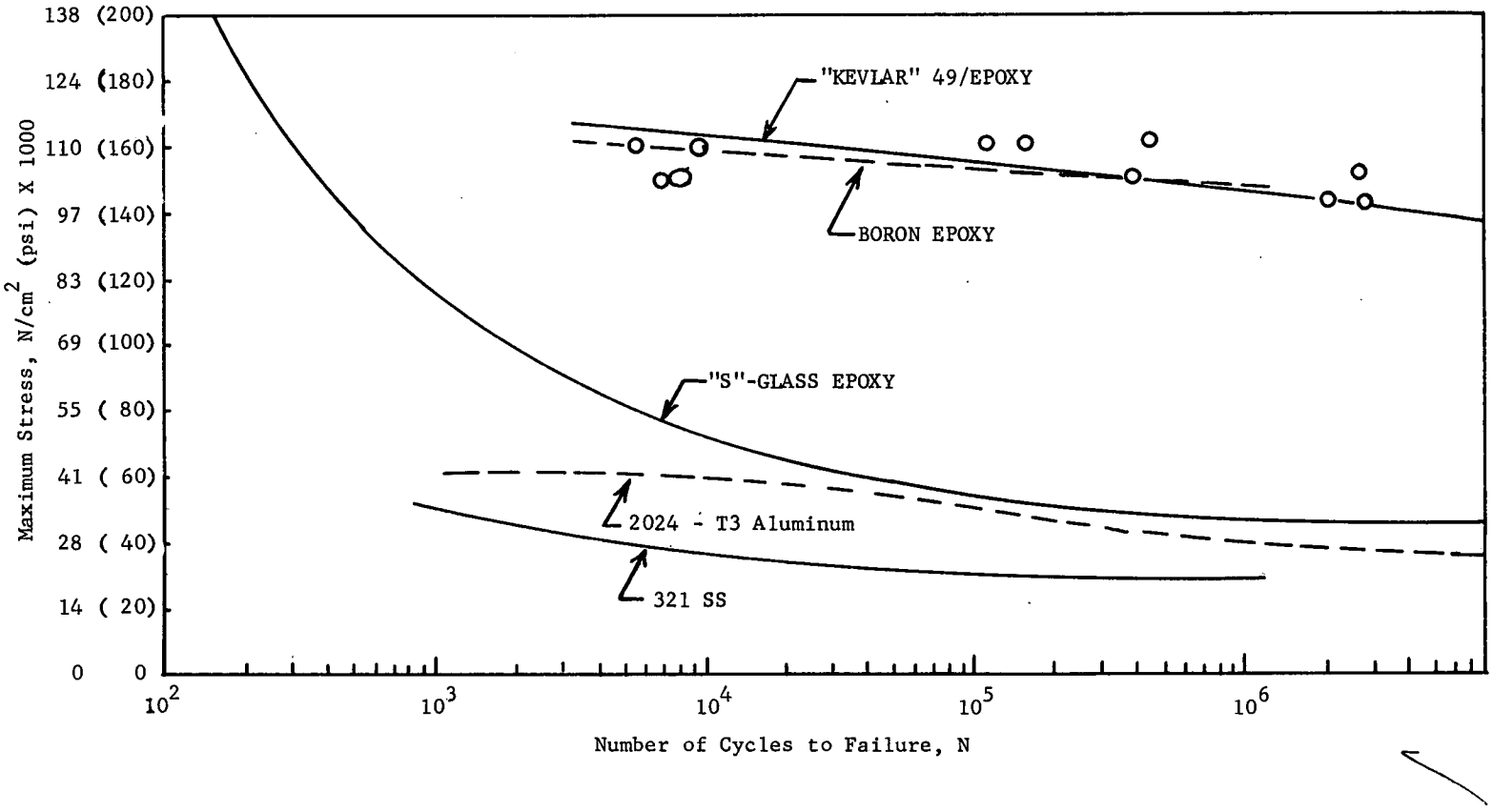

FIGURE 3.- TENSION-TENSION FATIGUE BEHAVIOR OF UNDIRECTIONAL COMPOSITES AND ALUMINUM

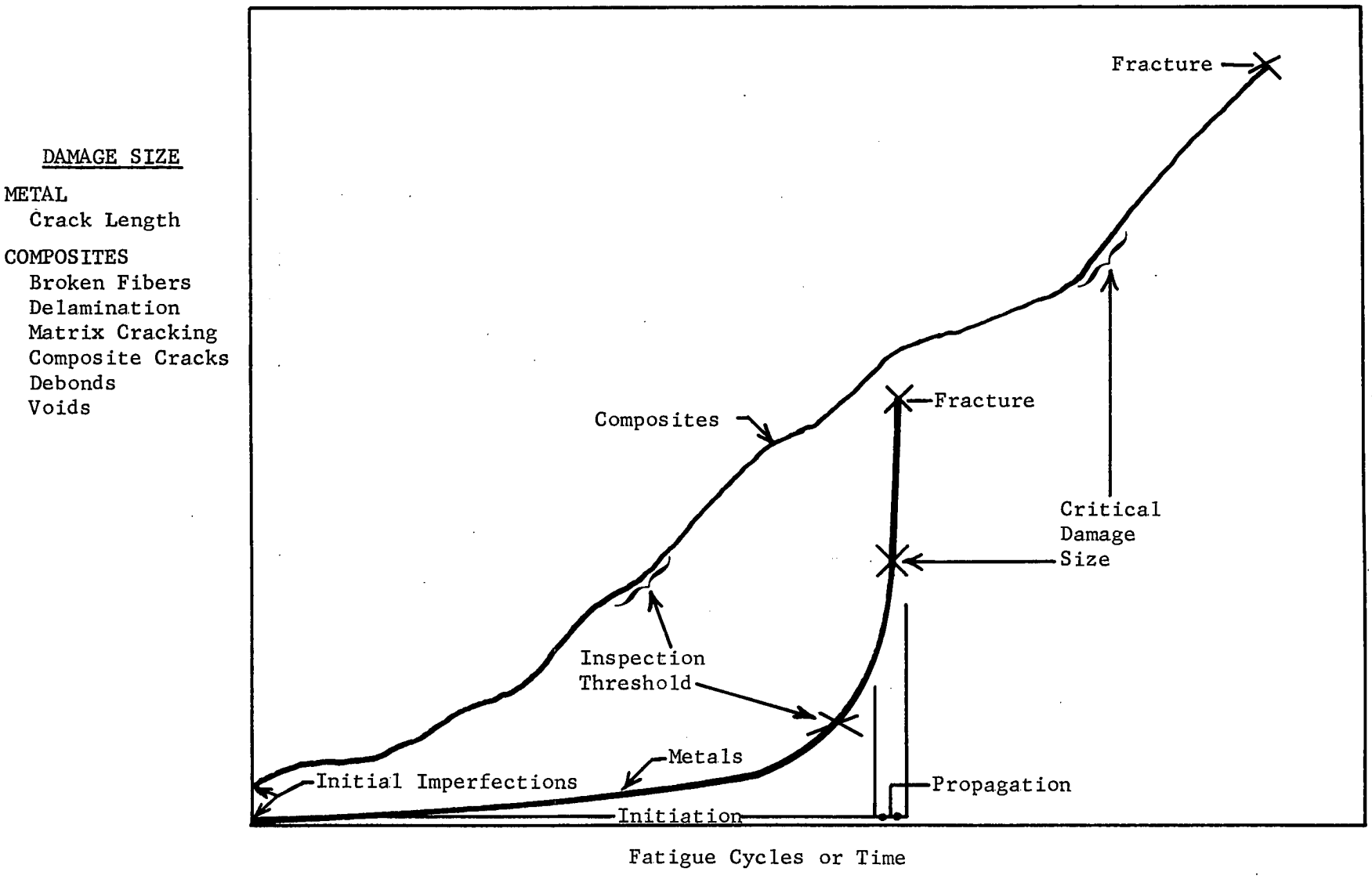

FIGURE 4.- COMPARISON OF FATIGUE BEHAVIOR OF COMPOSITES AND METALS

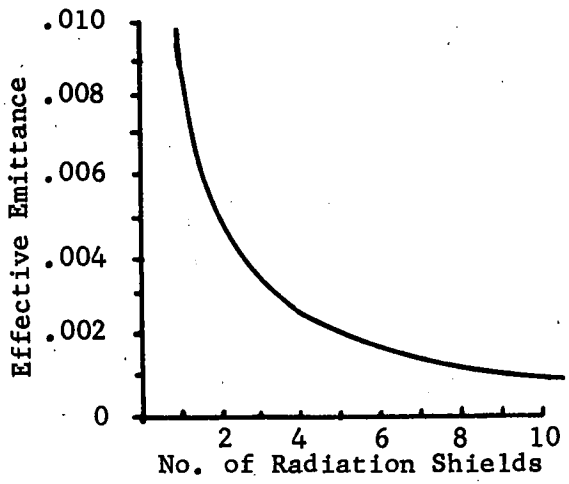

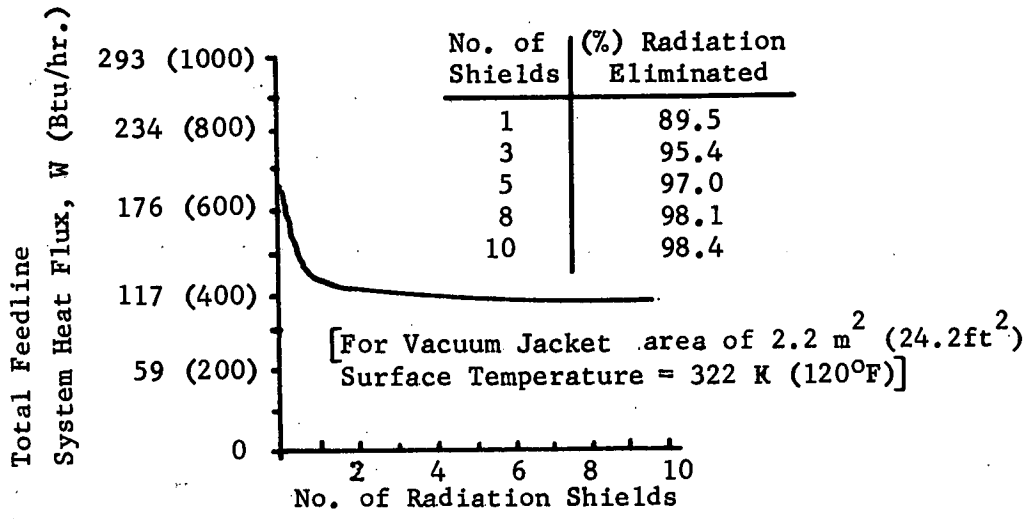

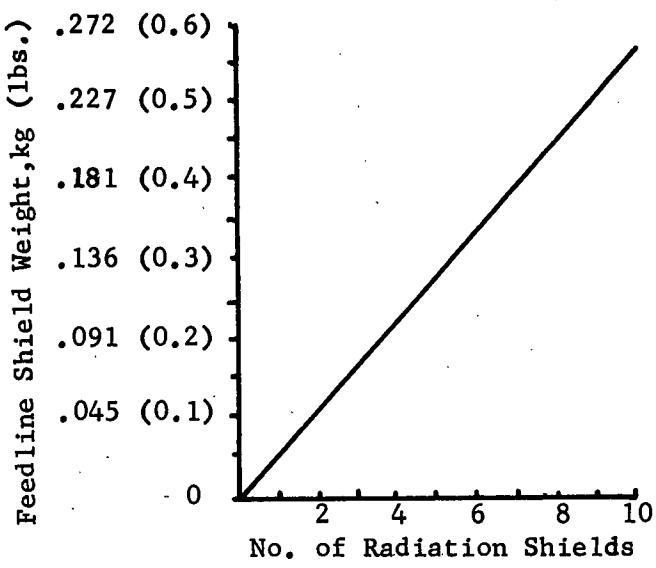

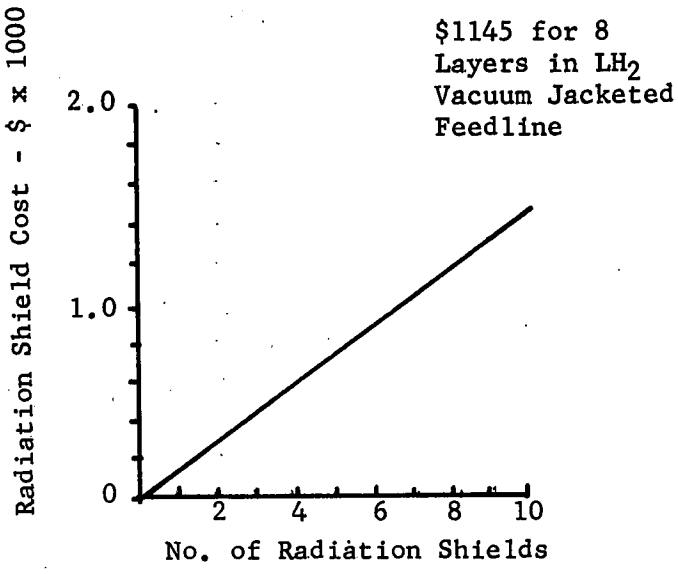

FIGURE 5.- CHARACTERISTICS OF RADIATION SHIELDS IN VACUUM JACKET ANNULUS

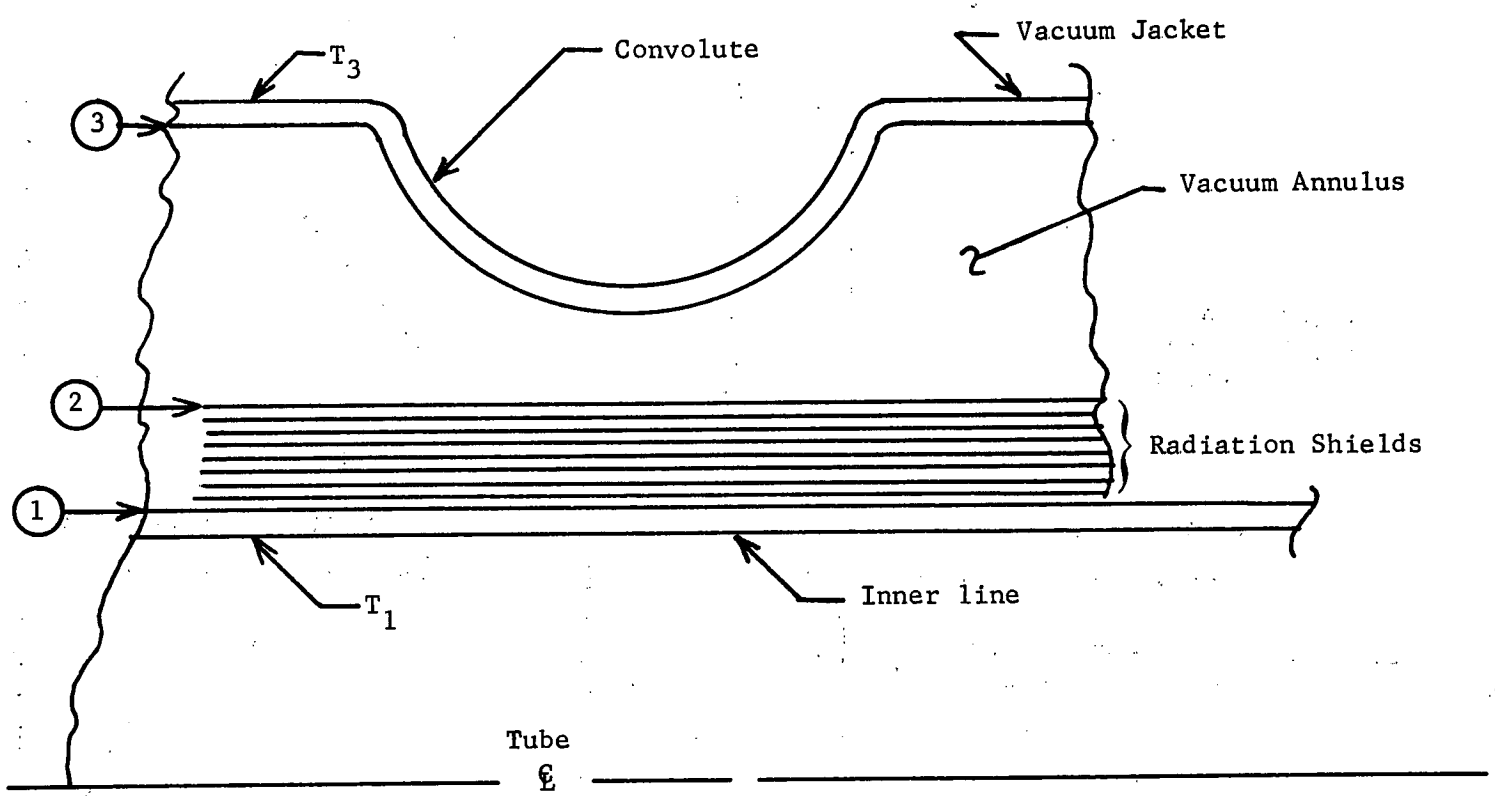

FIGURE 6.- THERMAL SCHEMATIC, RADIATION SHIELDS IN VACUUM ANNULUS

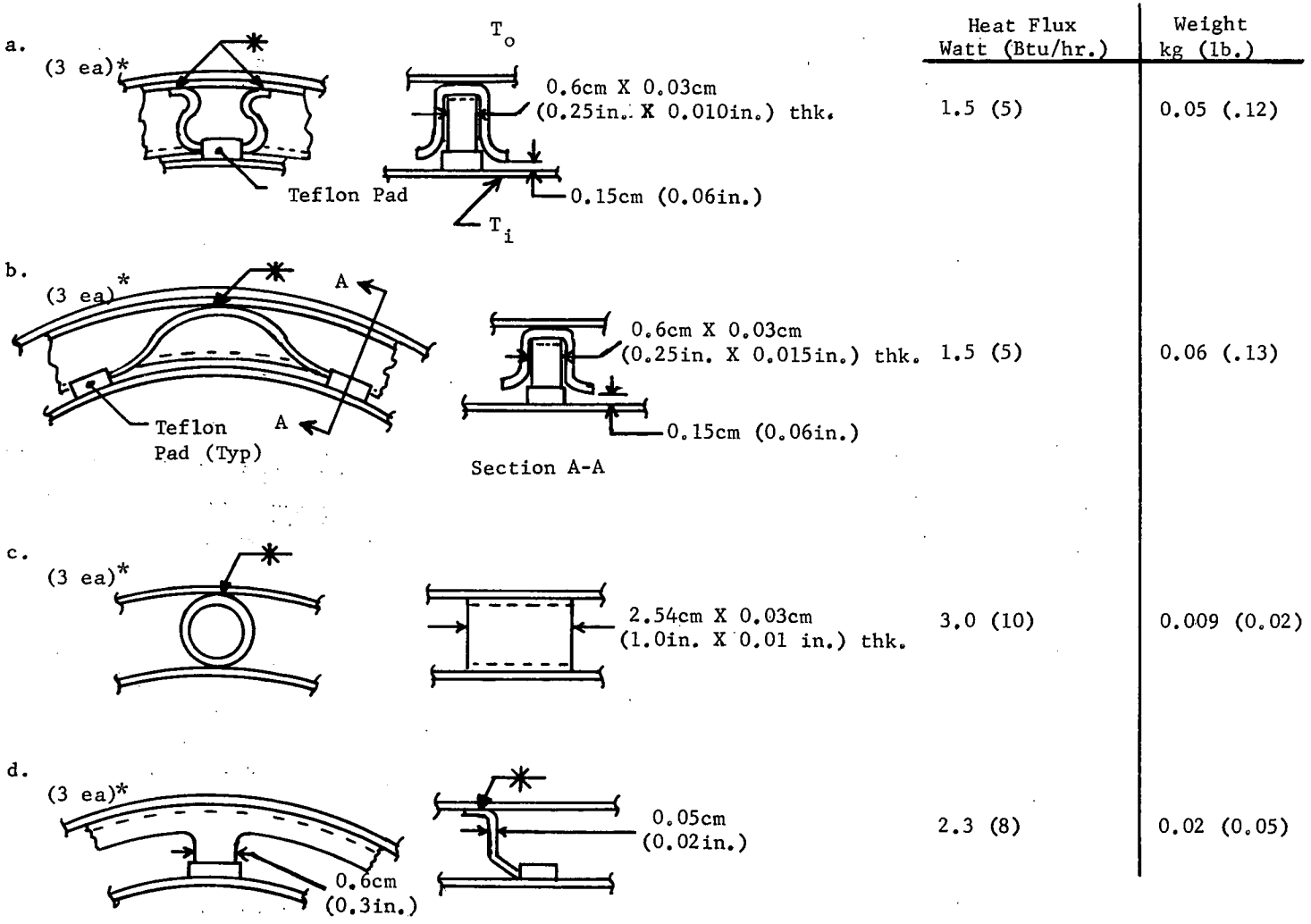

	Heat Flux Watt (Btu/hr.)	Weight kg (lb.)
a.	1.5 (5)	0.05 (.12)
b.	1.5 (5)	0.06 (.13)
c.	3.0 (10)	0.009 (0.02)
d.	2.3 (8)	0.02 (0.05)

Conditions: T_o = 300 K (80°F) Annulus = 1.3cm (0.5in.) Material: Stainless Steel
T_i = 22 K (-420°F) Line Dia. = 10.2cm (4.0in.)

*Three standoffs per radial location

FIGURE 7.- COMPARISON OF CANDIDATE VACUUM JACKETED LINE STANDOFF CONCEPTS

a. Half Torus

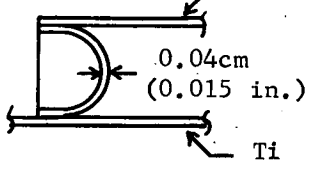

Conditions

To = 300 K (80°F)
Ti = 22 K (-420°F)
Annulus = 1.3cm (0.50 in.)
Line Dia = 10.2cm (4.0 in.)
Material = Stainless Steel

b. Axial Bellows

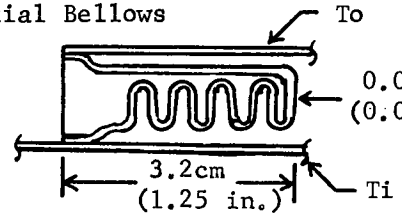

c. Cylindrical Cones

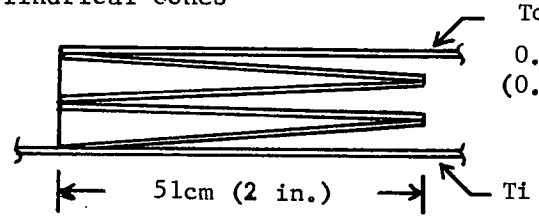

d. Conventional

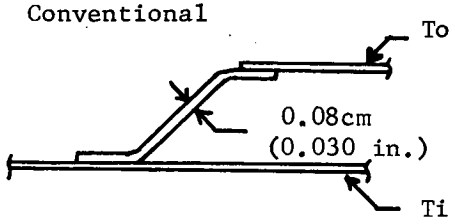

e. Thin Metal/Glass-Fiber

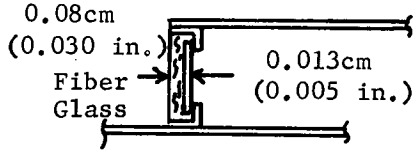

	Heat Flux Watt (Btu/hr.)	Weight kg (lb.)
a. Half Torus	33 (113)	0.02 (0.05)
b. Axial Bellows	7.3 (25)	1.0 (0.22)
c. Cylindrical Cones	3.2 (11)	0.1 (0.25)
d. Conventional	103.8 (354)	0.02 (0.05)
e. Thin Metal/Glass-Fiber	24.3 (83)	0.03 (0.06)

FIGURE 8.- COMPARISON OF VACUUM JACKETED LINE END CLOSURE CONCEPTS

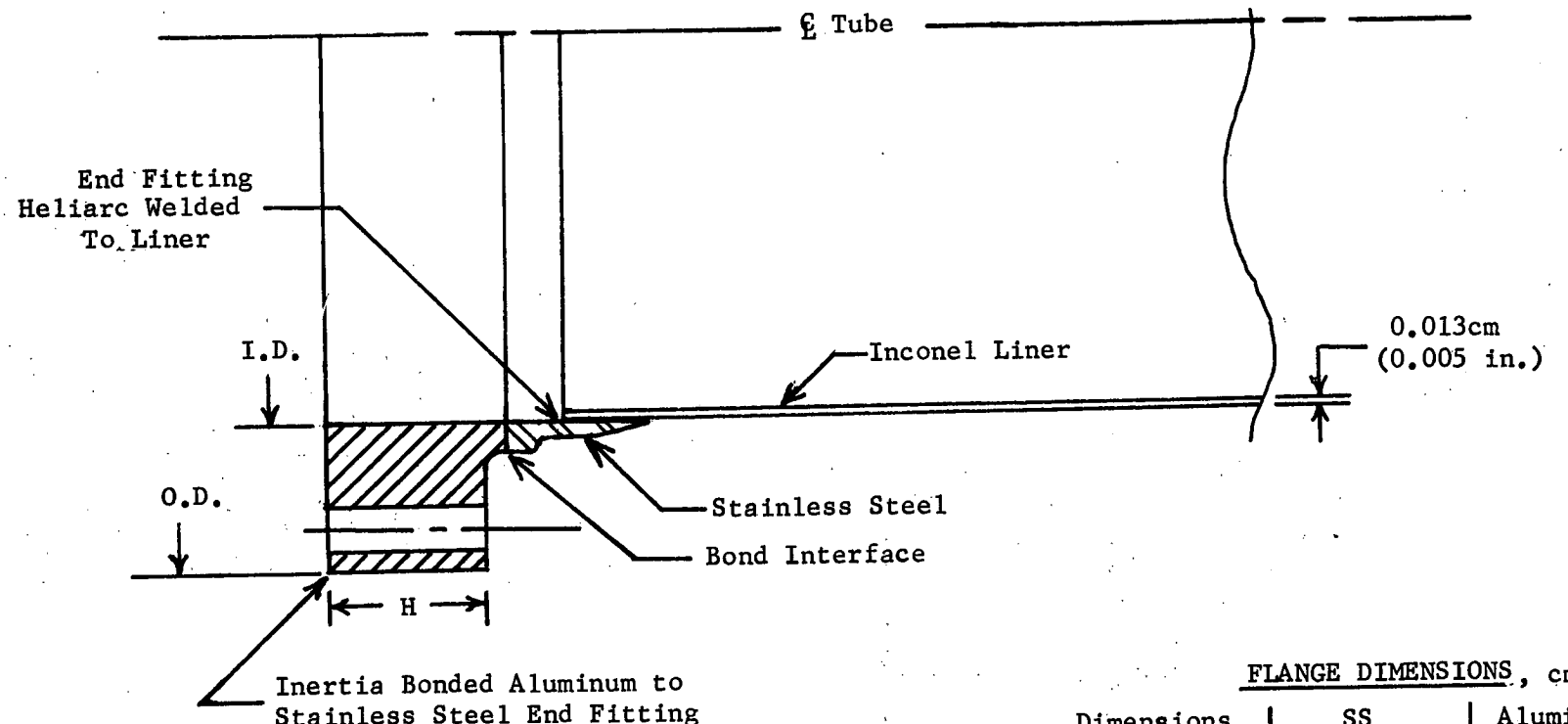

FLANGE DIMENSIONS, cm (in.)

Dimensions	SS	Aluminum
H	1.0 (0.4)	2.1 (0.84)
O.D.	13.2 (5.2)	13.2 (5.2)
I.D.	10.2 (4.0)	10.2 (4.0)

FIGURE 9.- TYPICAL DISSIMILAR METAL FLANGED JOINT CONFIGURATION

LINE DEFLECTIONS cm (in.)			
Point	X	Y	Z
A	+ 0.86 (0.34) - 2.87 (1.13)	± 0.5 (0.2)	± 0.5 (0.2)
B	± 2.54 (1.0)	± 2.54 (1.0)	± 0.25 (0.1)
C	+ 2.87 (1.13) - 0.86 (0.34)	± 0.5 (0.2)	± 0.5 (0.2)

POINT	ANGULATION Radians (Degrees)
A	± 0.02 (± 1)
B	± 0.02 (± 1)
C	± 0.01 (± 0.5)
	± 0.07 (± 4°) Engine Turbopump

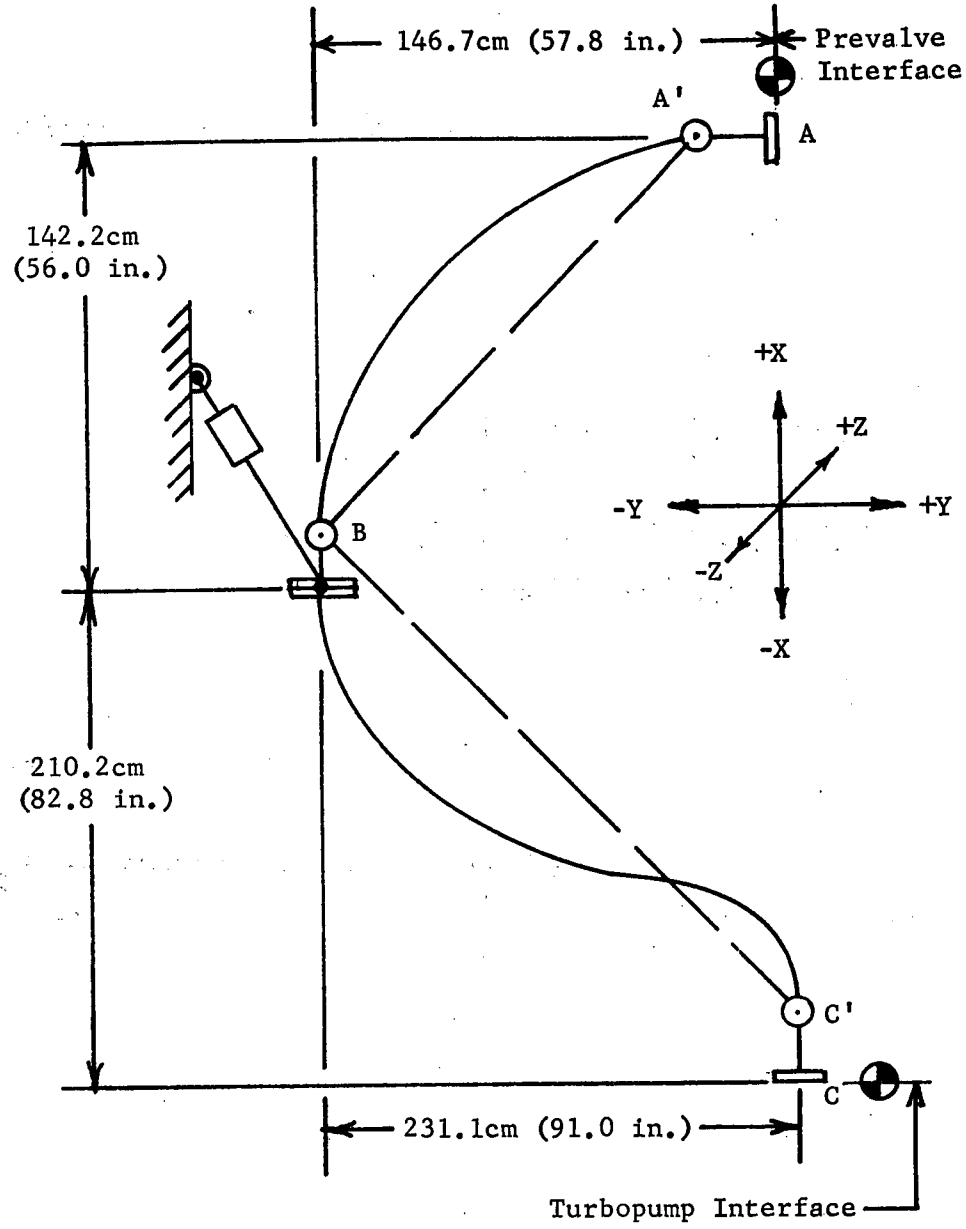

FIGURE 10.- FEEDLINE AND INTERFACE MOTIONS

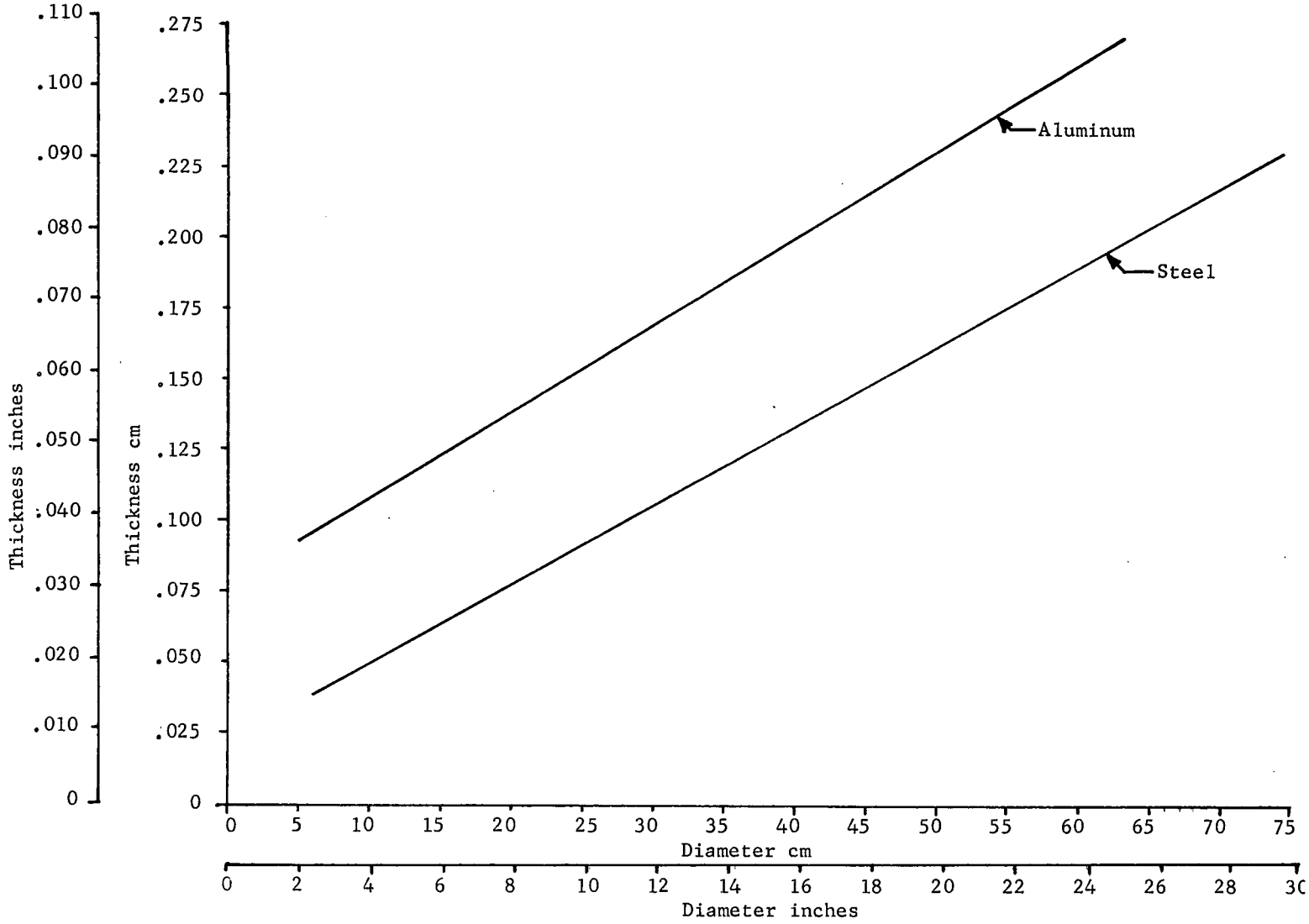

FIGURE 11.- DUCT MINIMUM WALL THICKNESS, MSFC CRITERIA

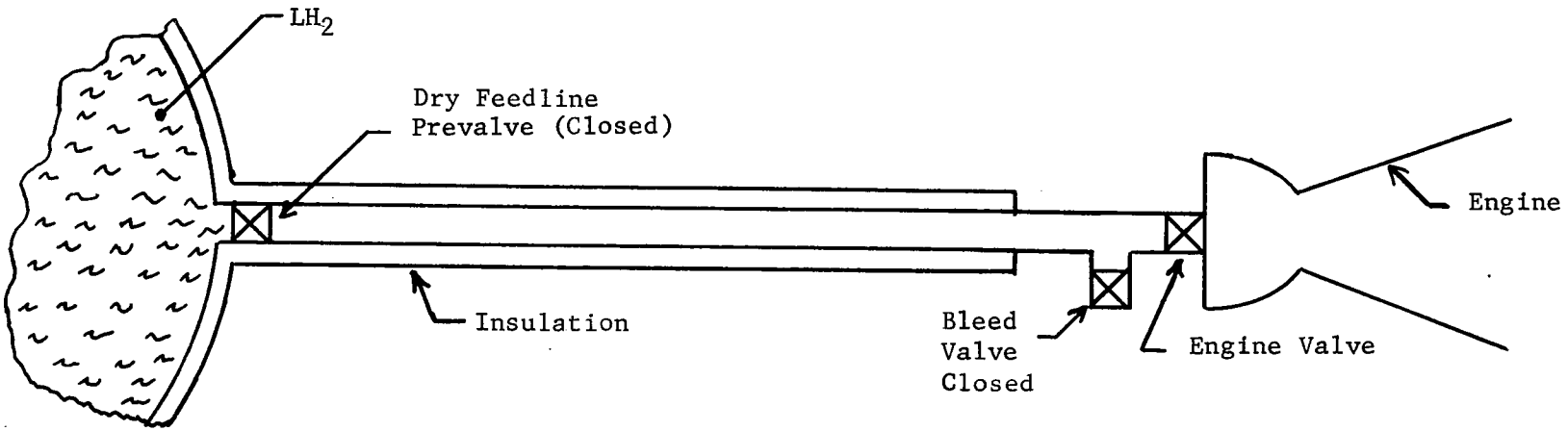

Configuration from Ground Fill to T + 14.74 Hrs, ie., first engine firing. See description of operational modes for configuration after first engine burn.

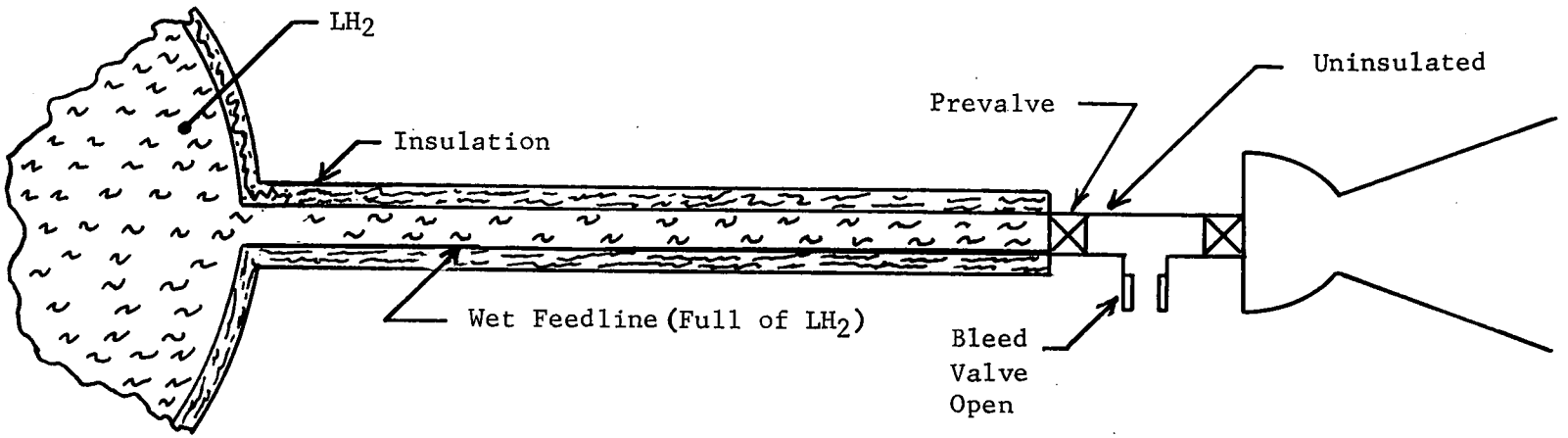

FIGURE 12.- DRY AND WET LH_2 FEEDLINE CONFIGURATIONS

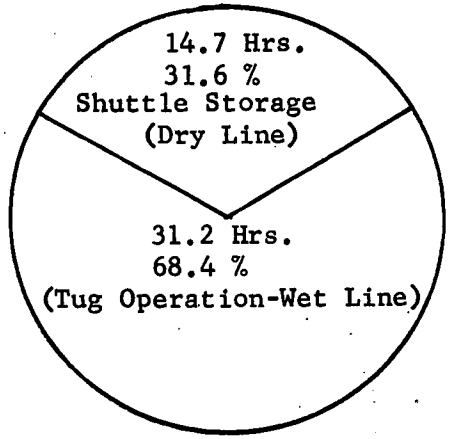

MODE II.- PREVALVE OPEN AFTER INITIAL ENGINE FIRING

CONDITIONS

Line Coated With Thermal Coating, Temperature of Line Surface, T_o = 225 K (0°F) for Tug Operation

T_o = 367 K (200°F) Shuttle Storage

Ground Hold Time - 2.0 Hrs. and T_o = 300 K (80°F)

Prevalve Remains Open Subsequent to Initial Engine Firing

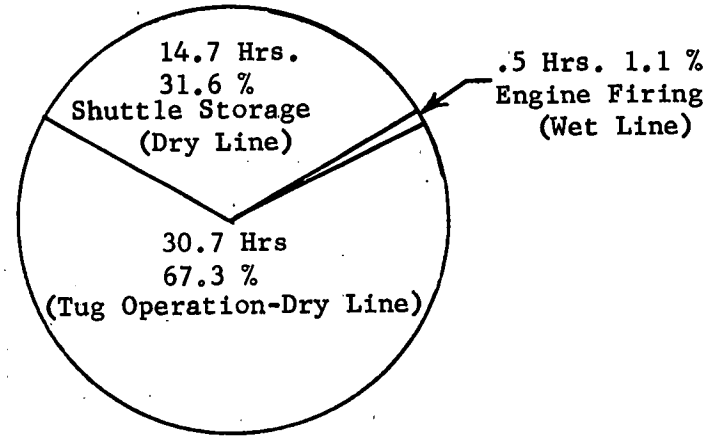

MODE III.- PREVALVE CLOSED AFTER EACH ENGINE FIRING AND LINE DUMPED

CONDITIONS

Line Coated With Thermal Coating, Temperature of Line Surface, T_o = 255 K (0°F) for Tug Operation and Engine Firing

T_o = 367 K (200°F) Shuttle Storage

Ground Hold Time - 2.0 Hrs. and T_o = 300 K (80°F)

LH_2 Dumped After each Engine Firing and Line is Void of Propellant Between Engine Firings

FIGURE 13.- FEEDLINE OPERATIONAL CONFIGURATIONS - DRY FEEDLINE

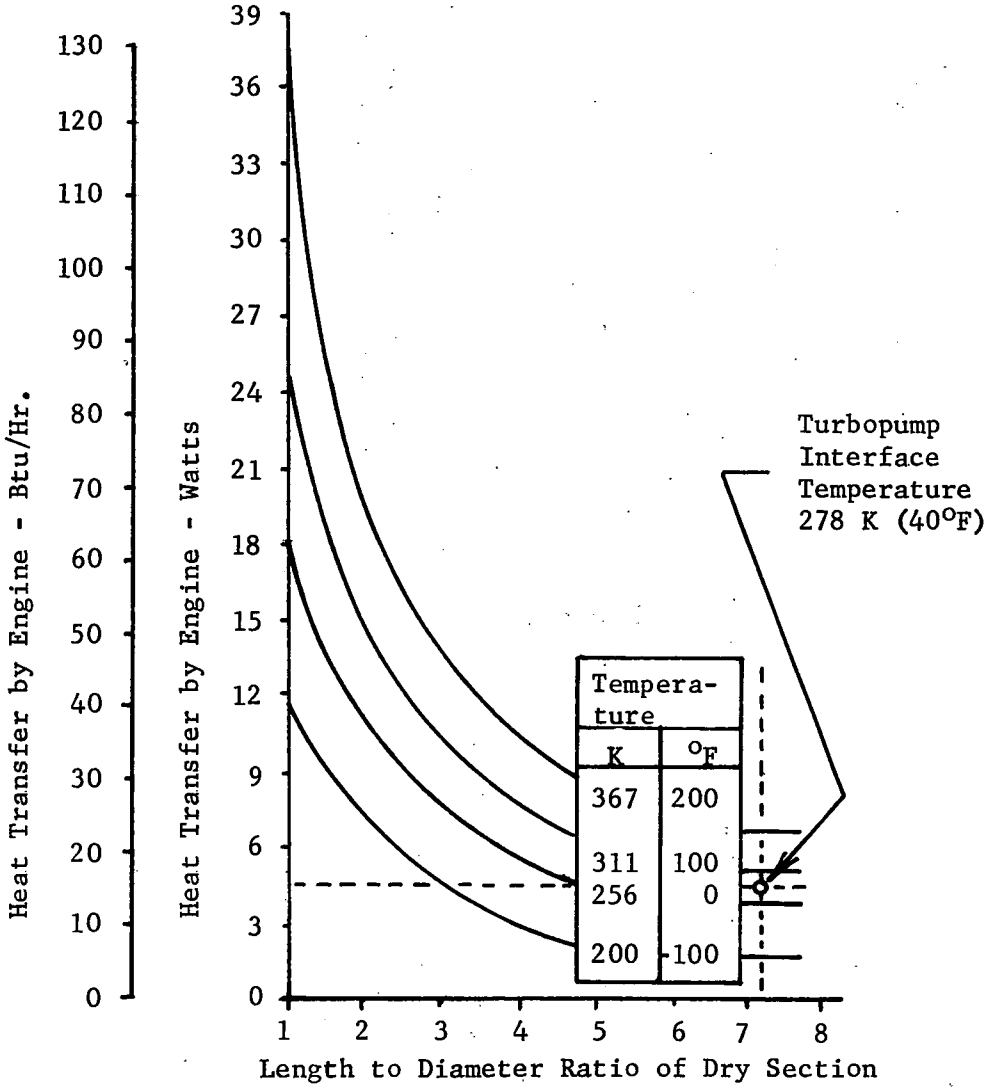

FIGURE 14.- HEAT TRANSFER FROM ENGINE TO FEEDLINE

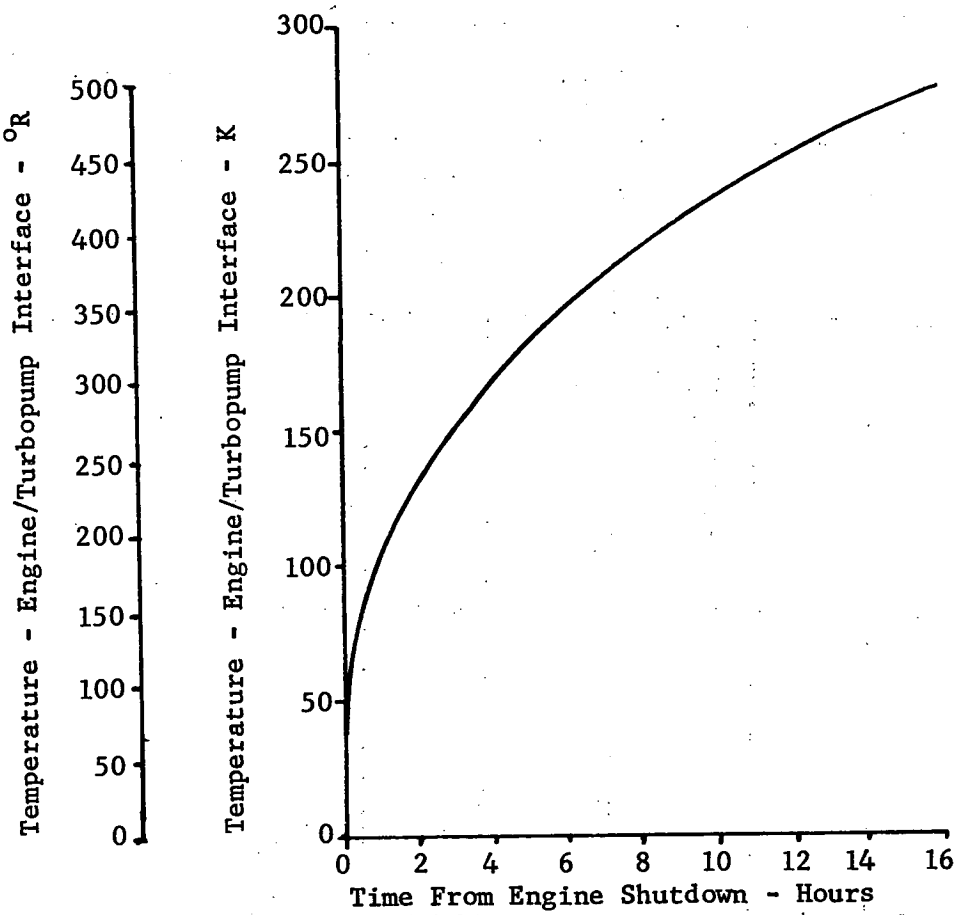

FIGURE 15.- TEMPERATURE VERSUS TIME PROFILE FOR ENGINE TURBOPUMP INTERFACE

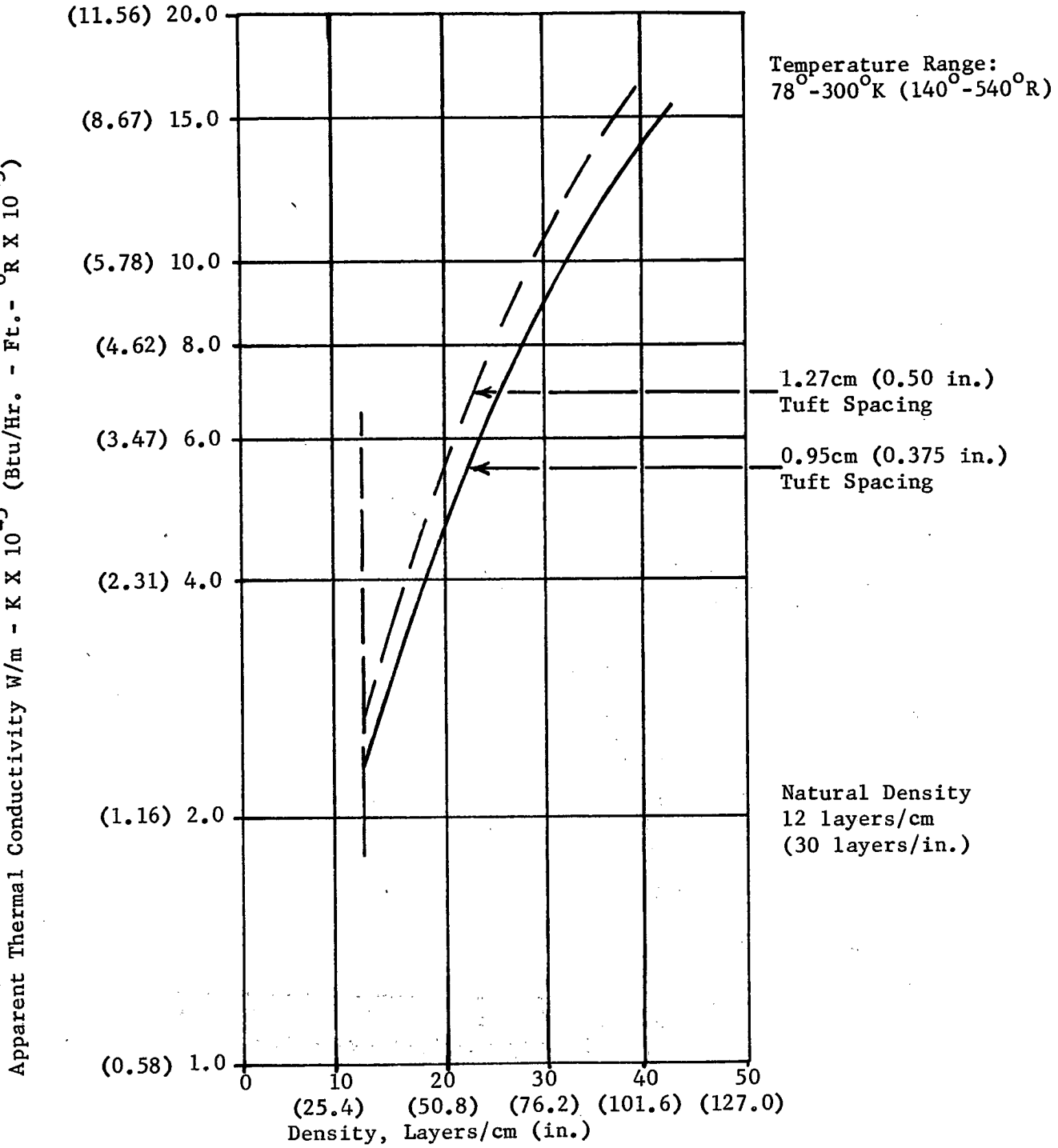

FIGURE 16.- MLI APPARENT THERMAL CONDUCTIVITY VERSUS LAYER DENSITY

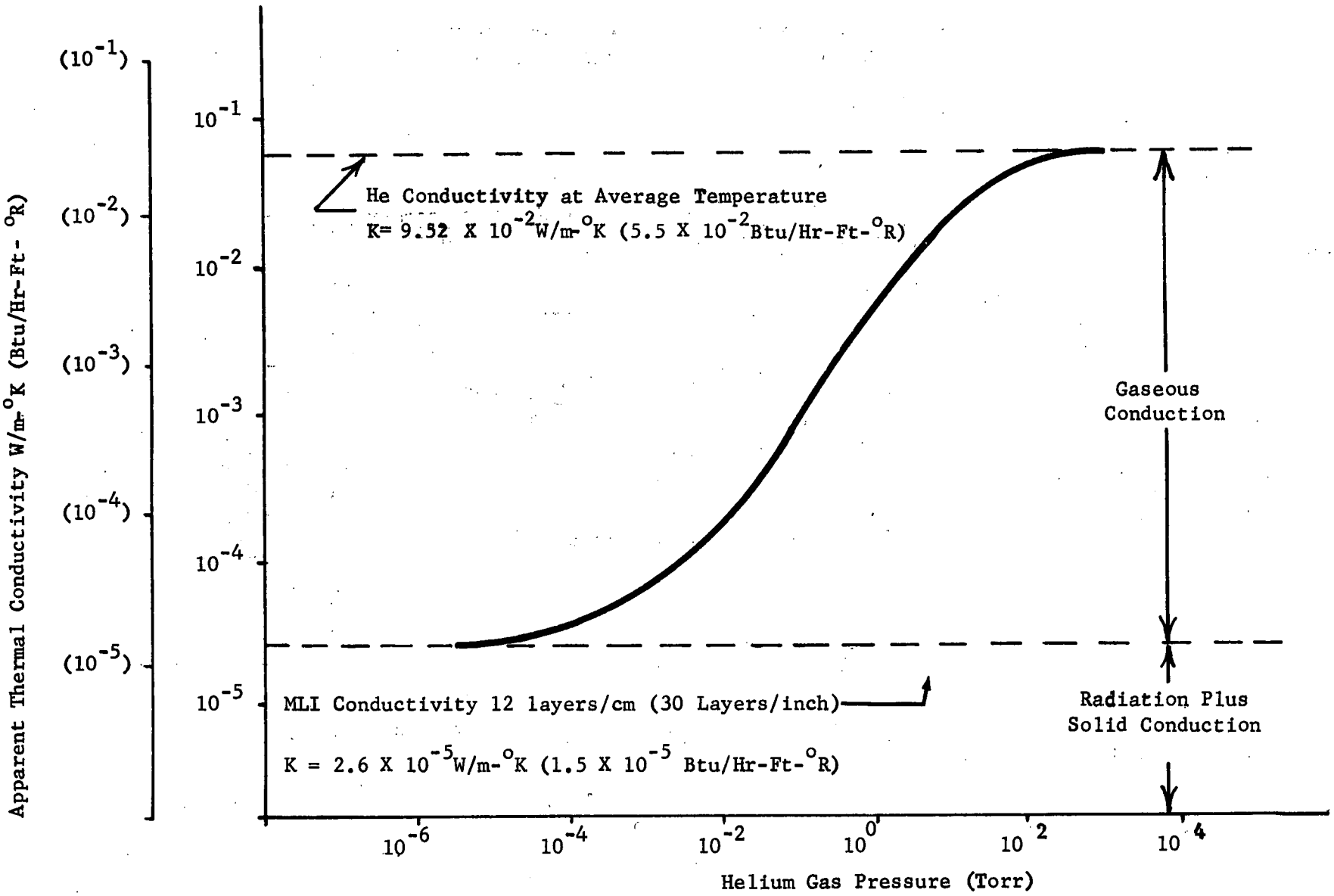

Figure 17.- APPARENT THERMAL CONDUCTIVITY VERSUS HELIUM GAS PRESSURE

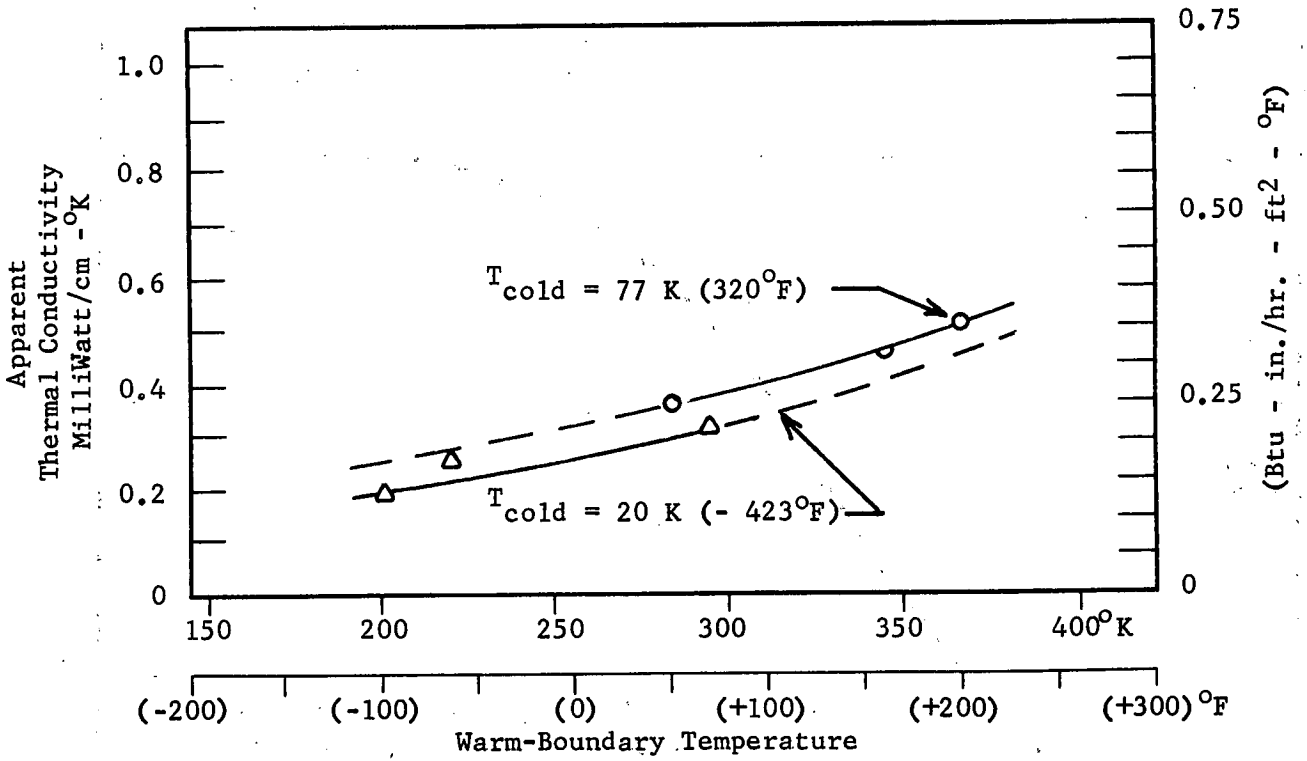

FIGURE 18.- EFFECT OF BOUNDARY TEMPERATURE ON THE MEAN APPARENT THERMAL CONDUCTIVITY OF A MULTILAYER INSULATION

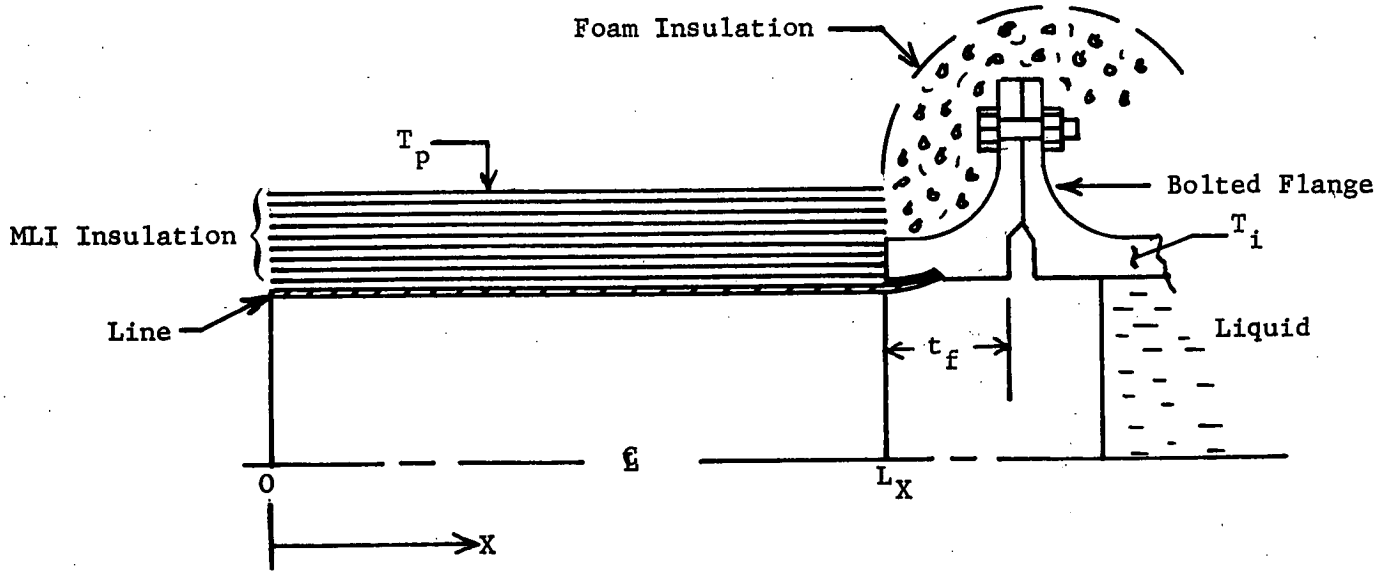

FIGURE 19.- AXIAL HEAT TRANSFER CONFIGURATION FOR A WARM LINE TO A COLD LINE

REVISIONS				
SYM	ZONE	DESCRIPTION	DATE	APPROVED

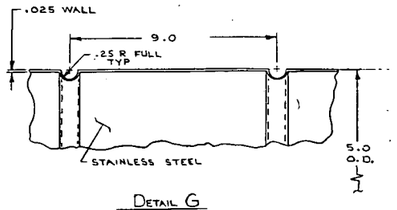

DETAIL G
NO SCALE
TYPICAL CONCEPT 1

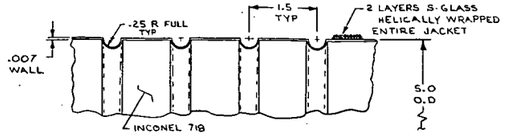

DETAIL F
NO SCALE
TYPICAL CONCEPT 2

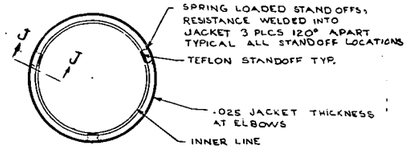

DETAIL H
NO SCALE
TYPICAL CONCEPTS 1 & 2

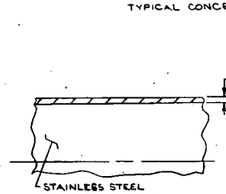

DETAIL D
NO SCALE
TYPICAL CONCEPT 1

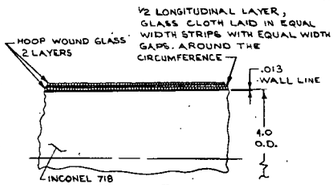

DETAIL E
NO SCALE
TYPICAL CONCEPT 2

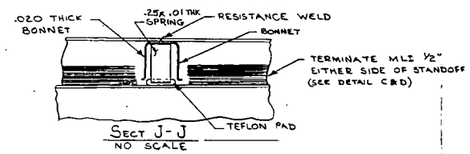

SECT J-J
NO SCALE

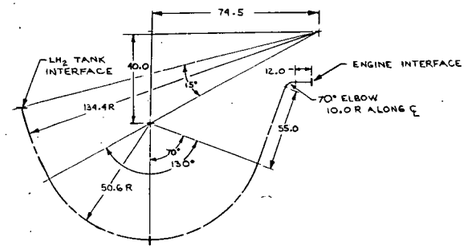

DIMENSIONAL LAYOUT
CONCEPT 1 & 2 LINE

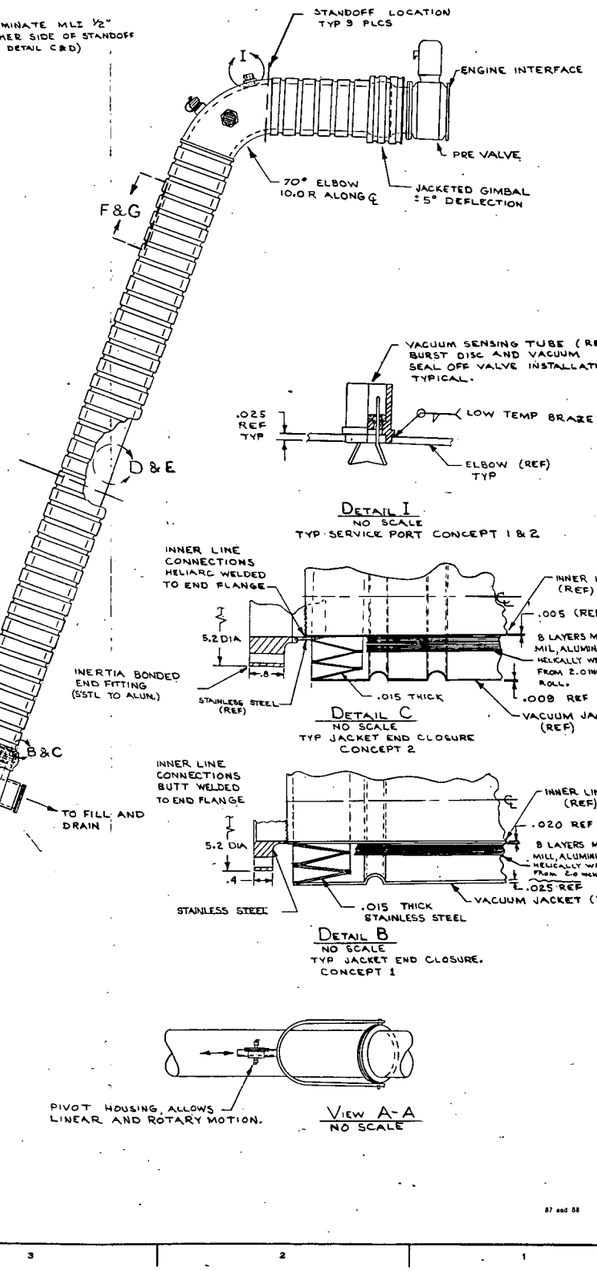

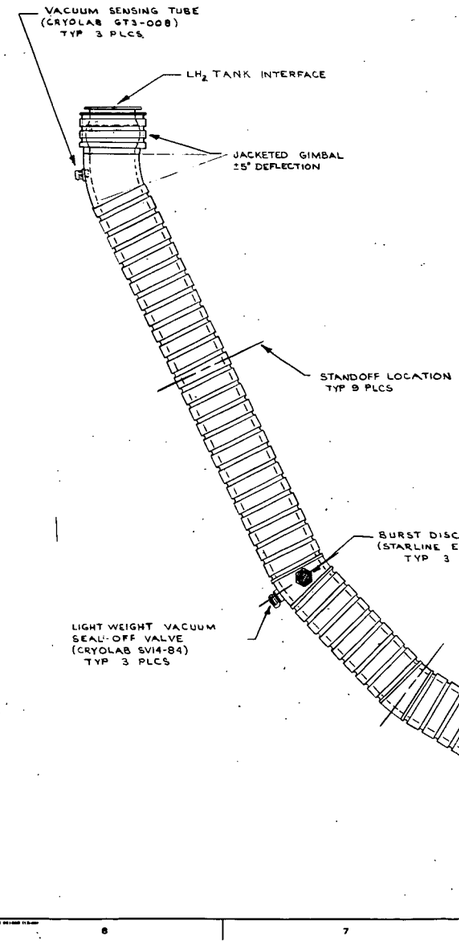

DETAIL I
NO SCALE
TYP SERVICE PORT CONCEPT 1 & 2

DETAIL C
NO SCALE
TYP JACKET END CLOSURE
CONCEPT 2

DETAIL B
NO SCALE
TYP JACKET END CLOSURE.
CONCEPT 1

DESIGN CONCEPTS 1 & 2			
VACUUM JACKETED, UNINSULATED, WET, FEEDLINE			
CONCEPT 1		CONCEPT 2	
INNER LINE	VACUUM JACKET	INNER LINE	VACUUM JACKET
4.0 OUTSIDE DIAMETER	5.0 OUTSIDE DIAMETER	4.0 OUTSIDE DIAMETER	5.0 OUTSIDE DIAMETER
.023 WALL	.025 WALL	.013 WALL	.007 WALL
STAINLESS STEEL (SEE DETAIL "D")	STAINLESS STEEL (SEE DETAIL "G")	INCONEL 718 OVERWRAPPED 2 ½ LAYERS, S-GLASS HOOP, & LONGITUDINAL & HOOP. (SEE DETAIL "E")	INCONEL 718 OVERWRAPPED 2 LAYERS, S-GLASS HELICALLY WRAPPED (SEE DETAIL "F")
EMISSIVITY IMPROVEMENT INSULATION TYP CONCEPTS 1 & 2			
¼ MIL (.00025 INCH) THICK DOUBLE ALUMINIZED MYLAR, "SUPER FLOC", 8 LAYERS HELICALLY WRAPPED FROM A 2.0 INCH WIDE SPOOL WITH 1.0 INCH OVERLAP. FASTEN START AND STOP WITH VACUUM COMPATIBLE TAPE.			

PIVOT HOUSING, ALLOWS LINEAR AND ROTARY MOTION.

VIEW A-A
NO SCALE

87 and 88

REVISIONS

ZTR	ECNO	DESCRIPTION	DATE	APPROVED

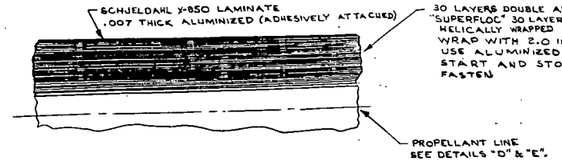

DETAIL F
NO SCALE
TYP CONCEPT 4 & 5

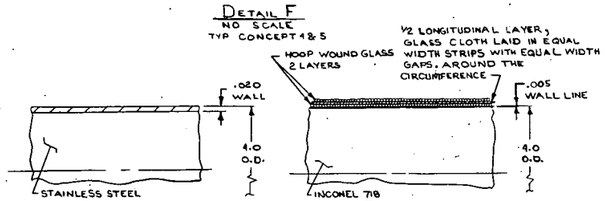

DETAIL D
NO SCALE
TYPICAL CONCEPT 4

DETAIL E
NO SCALE
TYPICAL CONCEPT 5

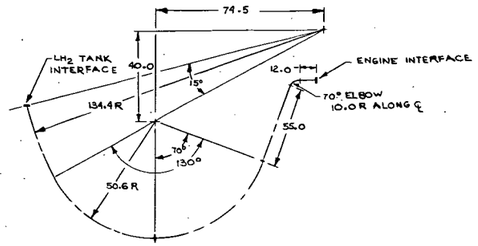

DIMENSIONAL LAYOUT
CONCEPT 4 & 5 LINE

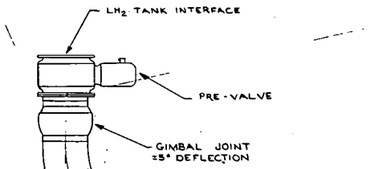

DESIGN CONCEPTS 4 & 5		
MLI INSULATED, DRY, FEEDLINE		
CONCEPT 4		CONCEPT 5
FEEDLINE	INSULATION (TYP BOTH CONCEPTS)	FEEDLINE
4.0 OUTSIDE DIAMETER .020 WALL STAINLESS STEEL (SEE DETAIL "D")	MLI INSULATION SYSTEM; ¼ MIL (.00025) THICK, DOUBLE ALUMINIZED MYLAR; 30 LAYERS HELICALLY WRAPPED OVER LINE FROM A 2.0 WIDE SPOOL WITH 1.0 OVERLAP. FASTEN START AND STOP WITH ALUMINIZED MYLAR TAPE. WRAP OUTSIDE WITH SCHJELDAHL X-850 LAMINATE. (SEE DETAIL F)	4.0 OUTSIDE DIAMETER .005 WALL INCONEL 718 OVERWRAPPED 2½ LAYERS, S-GLASS HOOP, ½ LONGITUDINAL & HOOP. (SEE DETAIL "E")

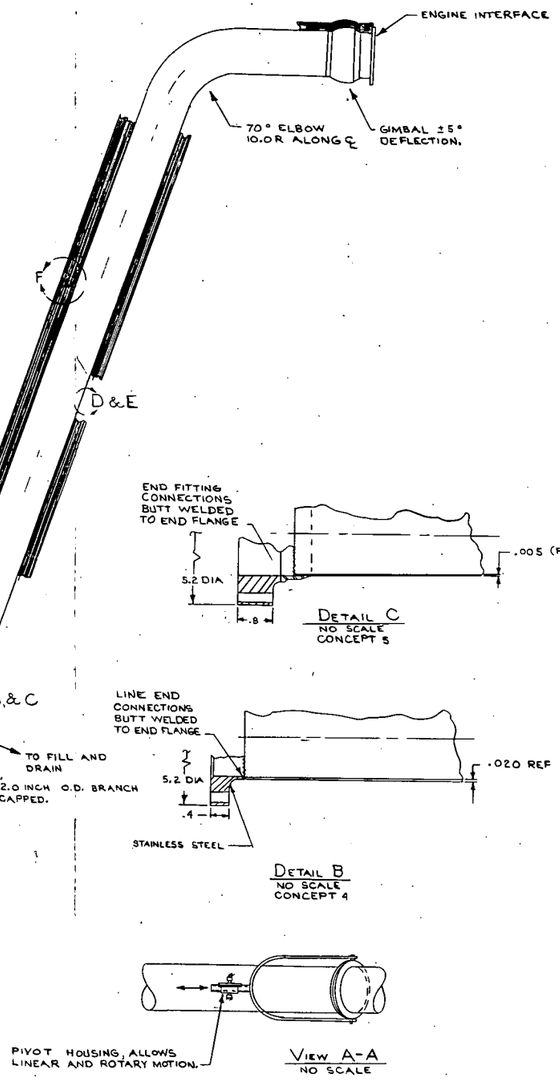

DETAIL C
NO SCALE
CONCEPT 5

DETAIL B
NO SCALE
CONCEPT 4

VIEW A-A
NO SCALE

89 and 90

REVISIONS				
QTY	ZONE	DESCRIPTION	DATE	APPROVED

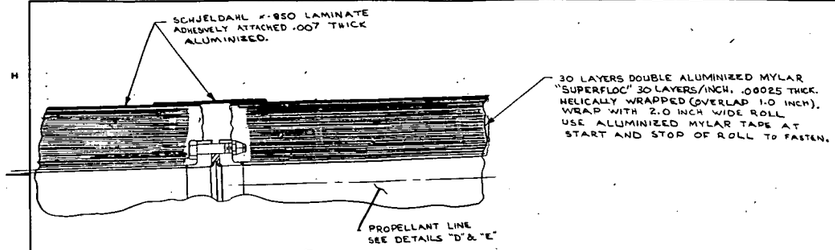

Detail F
TYP CONCEPTS 3&6
NO SCALE

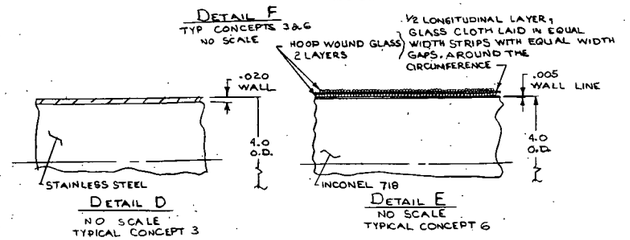

Detail D
NO SCALE
TYPICAL CONCEPT 3

Detail E
NO SCALE
TYPICAL CONCEPT 6

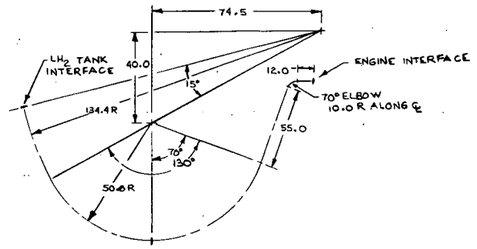

Dimensional Layout
Concept 3&6 Line

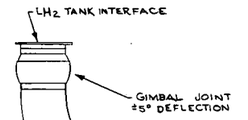

Design Concepts 3&6		
Purged MLI Insulated, Wet, Feedline		
Concept 3		Concept 6
FEED LINE	INSULATION (TYP BOTH CONCEPTS)	FEEDLINE
4.0 OUTSIDE DIAMETER .020 WALL STAINLESS STEEL (SEE DETAIL "D")	MLI INSULATION SYSTEM; ¼ MIL (.00025) THICK, DOUBLE ALUMINIZED MYLAR, 30 LAYERS SPIRALLY WRAPPED OVER LINE FROM A 2.0 WIDE SPOOL WITH 1.0 WIDE OVERLAP (MLI IS SUPER FLOC) FASTEN START AND STOP WITH ALUMINIZED MYLAR TAPE. WRAP OUTSIDE WITH SCHJELDAHL X-850 LAMINATE, CLOSE ENDS AND ATTACH PURGE. (SEE DETAIL F)	4.0 OUTSIDE DIAMETER .005 WALL INCONEL 718 OVERWRAPPED 2½ LAYERS, S-GLASS HOOP/½ LONGITUDINAL & HOOP. (SEE DETAIL "E")

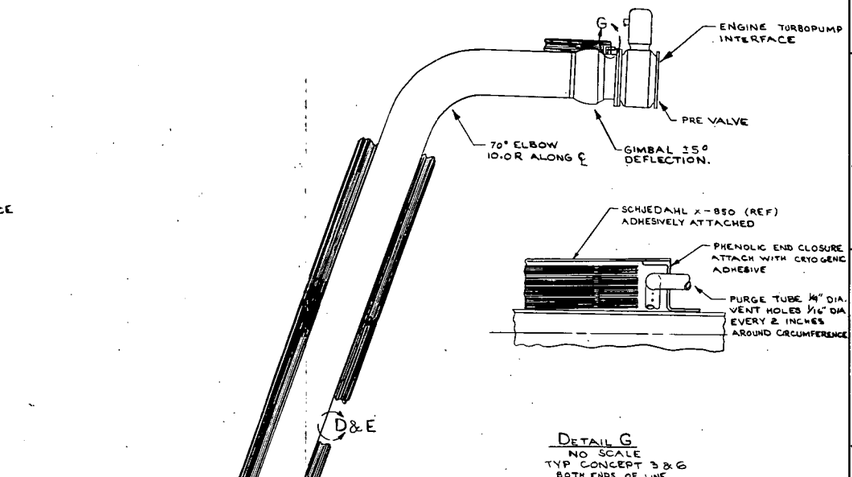

Detail G
NO SCALE
TYP CONCEPT 3&6
BOTH ENDS OF LINE

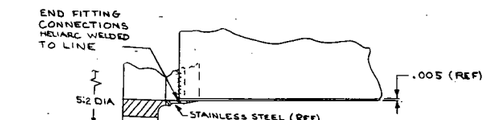

Detail C
NO SCALE
CONCEPT 6

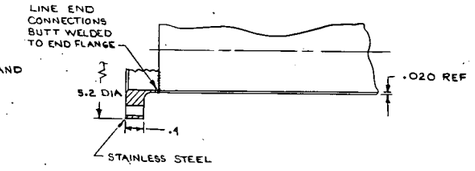

Detail B
NO SCALE
CONCEPT 3

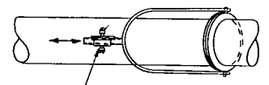

View A-A
NO SCALE

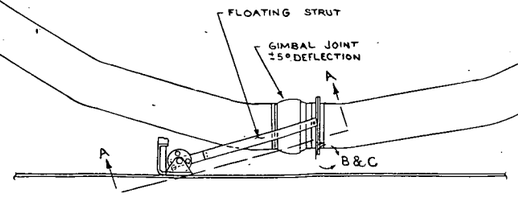

91 and 92

REFERENCES

1. Space Tug Point Design Studies
   McDonnell-Douglas Astronautics
   February, 1972

2. Space Tug Point Design Studies
   North American Rockwell
   February, 1972

3. Baseline Tug Definition Document - Rev. A
   George C. Marshall Space Flight Center
   June 26, 1972

4. "Space Tug Systems Study", 18 September 1973, GD/Convair, Contract No. NAS8-29676, Volume V - Systems Data Dump.

5. Space Tug Systems Study (Storable), Performed by the Martin Marietta Corporation under Contract NAS8-29675.

6. Hall, Laintz and Phillips: Volume I, Final Report, Composite Propulsion Feedlines for Cryogenic Space Vehicles.

7. Kevlar 49 Data Manual, E.I. DuPont DeNemours and Company Inc.

8. Final Report, "Development of Advanced Materials for Integrated Tank Insulation System for the Long Term Storage of Cryogens in Space", MCR-69-405, September, 1969, by John P. Gille.

9. "Fatigue of Composite", Salkind, M. J., Composite Materials: Testing and Design (Second Conference), ASTM STP 497, American Society for Testing and Materials, 1972, pgs. 143-169.

10. Final Report, "Design Criteria for Low Profile Flange Calculations", Report No. LMSC-HREC-TR D306492, Contract NAS8-28614, Lockheed Missiles and Space Company, Inc., by Karl R. Leimback, March, 1973.

11. Phase Report, "Design and Development of Pressure and Repressurization Purge System for Reusable Space Shuttle Multilayer Insulation Systems", Report No. 632-3-286, Contract NAS8-27419, General Dynamics, Convair Aerospace Division.

12. Aerospace Fluid Component Designers Handbook, Volume I, Rev. D, Technical Documentary Report No. RPL-TDR-64-25, February, 1970.

13. Roark, Formulas for Stress and Strain, McGraw-Hill Book Company, Third Edition, 1954.

14. Filament - Overwrapped Metallic Cylinderical Pressure Vessels, NASA TM X-52171, by Robert H. Johns and Albert Kaufman, Lewis Research Center, Cleveland, Ohio, April, 1966.

15. Thermal Insulation Systems, NASA SP-5027: 1967, P.E. Glaser, et.al.

DISTRIBUTION LIST

No. of Report Copies	Recipient
	National Aeronautics & Space Administration Lewis Research Center 21000 Brookpark Road Cleveland, Ohio 44135
1	Attn: Contracting Officer, MS 500-313
5	E. A. Bourke, MS 500-205
1	Technical Utilization Office, MS 3-16
1	Technical Report Control Office, MS 5-5
2	AFSC Liaison Office, MS 501-3
2	Library MS 60-3
1	Office of Reliability & Quality Assurance, MS 500-211
1	N. T. Musial, MS 500-113
12	J. J. Notardonato, Project Manager, MS 500-203
1	Director, Manned Space Technology, RS Office of Aeronautics & Space Technology NASA Headquarters Washington, DC 20546
2	Director Space Prop. and Power, RP Office of Aeronautics & Space Technology NASA Headquarters Washington, DC 20546
1	Director, Launch Vehicles & Propulsion, SV Office of Space Science NASA Headquarters Washington, DC 20546
1	Director, Materials & Structures Div., RW Office of Aeronautics & Space Technology NASA Headquarters Washington, DC 20546
1	Director, Advanced Missions, MT Office of Manned Space Flight NASA Headquarters Washington, DC 20546
2	Director Space Prop. and Power, RP Office of Aeronautics & Space Technology NASA Headquarters Washington, DC 20546

1 Director, Launch Vehicles & Propulsion, SV
Office of Space Science
NASA Headquarters
Washington, DC 20546

1 Director, Materials & Structures Division, RW
Office of Aeronautics & Space Technology
NASA Headquarters
Washington, DC 20546

1 Director, Advanced Manned Mission, MT
Office of Manned Space Flight
NASA Headquarters
Washington, DC 20546

1 National Aeronautics & Space Administration
Ames Research Center
Moffett Field, California 94035
Attn: Library

1 National Aeronautics & Space Administration
Flight Research Center
P.O. Box 273
Edwards, California 93523
Attn: Library

1 Director, Technology Utilization Division
Office of Technology Utilization
NASA Headquarters
Washington, DC 20546

1 Office of the Director of Defense
Research & Engineering
Washington, DC 20301
Attn: Office of Asst Dir (Chem Technology)

1 Office of Aeronautics & Space Technology, R
NASA Headquarters
Washington, DC 20546

10 NASA Scientific and Technical Information Facility
P.O. Box 33
College Park, Maryland 20740
Attn: NASA Representative

1 National Aeronautics & Space Administration
Goddard Space Flight Center
Greenbelt, Maryland 20771
Attn: Library

1 National Aeronautics & Space Administration
John F. Kennedy Space Center
Cocoa Beach, Florida 32931
Attn: Library
1 I. Moore

1 National Aeronautics & Space Administration
Langley Research Center
Langley Station
Hampton, Virginia 23365
Attn: Library

1 National Aeronautics & Space Administration
Manned Spacecraft Center
Houston, Texas 77001
Attn: Library
1 W. Chandler
1 W. Dusenberry
1 C. Yodzis
1 R. High
1 D. Medlock
1 R. Allgeier

1 National Aeronautics & Space Administration
George C. Marshall Space Flight Center
Huntsville, Alabama 35912
Attn: Library
1 J. M. Stuckey
1 I. G. Yates
1 E. H. Hyde
1 P. L. Muller

1 Jet Propulsion Laboratory
4800 Oak Grove Drive
Pasadena, California 91103
Attn: Library
1 L. Stimson
1 J. Kelly
1 R. Breshears

1 Defense Documentation Center
Cameron Station
Building 5
5010 Duke Street
Alexandria, Virginia 22314
Attn: TISIA

1 RDT (RTNP)
Bolling Air Force Base
Washington, DC 20332

1 Arnold Engineering Development Center
Air Force Systems Command
Tullahoma, Tennessee 37389
Attn: Library

1 Advanced Research Projects Agency
Washington, DC 20525
Attn: Library

1 Aeronautical Systems Division
Air Force Systems Command
Wright-Patterson Air Force Base,
Dayton, Ohio
Attn: Library
1 AFML (MAAE)
1 AFML (MAAM)

1 Air Force Rocket Propulsion Laboratory (RPM)
Edwards, California 93523
Attn: Library

1 Air Force FTC (FTAT-2)
Edwards Air Force Base, California 93523
Attn: Library

1 Air Force Office of Scientific Research
Washington, DC 20333
Attn: Library

1 Space & Missile Systems Organization
Air Force Unit Post Office
Los Angeles, California 90045
Attn: Technical Data Center

1 Office of Research Analyses (OAR)
Holloman Air Force Base, New Mexico 88330
Attn: Library
RRRD

1 U. S. Air Force
Washington, DC
Attn: Library

1 Commanding Officer
U. S. Army Research Office (Durham)
Box CM, Duke Station
Durham, North Carolina 27706
Attn: Library

1 Bureau of Naval Weapons
Department of the Navy
Washington, DC
Attn: Library

1 Director (Code 6180)
U. S. Naval Research Laboratory
Washington, DC 20390
Attn: Library

1 Picatinny Arsenal
Dover, New Jersey 07801
Attn: Library

1 Air Force Aero Propulsion Laboratory
Research & Technology Division
Air Force Systems Command
United States Air Force
Wright-Patterson AFB, Ohio 45433
Attn: APRP (Library)

1 Electronics Division
Aerojet-General Corporation
P.O. Box 296
Azusa, California 91703
Attn: Library

1 Space Division
Aerojet-General Corporation
9200 East Flair Drive
El Monte, California 91734
Attn: Library

1 Aerojet Ordnance and Manufacturing
Aerojet-General Corporation
11711 South Woodruff Avenue
Fullerton, California 90241
Attn: Library

1 Aerojet Liquid Rocket Company
P.O. Box 15847
Sacramento, California 95813
Attn: Technical Library 2484-2015A

1 Aeronutronic Division of Philco Ford Corp.
Ford Road
Newport Beach, California 92663
Attn: Technical Information Department

1 Aerospace Corporation
2400 E. El Segundo Blvd.
Los Angeles, California 90045
Attn: Library-Documents

1 Arthur D. Little, Inc.
20 Acorn Park
Cambridge, Massachusetts 02140
Attn: Library
1 R. B. Hinckley

1 Astropower Laboratory
McDonnell-Douglas Aircraft Company
2121 Paularino
Newport Beach, California 92163
Attn: Library

1 ARO, Incorporated
Arnold Engineering Development Center
Arnold AF Station, Tennessee 37389
Attn: Library

1 Susquehanna Corporation
Atlantic Research Division
Shirley Highway & Edsall Road
Alexandria, Virginia 22314
Attn: Library

1 Beech Aircraft Corporation
Boulder Facility
Box 631
Boulder, Colorado
Attn: Library

1 Bell Aerosystems, Inc.
Box 1
Buffalo, New York 14240
Attn: Library

1 Instruments & Life Support Division
Bendix Corporation
P.O. Box 4508
Davenport, Iowa 52808
Attn: Library

1 Boeing Company
Space Division
P.O. Box 868
Seattle, Washington 98124
Attn: Library
1 D. H. Zimmerman

1 Boeing Company
1625 K Street, N.W.
Washington, DC 20006

1 Chemical Propulsion Information Agency
Applied Physics Laboratory
8621 Georgia Avenue
Silver Spring, Maryland 20910

1 Chrysler Corporation
Missile Division
P.O. Box 2628
Detroit, Michigan
Attn: Library

1 Chrysler Corporation
Space Division
P.O. Box 29200
New Orleans, Louisiana 70129
Attn: Librarian

1 Curtiss-Wright Corporation
Wright Aeronautical Division
Woodridge, New Jersey
Attn: Library

1 University of Denver
Denver Research Institute
P.O. Box 10127
Denver, Colorado 80210
Attn: Security Office

1 Fairchild Stratos Corporation
Aircraft Missiles Division
Hagerstown, Maryland
Attn: Library

1 Research Center
Fairchild Hiller Corporation
Germantown, Maryland
Attn: Library

1 Republic Aviation
Fairchild Hiller Corporation
Farmington, Long Island
New York

1 General Dynamics/Convair
P.O. Box 1128
San Diego, California 92112
Attn: Library
1 R. Tatro

1 Missiles and Space Systems Center
General Electric Company
Valley Forge Space Technology Center
P.O. Box 8555
Philadelphia, Pa. 19101
Attn: Library

1 General Electric Company
Flight Propulsion Lab. Department
Cincinnati, Ohio
Attn: Library

1 Grumman Aircraft Engineering Corporation
Bethpage, Long Island, New York
Attn: Library
1 B. Aleck
1 M. Martin

1 Honeywell Inc.
Aerospace Division
2600 Ridgeway Road
Minneapolis, Minnesota
Attn: Library

1 IIT Research Institute
Technology Center
Chicago, Illinois 60616
Attn: Library

1 Ling-Temco-Vought Corporation
P.O. Box 5907
Dallas, Texas 75222
Attn: Library

1 Lockheed Missiles and Space Company
P.O. Box 504
Sunnyvale, California 94087
Attn: Library

1 Linde--Division of Union Carbide
P.O. Box 44
Tonawanda, N.Y. 11450
Attn: G. Nies

1 Marquardt Corporation
16555 Saticoy Street
Box 2013 - South Annex
Van Nuys, California 91409

1 Denver Division
Martin Marietta Corporation
P.O. Box 179
Denver, Colorado 80201
Attn: Library
1 R. W. Vandekoppel

1 Western Division
McDonnell Douglas Astronautics
5301 Bolsa Ave
Huntington Beach, California 92647
Attention: Library
1 P. Klevatt

1 McDonnell Douglas Aircraft Corporation
P.O. Box 516
Lambert Field, Missouri 63166
Attn: Library
1 L. F. Kohrs

1 Rocketdyne Division
Rockwell International
6633 Canoga Avenue
Canoga Park, California 91304
Attn: Library, Department 596-306

1 Space & Information Systems Division
Rockwell International
12214 Lakewood Blvd.
Downey, California
Attn: Library
1 E. Hawkinson
1 R. Boudreaux

1 Northrop Space Laboratories
3401 West Broadway
Hawthorne, California
Attn: Library

1 Purdue University
Lafayette, Indiana 47907
Attn: Library (Technical)

1 Goodyear Aerospace Corporation
1210 Massilon Road
Akron, Ohio 44306
Attn: C. Shriver

1 Hamilton Standard Corporation
Windsor Locks, Connecticut 06096
Attn: Library

1 Stanford Research Institute
333 Ravenswood Avenue
Menlo Park, California 94025
Attn: Library

1 TRW Systems Inc.
1 Space Park
Redondo Beach, California 90278
Attn: Tech. Lib. Doc. Acquisitions

1 United Aircraft Corporation
Pratt & Whitney Division
Florida Research & Development Center
P.O. Box 2691
West Palm Beach, Florida 33402
Attn: Library

1 United Aircraft Corporation
United Technology Center
P.O. Box 358
Sunnyvale, California 94038
Attn: Library

1 Vickers Incorporated
Box 302
Troy, Michigan

1 Airesearch Mfg. Div.
Garrett Corporation
9851 Sepulveda Blvd
Los Angeles, California 90009

1 Airesearch Mfg. Div.
Garrett Corporation
402 South 36th Street
Phoenix, Arizona 85034
Attn: Library

1 Commanding Officer
U.S. Naval Underwater Ordnance Station
Newport, Rhode Island 02844
Attn: Library

1 National Science Foundation, Engineering Division
1800 G. Street N.W.
Washington, DC 20540
Attn: Library

1 G. T. Schjeldahl Company
Northfield, Minn. 55057
Attn: Library

1 General Dynamics
P.O. Box 748
Fort Worth, Texas 76101

1 Cryonetics Corporation
Northwest Industrial Park
Burlington, Massachusetts

1 Institute of Aerospace Studies
University of Toronto
Toronto 5, Ontario
Attn: Library

1 FMC Corporation
Chemical Research & Development Center
P.O. Box 8
Princeton, New Jersey 08540

1 Westinghouse Research Laboratories
Beulah Road, Churchill Boro
Pittsburgh, Pennsylvania 15235

1 Cornell University
Department of Materials Science & Eng.
Ithaca, New York 14850
Attn: Library

1 Marco Research & Development Co.
Whittaker Corporation
131 N. Ludlow Street
Dayton, Ohio 45402

1 General Electric Company
Apollo Support Dept. P.O. Box 2500
Daytona Beach, Florida 32015
Attn: C. Ray

1 E. I. DuPont, DeNemours and Company
Eastern Laboratory
Gibbstown, New Jersey 08027
Attn: Library

1 Esso Research and Engineering Company
Special Projects Unit
P.O. Box 8
Linden, New Jersey 07036
Attn: Library

1 Minnesota Mining and Manufacturing Company
900 Bush Avenue
St. Paul, Minnesota 55106
Attn: Library